Dr.-Ing. Roland Schmidt[1]
Dr. rer. nat. Günther Klingenberg[1]
Dr.-Ing. Mathias Woydt[2]

[1]Physikalisch-Technische Bundesanstalt (PTB)
[2]Federal Institute for Materials Research and Testing (BAM)

New lubrication concepts for environmental friendly machines

– Tribological, thermophysical and viscometric properties of lubricants interacting with triboactive materials –

Research Report Nr. 277
Compiling the achievements of the project BMWA 14/02
Berlin and Braunschweig, Germany, 2006

Forschungsbericht 277
Berlin 2006

Impressum

Forschungsbericht 277:
New lubrication concepts for environmental friendly machines – Tribological, thermophysical and viscometric properties of lubricants interacting with triboactive materials –
2006

Herausgeber:
Bundesanstalt für Materialforschung und -prüfung (BAM)
Unter den Eichen 87
12205 Berlin
Telefon: +49 30 8104-0
Telefax: +49 30 8112029
E-Mail: info@bam.de
Internet: www.bam.de

Verlag und Vertrieb:
Wirtschaftsverlag NW
Verlag für neue Wissenschaft GmbH
27568 Bremerhaven
Telefon: +49 471 94544-0
Telefax: +49 471 94544-77

Umschlag: Lutz Mittenzwei
Layout: BAM-Arbeitsgruppe Z.67

ISSN 0938-5533
ISBN 3-86509-528-3

Summary

The present research report was elaborated in close cooperation with Renault SAS, FUCHS Petrolub AG and Ingenieurgesellschaft Auto und Verkehr (IAV).

The use of alternative oils for the lubrication of automobile engines has a potential of ecological and technical advantages. It requires the detailed knowledge of several thermophysical and viscometric properties in a large temperature range (mapping). Therefore, the following properties of up to twenty-eight different oils have been measured in the temperature range from 22 °C to 150 °C: density, heat capacity, thermal conductivity, viscosity at ambient pressure, viscosity under shear rates above 10^6 s^{-1}, and the viscosity at elevated pressures (maximum 100 MPa). The last two have been measured with a substantially improved and a newly developed apparatus, respectively. The pressure-viscosity coefficient has been measured on four hydrocarbon-based, factory-fill oils, a paraffin oil and twenty-three alternative oils. Nine of the alternative oils are based partly or completely on esters, the other fourteen on polyglycols, two of them additionally on water.

Based on the piston ring/cylinder liner simulation tests of BAM performed outside of engines and the SRV® tests both performed only under conditions of mixed/boundary lubrication, it is reasonable that thermally sprayed TiO_x-based, $Ti_{n-2}Cr_2O_{2n-1}$ and (Ti,Mo)(C,N)+23NiMo piston ring coatings, so called “lubricious or triboactive oxides”, can substitute common materials and serve as a promising alternative to commercial piston ring coatings made of strategic Molybdenum and super-finishing intensive blends of WC/Cr_3C_2. Some couples qualified for “zero” wear.

In combination with bionotox ester- and polyglycol-based lubricants the coefficient of friction can be reduced fulfilling simultaneously stronger European exhaust emission regulations. Thermally sprayed Ti-based coatings with their high wear resistance can additionally be used on aluminium liners to increase the resistance of critical components against wear, adhesive wear and thermomechanical stresses. For given tribological test conditions all APS[1] coatings on piston rings showed no friction reducing effect. The coefficient of friction is more determined by the lubricants than by the materials or by an individual interaction between lubricants and a specific material or tribopairing.

Lubricious oxides or triboactive materials and/or polar base oils may substitute the extreme pressure (EP) and anti-wear (AW) properties realized by the additives, thus enabling long drains and responding to “eco-tox” or “bio-no-tox” requirements as well as restrictions from the “chemical box”.

Overall, the different polymer-free bionotox and low-ash prototype engine oils with reduced additive contents displayed isoperformance regarding the tribological behaviour against cast iron with high carbon content and triboreactive materials.

Keywords

Ester, polyglycol, PAG, PPG, factory fill, hydrocarbon, engine oil, bio-oils, eco-lubricants, EAL, bio-no-tox oils, heat capacity, density, viscosity, pressure-viscosity, viscosity at high shear rate, thermal conductivity, mixed, boundary, lubrication, low sap, mid sap, wear, friction, triboactive materials, water-based oils, steam

[1] abbeviation for “atmospheric plasma spraying”

Zusammenfassung

Der vorliegende Forschungsbericht entstand in enger Zusammenarbeit mit der Renault SAS, der FUCHS Petrolub AG und der Ingenieurgesellschaft Auto und Verkehr (IAV).

Die Anwendungsfähigkeit alternativer Schmierstoffformulierungen in Verbrennungsmotoren hängt von der umfassenden Kenntnis des funktionalen Eigenschaftsprofiles ab. Dazu ist die detaillierte Kenntnis thermophysikalischer und viskosimetrischer Größen in einem weiten Temperatur- und Druckbereich erforderlich. Daher wurden folgende Größen an bis zu 28 verschiedenen Ölen im Temperaturbereich von 22 °C bis 150 °C gemessen: Dichte, Wärmekapazität, Wärmeleitfähigkeit, Viskosität bei Atmosphärendruck, Viskosität bei Schergeschwindigkeiten bis 10^6 s^{-1} und die Viskosität bei erhöhten Drücken (maximal 100 MPa). Die beiden letzten Größen wurden mit einer grundlegend verbesserten bzw. mit einer neu entwickelten Apparatur gemessen. An vier Ölen auf Kohlenwasserstoffbasis, einem unadditivierten Paraffinöl und 23 alternativen Ölen wurde der Druckkoeffizient der Viskosität gemessen. Neun der alternativen Öle basierten teilweise oder vollständig auf Estern, die anderen 14 auf Polyglykolen, zwei davon zusätzlich auf Wasser.

Die außermotorische Charakterisierung des tribologischen Verhaltens des Tribosystems „Kolbenring/Zylinderbahn“ unter Misch-/Grenzreibung beruhte auf zwei völlig verschiedenen Testphilosophien: dem BAM- sowie dem SRV®-Test.

Im Rahmen des Projektes neuentwickelte, thermisch gespritzte, TiO_x – und $Ti_{n-2}Cr_2O_{2n-1}$ – basierte und (Ti,Mo)(C,N)+23NiMo Kolbenringbeschichtungen, so genannte „schmierwirksame oder triboaktive Oxide“, offenbarten sich als vielversprechende Alternativen zu den kommerziellen Kolbenringbeschichtungen auf Basis von Molybdän und der endbearbeitungsintensiven Hartmetallbeschichtung aus WC/Cr_3C_2. Einige neuentwickelte Werkstoffpaarungen offerieren sogar „Null-Verschleiß“.

In Verbindung mit den biologisch schnell abbaubaren und Bionotox-Schmiermitteln auf Ester- und Polyglykol–Basis können die Misch-/Grenzreibungszahlen nachhaltig reduziert werden und außerdem können die strengeren europäischen Abgasemissionsvorschriften eingehalten werden, da diese Formulierungen entweder aschearm oder aschefrei sind und/oder über „lean burn“-Eigenschaften verfügen.

Thermisch gespritzte Beschichtungen auf Ti-Basis mit ihrer hohen Verschleißbeständigkeit können zusätzlich auf Aluminium–Zylinderbahnen aufgebracht werden, um den Verschleißwiderstand kritischer Komponenten auf das Niveau von hochgekohltem Grauguß zu bringen. Alle APS[1]-Beschichtungen auf Kolbenringen zeigten unter den verwendeten tribologischen Testbedingungen keinen die Reibungszahl verringernden Effekt. Unter Misch-/Grenzreibung bestimmen eher die Schmierstoffformulierungen die Reibungszahl, wobei in bestimmten Kombinationen durch individuelle Wechselwirkungen zwischen den Schmierstoffen und Werkstoffoberflächen niedrige Reibungszahlen gemessen wurden.

Schmierwirksame Oxide oder triboaktive Materialien und/oder polare Basisöle können die Hochdruck(EP) – und Verschleißschutz(AW) – Eigenschaften der Additive substituieren. So sind verlängerte Ölwechselintervalle möglich, die Erfüllung der Zielforderungen „eco–tox“ oder „bio–no–tox“ sowie die jüngst sich aus der „chemical box“ ableitenden Restriktionen können funktional eingehalten werden.

Trotz des abgesenkten Additivgehaltes zeigten die verschiedenen polymerfreien, biologisch schnell-abbaubaren Prototypenformulierungen mit reduzierten Aschegehalten und verringertem Additivkonzentrationen gegenüber hochgekohltem Grauguß und den triboaktiven Werkstoffen keine tribologischen Nachteile im Vergleich zu Erstbefüllungsölen auf Basis von Kohlenwasserstoffen.

Schlüsselwörter

Ester, Polyglykole, PAG, PPG, Erstbefüllung, Kohlenwasserstoff, Bioöl, Bio-no-tox-Öl, Wärmekapazität, Dichte, Viskosität, Druckviskosität, Viskosität unter hohen Scherraten, Wärmeleitfähigkeit, Misch/Grenzreibung, Schmierung, lowsap, midsap, Verschleiß, Reibung, triboaktive Werkstoffe, wasserbasiertes Öl, Dampf

[1)] Abkürzung für „atmospheric plasma spraying“

Contents

1 Introduction

More and more, the impact of engine oils on durability of particulate filters and catalysts has to be minimized or avoided, on fuel economy (FE) maximized, as well as their impact on terrestrial and aquatic environment. Replacing hydrocarbon-based oils with environmental friendly products is one of the ways to reduce adverse effects on the ecosystem caused by the use of lubricants.

The competition between hydrocarbons and new alternative base oils is not yet technologically decided in favor for hydrocarbons or esters or polyglycols.

1.1 General context for internal combustion engines

Original equipment manufacturers (OEMs) are more and more interested in passenger car engine oils (PCMO) with reduced metal-organic additives thus contributing to the vision of an environmentally friendly and sustainable car. This is necessary in order to reduce the ash build-up in the after-treatment system caused by engine oils and therefore improve its filter efficiency and lifetime. High fuel efficiency retention and long drain intervals are expected, as well, from the engine oils. Easy removal of bio-no-tox-fluids and recycling supports a sustainable development.

As displayed by the RENAULT demonstrator ELLYPSE [1] and the FORD Model U, additional requirements may be in the future demanded, like

a. biodegradability and non-toxicity and/or
b. a content of renewables.

The criteria for attribution of the european environmental label “EUROMARGUERITE” require for hydraulic fluids a content of >50 % of renewables. A smaller figure was proposed for engine oils [2].

Besides, the fragmentation of standardized oil specifications between Europe, Asia and US persists, and the diversification in original equipment manufacturer (OEM) specifications is spreading more and more since engine designs requiring specific oil formulations or using specific combustion processes have been released.

Pure hydrocarbons it self can be US-FDA proof. The additive packages, which make hydrocarbons functional, determine the eco-tox and/or bio-no-tox and/or ash formation properties of hydrocarbon based formulations. It is obvious to look for the substitution of critical additives by others or new functional concepts,

a. EP/AW properties by triboactice materials and coatings and/or
b. Viscosity improvers by the high VI of base oils, like esters and polygycols and/or
c. Polar base oil molecules for lubricity.

One of the key questions is: How will the 2010+ engine oil look like?

The two main tasks of engine lubricants are energy saving (friction, FE) and wear prevention. The first task requires comparatively low viscosities at low temperatures and reduced coefficients of friction under mixed/boundary lubrication. The second task – which is another key issue of this research report - is connected with the ability of the lubricant to form a liquid film that separates the moving surfaces of the engine tribosystems from each other at high temperatures (in the case of IC engines at up to 150 °C). The higher the film thickness, the lower is the risk of direct contact of surface asperities which might damage the surface. The most critical tribosystems in an engine are:

a. the cam/follower (highest contact pressures, moderate sliding speed),
b. the piston ring /cylinder (lower contact pressures, high sliding speed) and
c. the crank shaft (highest sliding speeds, moderate pressure).

Engine designers seeking for alternative engine oils need a methodology to compare the hydrodynamic film forming behavior of base oils and formulations which are chemically completely different. The existing criteria in the oil specifications (ν_{40C}, ν_{100C} and HTHS) seem to be not descriptive enough.

Heat capacity and thermal conductivity are other important issues for comparing alternative oils [3, 4], and are therefore discussed in this research report, too.

The frictional and wear behavior of alternative lubricants when interacting with current state-of-the-art materials and new, triboactive materials need to be mapped.

1.2 Steam technology

The thermodynamic and caloric properties of steam makes it attractive for heat conversion and propulsion systems.

Combining a 19th century technology (steam $T_{max.} \approx 280$ °C and <28 bar) with the advanced materials, design tools and manufacturing processes of the 21st century for steam with 600 °C and up to 100 bar could truly result in revolutionary new steam applications. A sound understanding and tribological data base is needed to ensure the success of these machines. The success of the development of advanced water-lubricated steam engine systems depends strongly on the identification of triboactive materials and water-based crank shaft lubricants.

This approach was nowadays pushed by IAV [5] GmbH (Ingenieurgesellschaft Auto und Verkehr GmbH, www.iav.de, ca. 50 patent applications for steam engines) with the development of a three cylinder reciprocating steam engine (Zero Emission Engine) using the Rankine cycle. This work is today continued by EGINION/AMOVIS for APUs (Auxiliary Power Units) in passenger cars and trucks as well as for cogeneration (SteamCell®), a venture capital financed company.

Also in Germany was recently marketed of linear, reciprocating steam engine “Lion” for cogeneration (www.otag.de).

Spilling Energiesysteme [6] (see DE29906867U; EP1045128) markets since 2001 oil-free, reciprocating steam engines up to 2 MW for heat recovery using steam at 30 bar and 300 °C, but displayed a clear trend to use 450 °C and 60 bar.

Yankee Scientific, Inc., (www.yankeescientific.com e.g. www.climate-energy.com) develops a steam scroll expander for cogeneration or energy supply. The miniaturization, simplification and cost reduction of system components is achieved through the use of a two-phase working fluid and an oil-free positive-displacement scroll expander.

Steam technology is considered to be from the material science point of view more proven than fuel cells and much cheaper per kW.

Beginning 2006, BMW AG unveiled the concept of a hydrid propulsion system for passenger cars combining inline "classic" IC engine with a reciprocating steam expander directly linked to the crank shaft using waste exhaust heat to generate steam.

2 Tested Lubricants

In future, lubricants will more and more determine the functional performances and environmental properties of machineries and engines. Esters and polyglycols were identified as alternative base oils and blended to environmental friendly prototype engine oils meeting following properties:

a. low viscosity,
b. low contributions to exhaust emissions (lean burning),
c. high oxidative stability,
d. high biodegradability and
e. low toxicity (bio-no-tox) as well as
f. low ash formation or ash-free and
g. polymer-free.

The results from the eco-toxicological tests (Erebio-EC-project) are published elsewhere [7, 8]. Polymer-free lubricants are advantageous for direct injecting engines in view of deposit formation on intake valves. The content of ash and metal must be limited because the exhaust treatment devices and in consequence the fuel economy might be influenced by it.

Supplementarily, the requirement of reduced sulfur and phosphorus contents was taken into consideration.

Bio-no-tox engine oils offer the chance of better fuel efficiency, i.e. lower fuel consumption. This is a relevant contribution to the actual European "Climate Change Policy". Additionally, environmentally compatible engine oils based on synthetic esters can be formulated on renewable raw material, consequently offering further CO2 savings. Vegetable oils are one of the major source of these synthetic base fluids.

The results of the viscometric and thermophysical measurements will be presented in diagrams in chapter 4. Most diagrams show data for one of the three groups of oils. The names of the oils are listed in the following table.

Group 1

Three factory-fill, hydrocarbon-based engine oils as high performance formulations Titan SL PCX 0W-30, Castrol SLX HC 0W-30 and TOTAL HC 5W-30 served as references with a HTHS of ca. 3.0 mPas (target for the prototype oils), also for the tribological properties under mixed/boundary lubrication.

The commercially available Fuchs Titan GT1 0W-20 (1.2 wt.-% ash) with a portion of 50 % ester is listed on the positive list of the German Market Introduction Programme (MIP) for „Biolubricants and Biofuels", funded by the Ministry of Consumer Protection, Food and Agriculture (BMVEL). Also, fully ester-based, prototype oils of Fuchs Titan 100E SAE 0W-20, 100E HDDO and TOTAL 100E, were used. The formulations GT1, GTE/100E and HCE low SAP of FUCHS conform with the requirement of >50% of renewables. The GT1 and 100E/GTE are polymer-free.

The TOTAL HCE midSAP (0.75 wt.-% of sulfated ash) is a blend of hydrocarbons with esters.

The FUCHS GT1, HCE low SAP as well as the Total 100E and Total HCE (SAE 0W-30) comply with the bio-no-tox criteria in EC/1999/45. The Fuchs HCE lowSAPs, HCE 0W-20 and 100E 0W-20/10W-30 are zinc-free. The Fuchs HCE lowSAPs form only 0.5 wt.-% sulfated ash.

Group 1	Group 2	Group 3
Oils based on hydrocarbons and /or blends with esters	Oils for the Steam Rankine power cycle	Polyglycols and others
HC 5W-30	IAV-PAS 8	PAG 46-2
HC 5W-30 + 3.7% soot	IAV 65-2	PAG 46-4
Fuchs HCE 0W-20	IAV 65-2 + water	PPG 32-2
Total 100E	IAV 65-3	PPG 32-3
100E 0W-20	IAV 65-3 + water	Triol-PO
Total HCE		Triol-EO
Titan SL PCX 0W-30		Diol-PO
Castrol HC 0W-30 (SLX)		Paraffin 46
Fuchs HCE-Low-SAP		PG WS55
Total HCE-Mid-SAP		PAG 68
100E Aero		
Fuchs HCE-Low-SAP2 0W-20		
Fuchs 100E-Low-SAP 10W-30 (HDDO)		

The 100E aero is a pentaerythritester-based engine oil developed by SHELL in the eighties for adiabatic engines and displays an outstanding oxidation resistance forming 0.96 wt.-% sulfated ash.

The Fuchs 100E-Low-SAP 10W-30 (HDDO) is a 100 % ester-based engine oil forming 0.8 wt.-% sulfated ash.

The HC 5W-30 having 3.7 wt.-% soot was aged in a fired 1.9 liter turbodiesel engine with 89 kW by Renault SAS. The aim of this oil sample was to investigate the influence of soot on friction and wear.

The paraffinic oil (MERCK) in VG 46 was unadditivated.

Group 2

The IAV-PAS 8 is a water-based polyethylene glycol (PEG 3350 g/mol) crank case oil with 50 wt.-% water according to DE 100 49 175 for reciprocating steam expanders using the Rankine cycle, which is considered as a competitor to the fuel cells, since the combustion process applied by IAV fulfils “zero-emission” or “lean-burn” criteria, except for CO_2, H_2O and N_2. Due to steam blow-by, the crank case oil needs to be tolerant vis-à-vis water.

The IAV 65 formulations contains a base oil composed of 50 wt.-% PEG 450 and 50 wt.-% triethyleneglycol. The very high viscosity index of 266 associated with a low viscosity at 40 °C underlines this robust concept, which is designed not to suffer under a high water take-up.

The PAG 68 is a polyethyleneglycol-based formulation from FUCHS with 20 wt.-% water. The boiling temperature was above 120 °C.

The polyethyleneglycols (CAS: 25322-58-3) comply with bio-no-tox and pharmaceutical requirements. The aim of all

Table 1
Properties of engine and prototype oils

Lubricants	Noack evapo-ration in %	Pour point in °C	*VI*	ν_{40} in mm²/s	ν_{100} in mm²/s	ν_{150} in mm²/s	HTHS at 150 °C in mPa·s
Factory fill oils							
Total HC 5W-30	12.8	-42	159	55.15	9.57	4.197	3.0
Total HC 5W-30+ 3,7% soot	./.	./.	162	67.85	11.48	4.93	./.
Castrol SLX 0W-30	8.1	-57	168	57.0	10.2	4.42	3.0
Titan SL PCX 0W-30	9	- 45	162	53.19	9.44	4.14	2.95
Paraffin 46 b.o.	./.	./.	118	51.96	7.39	2.4	./.
Ester oils							
TOTAL 100E	4.8	<-42	153	40.98	7.6	3.46	2.95
100 E 0W-20	5.5	-39	167	43.26	8.23	3.64	2.95
100E aero			90	118.74	12.22	4.34	
100E LowSAP (HDDO)	7	<-48	151	56.22	9.44	4.03	3.0
TOTAL HCE	./.	<-42	159	46.32	8.41	3.73	2.98
Fuchs HCE 0W-20	6	- 45	160	47.03	8.64	3.78	2.95
TOTAL HCE midSAP	6.6	<-48	165	57.8	10.4	4.53	2.99
FUCHS HCE LowSAP	5.2	-45	184	44	8.8	4.26	2.9
Polyalkyleneglycols							
PAG 46-2	19.3	-31	*203*	47.4	9.94	4.81	4.3
PAG 46-3	19.5	-<27	*207*	46.7	9.95	./.	4.5
PAG 46-4 (Base oil)	11.3	-33	*146*	52.2	8.56	3.61	3.6
Diol-PO b.o.	./.	./.	*147*	39.8	7.31	3.39	./.
PPG 32-2	4.8	-45	*149*	34.3	6.7	3.2	2.78
PO-Triol b.o.	./.	-29	*41*	119.1	8.95	3.04	./.
EO-Triol b.o.	./.	./.	*89*	104.1	11.1	4.0	./.
Water-based formulations on polyethyleneglycols							
IAV PAS-8	./.	-30	265	39.5	10.4	./.	./.
PAG 68			*172*	70.12	12.39	./.	./.
IAV 65	./.	-27	61	26.11	4.76	2.11	./.
PAG WS 55		-55	./.	9,21	2,57	1,38	

water-based or water diluable formulations was to achieve at 100 °C a kinematic viscosity comparable to engine oils at 150 °C, thus enabling the use of state-of-the-art crank shaft bearings in engines.

Group 3

The polymer-free polyalkylene glycols (PAG 46-2/PAG 46-3 (Mw= 1 205/1 280 g/mol) and 46-4) were diols with EO: PO = 1:1 or 7:1 (EO= ethylene oxide, PO= propylene oxide). The polyalkylene glycols (PAG 46-2/46-3 and PAG 46-4) have different molecular weight distributions and EO:PO portions and were first blended with a gear/hydraulic oil additive according to patent US 6,194,359 and then modified by BAM in view of oxidation resistance and tribological properties. The PAG 46-4 is a custom-made prototype PAG elaborated by DOW Europe SA with Mw= 664 g/mol. The PAGs are not obliged to be labeled with the symbol „N“, they are polymer-free, ash-free, and do not contain any zinc or calcium.

The PPG 32-2 formulation uses a polypropylene glycol monobutyl ether base oil and a gear/hydraulic oil package which does not contain any polymers, is free of Zn, Ca and sulfur, and does not have to be labeled with the symbol “N” (Bio-no-tox). This PPG 32-2 has a comparatively low kinematic viscosity (only about 34 mm²/s at 40 °C) and at the same time a low NOACK-volatility of less than 5 %. The polymer-free PPG 32-2 contains 1 700 ppm sulfur and 200 ppm phosphorus respecting bio-no-tox criteria. Polypropylene glycol monobutyl ethers are classified as “slightly hazard“ to water (WGK 1) by the German Environmental Agency (www.umweltbundesamt.de) under the number #3530.

Additionally, the oxidation resistance of the PAG 46-4 and PPG 32-2 was boosted by proprietary additive packages “Phepani”, “Phopani”, “Chopani” or “Papani”. The amount of phosphorus and sulfur is reduced to about 650-780 ppm [P] and to about 600-800 ppm [S].

The “triols” are trifunctional polyglycols, either based on 100 % ethylenoxide (EO-Triol) or 100 % propylene oxide (PO-Triol).

All viscosity indices of the polyglycols were labeled in italic, as they don’t follow a linear relation between viscosity and temperature in a logarithmic plot.

The Diol-PO is a polypropylene glycol without a butanol starter having a molar mass Mw of 490 g/mol and a surprisingly high α at 20 °C of 19.4 GPa^{-1} (compare with 19.2 GPa-1 of PPG 32-2 having Mw = 900 g/mol).

The PAG WS 55 is a water-soluble, linear polymer with a very low viscosity having a molecular weight of ca. 250 g/mol.

Some relevant properties of the different lubricants are summarized in *Table 1*.

The eco-toxicological properties of most formulations presented in *Table 1* are detailed in [7, 8].

3 Equipment used for the measurements of viscometric and thermophysical properties and tribological behavior

3.1 Viscosity at ambient pressure

For a part of the engine oils, the viscosity at ambient pressure has been measured at seven different temperatures using capillary viscometers of the Ubbelohde type. This type of measurement yields the kinematic viscosity. For other engine oils, the dynamic viscosity at ambient pressure has been measured in the same temperature range, using the rolling-ball viscometer being described in the next section. It is sufficient to measure either the kinematic viscosity ν or the dynamic viscosity η. The conversion ($\eta = \rho\nu$) requires only the density ρ.

3.2 Density

The density has been measured at ambient pressure using pycnometers in the temperature range from 20 °C to 150 °C.

3.3 High-pressure viscosity

Figure 1 shows the rolling-ball viscometer that is used at PTB. Driven by the gravitational force, a hardened steel ball rolls downwards in a tube that is slightly (10°) inclined against the vertical. The diameter of the ball (15.721 mm) is only 214 µm smaller than the inner diameter of the tube (15.935 mm). The tube is filled with the liquid under test which has a lower density than the ball. The speed of the ball depends on the dynamic viscosity and on the density of the liquid. The latter must be known, as the buoyancy of the ball has an effect on its speed. The density has to be measured in a separate experiment.

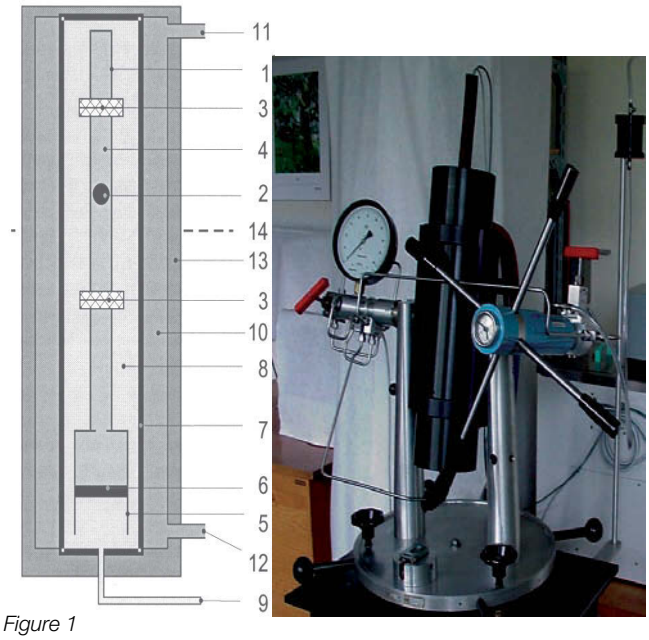

Figure 1
Photo and schematic diagram of the rolling-ball viscometer used at PTB: 1: fall tube, 2: steel ball, 3: double-coil, 4: sample, 5: cylinder, 6: piston, 7: pressure vessel, 8: pressure-transmitting oil, 9: pressure connection to screw press, 10: oil, 11 thermostat flow, 12: return of oil to thermostat, 13: insulation, 14: axis

The tube is located in a pressure vessel filled with oil. The pressure inside the vessel can be regulated by a screw press. A piston moving in a cylinder separates the liquid under test from the pressure-transmitting oil, guaranteeing the pressure equilibrium inside and outside the tube.

Thermostatisation is performed by a silicone oil which circulates around the pressure vessel in a channel which forms a spiral. The temperature of this oil is kept constant by a thermostat.

The ball‘s position is detected inductively by coils which enclose the tube. The ball, which consists of magnetic steel, augments temporarily the inductivity of the coil because it acts as an iron core as long as it is in the coil. A combination of two coils forming a differential transformer allows to determine exactly the point of time at which the ball passes through the beginning or the end of a measurement section. In order to get a clear signal from the differential transformers, the pressure vessel and the tube are made of stainless, non-magnetic steel.

When a measurement is finished, the pressure vessel is turned round to bring the ball back into its original position. All parts of the apparatus containing liquid under pressure have to be turned round, too. For this purpose, the pressure vessel, the screw press, the manometers and the pressure valves are mounted on a common axis.

The following quantities are recorded during a measurement:

– pressure p by a digital manometer
– temperature T by two platinum resistors which are located in the thermostat spiral channel
– the runtime t of the ball

A fourth quantity of importance is the density of the fluid which is known at ambient pressure. A simple experiment has been assembled to measure the increase in density caused by the pressure. In this experiment, a screw press is filled with the tested oil. The number of rotations necessary to achieve the maximal pressure of 100 MPa is dependent on the compressibility at ambient temperature. The higher compressibility at higher temperatures is estimated on the basis of the measured value at ambient temperature.

A feature of the measurements is the large range of viscosity. The maximal viscosity (at maximal pressure and ambient temperature) can be 200 times the minimal viscosity (at ambient pressure and maximal temperature). Exchanging the ball several times in order to adapt the size to the expected viscosity would be too time-consuming because the apparatus would have to be opened. Thus, the complete viscosity range is covered with just one ball, which leads to runtimes of up to 65 min. As the measurement values are recorded automatically by a computer, most of this time can be spent on other purposes.

To prepare the experiment, a long thermostatisation time is required. This is due to the pressure vessel which is located between the tube and the thermostatisation oil. It has a large mass and a limited thermal conductivity (about 15 W/(m · K)). The thermostatisation process can be started in the early morning by means of a time switch so that a thermal equilibrium will have developed at the beginning of a working day.

The rolling-ball viscometer has been calibrated with a special oil provided by the Fuchs Petrolub AG, one of the project partners. The viscosity and density of this oil in the temperature range of interest have been measured with capillary viscometers and pycnometers, respectively.

A calculation of the uncertainty following the GUM [9] resulted in a relative uncertainty (k = 2) for the viscosity of 1 % to 1.5 %. The most important contribution to this uncertainty is caused by the uncertainty of the temperature measurement.

On the one hand, the uncertainty of the temperature measurement is significantly higher at high temperatures, compared to the ambient temperature. On the other hand, the viscosity-temperature-coefficient β

$$\beta(T) = -\frac{1}{\eta}\left(\frac{\partial \eta}{\partial T}\right)\Bigg|_{p=\text{const.}} \tag{1}$$

is significantly smaller at high temperatures, resulting in a roughly constant contribution to the total measurement uncertainty.

The uncertainty of the estimation of the oil compressibility contributes only slightly to the total uncertainty because the difference to the high density of the steel ball is of interest, and this difference is known with an uncertainty of 0.25 %, even if the density of the oil is only known with an uncertainty of 2 %.

3.4 Heat capacity

The heat capacity measurements have been carried out using a power-compensated differential scanning calorimeter. This apparatus contains two crucibles. One of them is filled with the sample, the other one is empty. Both crucibles are heated with the same heating rate. The additional power that is necessary for the crucible which contains the sample is used to calculate the heat capacity of the sample. More details about the apparatus are given by Watson et al. [10] and by Höhne et al. [11].

3.5 Thermal conductivity

The conductivity of eight oils has been measured using a plate apparatus. In this experiment, a known flow of thermal energy $\dot{Q}$ is driven through a gap between two parallel plates. The gap is filled with the sample. The temperature difference ΔT that is necessary for this heat flux is measured. From these data and some geometrical information (area of the circular plates A_c, width of the gap d), the thermal conductivity λ can be calculated using

$$\lambda = \frac{\dot{Q} \cdot d}{A_c \cdot \Delta T} \tag{2}$$

For more details about the apparatus, see *Hammerschmidt* [12].

3.6 Tribological testing outside of engines

The tribological properties of a new triboreactive coating interacting with prototype engine oils based on esters and polyglycols were tribologically characterized outside of engines only under mixed/boundary lubrication using the SRV® [13] and BAM [14] test method in order to rank by two distinct different test methods.

SRV® tests are complementary to those the BAM-tests and were additionally performed according to a new ASTM Dyyyy-xx draft method [13] as cross-check to the BAM test method.

For the comparison of the results achieved with both tests, it has to be noted that the load in the SRV® test is six times higher than in the BAM test and both differ in the oil temperature (See *Figure 64* and *Figure 65*).

Piston ring/cylinder liner simulation tests were performed under mixed lubrication conditions in different lubricants at 170 °C and 0.3 m/s, whereby a thermal sprayed piston ring segment was pressed with 50 N against the rotating

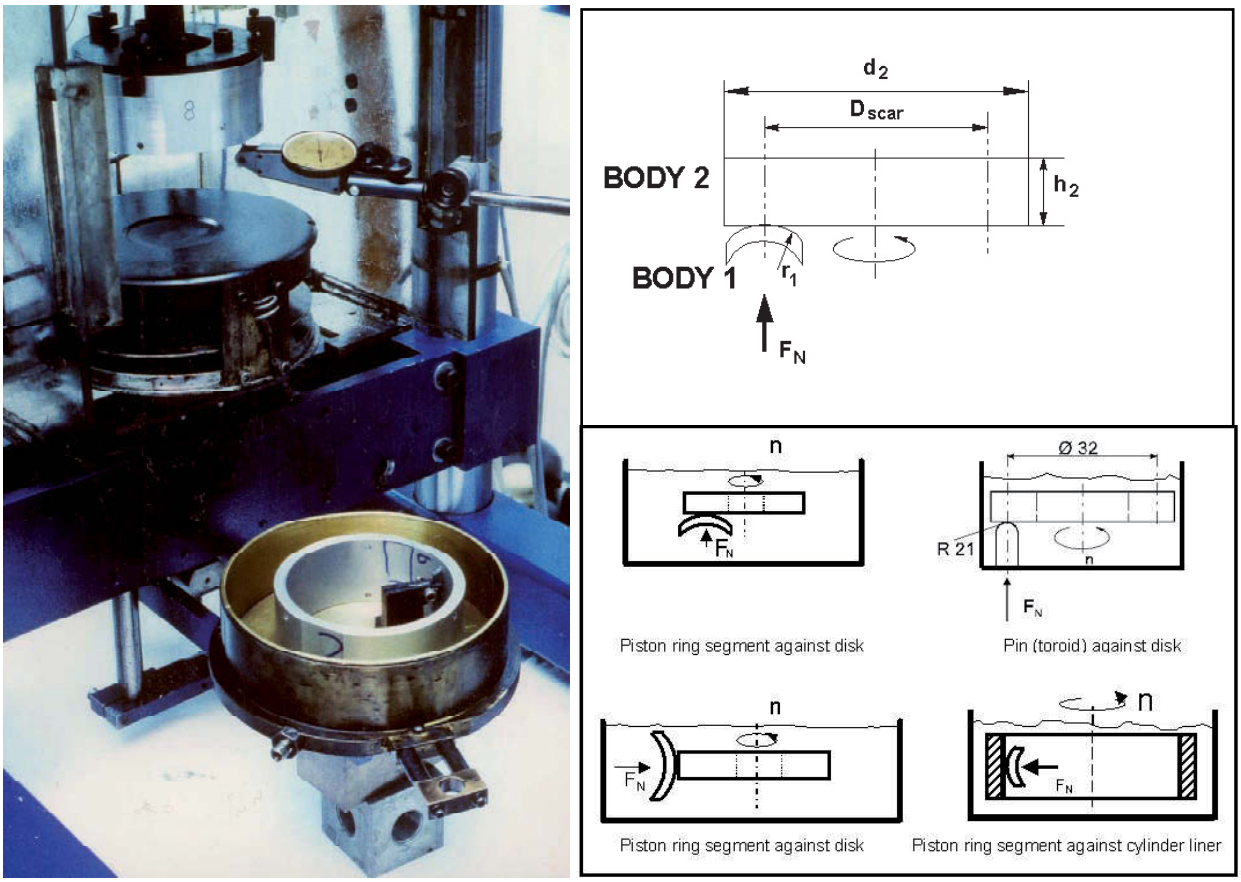

Figure 2
BAM test rig and piston ring / cylinder liner test configurations for mixed/boundary lubrication conditions under unidirectional sliding

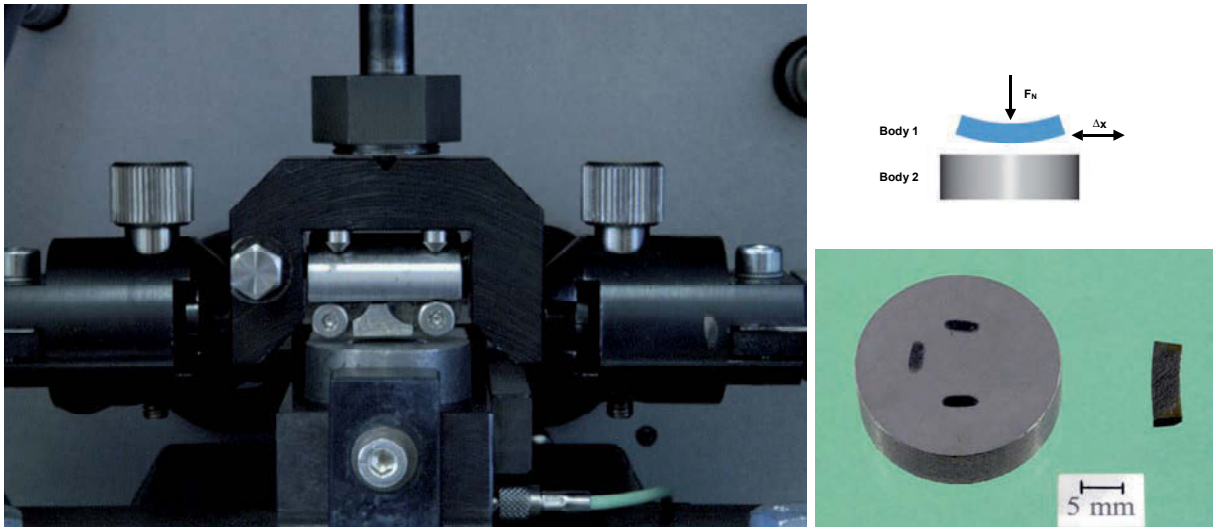

Figure 3
SRV® test rig with piston ring-on-disk (or cylinder liner) configuration

cylinder liner segment (or flat disk) up to a sliding distance of 24 000 m. An fresh oil amount of 0.3 to 0.4 l was used for each test. The test rig and the piston ring/cylinder liner configuration are shown in [14] using liner segments and in *Figure 2*.

The SRV® sample configuration with piston ring segments and wear scars [15] used here is shown in *Figure 3*. The resistance of different lubricants against scuffing was determined with 100Cr6/100Cr6 (AISI 52100) pairings according to modified ASTM D5706-05 [16].

The grey cast iron SRV-disks (GGL20HCN) corresponding to Renault GL1 have been produced and lapped to C.L.A. (R_a) = 0.343 µm, R_z = 2.483 µm, R_{pK} = 0.451 µm and R_{vK} = 0.596 µm.

3.7 Tribological materials

Wear protection represent another concern while using "mid-SAP" or even "lowSAP" oils or oils without or low contents of extreme pressure (EP) and/or anti-wear (AW) additives associated with bio-no-tox-properties according to directive EC/1999/45.

Lubricious oxides (LO) and triboactive materials appeared recently in scientific literature [17] and display estimated functional properties by different approaches. There exists within the scientific community no official consensus about their meaning.

The term of "lubricious oxides" was created 1989 by Michael N. Gardos [18, 19] for TiO_{2-x} as well as thematized by [20] and aim low wear with may be associated low dry coefficient of friction. The correct term for TiO_{2-x} is Magnéli-phases of titania, Ti_nO_{2n-1} with $4 \leq n \leq 9$, whereas TiO_{2-x}, with $x \leq 0.01$, describe "Wadsley"-defects.

The term "triboactive materials" appeared in Europe end of the nineties describing more a beneficial reaction between the surface and the lubricant or the ambient, thus indicating a more overall functional approach. Oxides, hydroxides or hydrates cover this understanding.

Novel and non-commercial "triboactive" or "triboreactive" materials were selected from Magnéli-type phases, like Ti_nO_{2n-1} and $Ti_{n-2}Cr_2O_{2n-1}$ (see FR 2 793 812), as well as substrates, like (Ti,Mo)(C,N)+23NiMo-binder (see DE 195 30 517), which forms by triboxidation these, namely γ-Ti_3O_5, Ti_5O_9, Ti_9O_{17} and $Mo_{0.975}Ti_{0.025}O_2$ as well as double oxides like $NiTiO_3$ and β-NiMoO4.

Experimental Ti_nO_{2n-1}, $Tin_{-2}Cr_2O_{2n-1}$ and (Ti,Mo)(C,N)-23NiMo as novel and non-commercial, triboactive powders applied by thermal spraying for automotive applications as cylinder liner and/or ring coatings were developed, produced and deposited for the first time on piston rings and cylinder liner samples.

With 550-880 HV0,2, the triboactive coatings follow not a metallurgically "hard" concept (See *Table 2*).

3.7.1 Spray powder

For the deposition of these coatings different Ti-based and substoichiometric powders were developed and purchased from H.C. Starck GmbH and FhG-IKTS (both Germany).

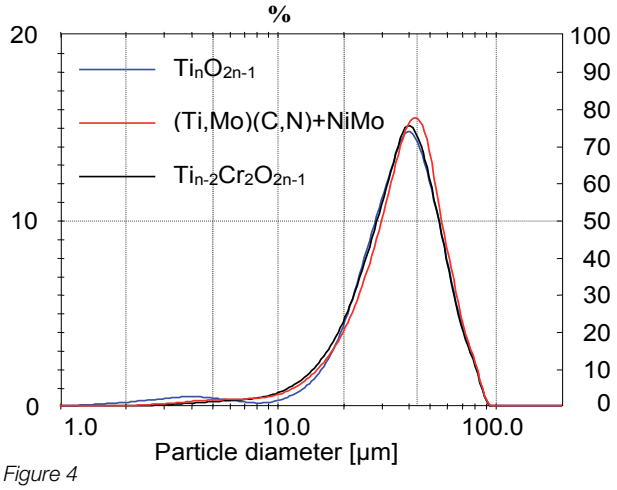

Figure 4
Particle size distribution of three different triboactive spray powders (agglomerated and sintered)

Table 2
Porosity and hardness of plasma sprayed Ti-based coatings on piston rings and on cylinder liners

Coating	Porosity by volume	Vickers hardness
MKP81A®		566 ± 144 HV0,2
APS Ti_nO_{2n-1} (n = 4 …6; $TiO_{1,60}$ to $TiO_{1,80}$) on piston **ring** (TARABUSI)	2 %	657 ± 88 HV0,2
APS $Ti_{n-2}Cr_2O_{2n-1}$ on piston **ring** (TARABUSI)	5 %	530± 55 HV0,5
APS (Ti,Mo)(C,N)+23NiMo (TM23-1) on piston **ring** (TARABUSI)	15 %	699 ± 99 HV0,5
APS (Ti,Mo)(C,N)+23NiMo (TM23-2) on piston **ring** (TARABUSI)	10 %	650 ± 59 HV0,5
APS Ti_nO_{2n-1} (n = 4 …6; $TiO_{1,60}$ to $TiO_{1,80}$) on cylinder **liner** (FhG-IWS)	2 %	846 ± 54 HV0,2
VPS Amperit 782.1 ($TiO_{1,95}$) on cylinder **liner** (FhG-IWS)	2 %	785 ± 39 HV0,2
APS $Ti_{n-2}Cr_2O_{2n-1}$ on cylinder **liner** (FhG-IWS)	2 %	851 ± 36 HV0,2
HVOF (Ti,Mo)(C,N)+23NiMo on cylinder **liner** (FhG-IWS)	10 %	816 ± 36 HV0,2

Before thermal spraying the spray powders were thoroughly characterized. Spray powder composition, particle morphology and resulting phase composition of coatings as well as particle size distribution are compiled in *Figure 4*.

3.7.2 Cylinder liner materials

The deposition of substoichiometric $TiO_{1.93}$, Ti_nO_{2n-1} ($TiO_{1.60}$ to $TiO_{1.80}$) and of (Ti,Mo)(C,N) cylinder liner coatings with different thermal spray processes (APS: Atmospheric plasma spraying, VPS: Vacuum plasma spraying, HVOF: High-Velocity-Oxy-Fuel) was described in more detail elsewhere [21, 22, 23]. The $T_{in-2}Cr_2O_{2n-1}$- and (Ti,Mo)(C,N)-23NiMo-powders were sprayed on GG20HCN disks by FhG-IWS using MF-P-1000 plasma spray equipment with F6 spray gun.

A $TiO_{1.95-x}$ coating was deposited with a vacuum plasma spray (VPS) process using a commercial, fused and crushed $TiO_{1.95}$ powder (Amperit 782.1 (22.5-45 µm; H.C. Starck GmbH, Goslar, Germany) directly on GGL20HCN without a bond layer as economic alternative to Ti_nO_{2n-1}. The advantage of vacuum plasma spraying (VPS) is that in this process no re-oxidation of the TiO_x powders can occur.

Analysis with XRD on the APS sprayed Ti_nO_{2n-1} coatings exhibit besides Rutile and Anatase peaks of Magnéli phases, mainly of Ti_4O_7 (Compare with ca. 66 wt.-% Ti_5O_9, ca. 17 wt.-% Ti_6O_{11} and ca. 17 wt.-% Ti_4O_7 in the spray powder).

The surfaces of $Ti_{n-2}Cr_2O_{2n-1}$-coatings were lapped to R_{PK} ca. 0.61 µm and in some cases smoothly finished to R_{PK} < 0.05 µm as well as those of (Ti,Mo)(C,N)-23NiMo-coatings to R_{PK} < 0.03 µm. In the sprayed $Ti_{n-2}Cr_2O_{2n-1}$-coatings were analyzed by means of ESMA 26.2 at.-% Titanium, 9.80 at.-% Chromium and 64.0 at.-% Oxygen.

Those newly developed triboactive Ti-based coatings were tribologically compared with uncoated grey cast irons (GGL20HCN with 3.7 wt.-% C) and GG26Cr [24] used as cylinder liner materials. It has to be noted, that dry running brake disks in passenger cars apply these cast iron grades with a high carbon contents.

The triboactive liner coatings were deposited without intermediate layer/bond coating on grey cast iron GGL20HCN supplied from Schwäbische Hüttenwerke (SHW) used as reference material. The structure of GGL20HCN is characterized by a perlitic matrix, a small amount of ferrite (<5 %), Fe_3P and small MnS inclusions as well as homogeneous distributed lamellar graphite. In comparison to common grey cast iron materials, GGL20HCN contains a relative high carbon content (3.66 wt.-% C) besides 2.0 % Si, 0.236 % Cr, 0.564 % Mn, 0.5 % Ni, 0.39 % Mo, 0.057 % S, 0.045 % P, 0.206 % Cu (all in wt.-%).

3.7.3 Piston ring materials

The ring diameters ranged from 79 mm to 89 mm. On piston rings (∅ = 80 mm x 2.5 mm) triboactive Ti_nO_{2n-1}, $Ti_{n-2}Cr_2O_{2n-1}$ and (Ti,Mo)(C,N)+23NiMo coatings were deposited by TARABUSI on a 94(NiCr)6Al bond layer using the APS process with a plasma gun SG 100 (Miller Thermal Inc.) in an Ar/He mixture as plasma forming gases. Piston ring substrate material is “AT 126”, a grey cast iron with spheroidal graphite and high carbon content.

These newly developed coatings were compared with two Mo coatings (PL72; APS-MKP81A® composed of Mo-NiCrBSi). The molybdenum in the VL® (Mo, ∅ = 122 mm) coating was deposited by means of flame spraying. The commercially available Mo-based piston rings differ mainly in the content of oxygen and in the amount of hard phases.

Porosity, hardness and roughness values before tribotesting are given in *Table 2* and *Table 3*. The roughness of Ti_nO_{2n-1} and MKP81A® coated piston rings are similar, but the hardness of Ti_nO_{2n-1} is much greater *(Table 4)*.

Figure 5 and *Figure 6* present the cross sections of triboactive APS sprayed coatings with NiCrAl bond coatings on piston rings. Ring substrate material is a grey cast iron with modular graphite (AT126). APS Mo (PL72) has a dense and lamellar structure and is used as reference coating and sprayed and complies with MKP81A®. To improve the bonding a NiCrAl intermediate layer was used. Concerning structure, phase composition and tribological behaviour APS Mo (PL72) and additionally investigated APS Mo (MKP81A®) *(Figure 7)* coatings are very similar. The PCF251® as well as PCF278® were supplied by DANA Corp. (Perfect Cycle Division). The PCF 278® consists of 59 wt.-% of Mo and 35 wt.-% CrNi as well as the PCF 251® of 80 wt.-% Mo and 18 wt.-% NiCr as well as the MKP81A® of 67-77 wt.-% Mo and 19-31 wt.-% NiCr.

Table 3
Roughness of uncoated grey cast iron and coated cylinder liner (or disk)

Specimen	Machining	R_a in µm	R_z in µm	R_{pk} in µm	R_{vk} in µm
GGL20HCN (BAM disks)	Lapped	1.07	5.9	0.53	1.45
VPS $TiO_{1,95-x}$ (Amperit 782.1)	Lapped	0.18	1.37	0.21	0.32
APS Ti_nO_{2n-1} (n = 4…6)	Lapped	0.135	0.863	0.164	0.200
APS- $Ti_{n-2}Cr_2O_{2n-1}$	Lapped or polished	0.57 0.152	4.49 1.44	0.61 0.054	1.25 0.571
HVOF (Ti,Mo)(C,N)+23NiMo	Lapped or polished	0.38 0.05	2.73 0.39	0.38 0.03	0.70 0.17

Table 4
Roughness of different piston rings

Metallurgy of running surfaces	R_z	Ra / C.L.A.	R_{pk}	R_{vk}	HV0,2	Supplier
APS 67-77 wt.-% Mo + Ni (MKP 81A)	1.9	0.5	**0.2**	2.2	570	Goetze
APS 67-77 wt.-% Mo + Ni (PL72)	0.98	0.149	**0.105**	0.559	530	TARABUSI
APS 80 wt.-% Mo +Ni (PCF-251)	0.455	0.090	**0.069**	0.137		DANA
Flame Mo (VL)	1.34	0.2	**0.22**	1.35	>900	Goetze
APS 59 wt.-% Mo +Cr+Ni (PCF-278)	0.902	0.190	**0.311**	0.210		DANA
APS Ti_nO_{2n-1} (n = 4 – 6)	2.3	0.5	**0.2**	1.6	830	TARABUSI
APS (Ti,Mo)(C,N) + 23NiMo (TM23-1)	15.1	3.1	**0.8**	6.00	700	TARABUSI
APS (Ti,Mo)(C,N) + 23NiMo (TM23-2)	1.76	0.36	**0.18**	1.24	660	TARABUSI
APS $Ti_{n-2}Cr_2O_{2n-1}$	0.81	0.14	**0.14**	0.52	550	TARABUSI
HVOF WC/Cr_3C_2 (MkJet 502)	0.574	0.111	**0.08**	0.305	1 200	Goetze
CKS-36 (Cr+ 2-6 Vol.-% Al_2O_3)	0.142	0.027	**0.014**	0.065	660	Goetze
GDC-50 (Cr+0.5-2.0 Vol.-% diamond)	0.204	0.040	**0.026**	0.108	830	Goetze
Nitrided	0.176	0.030	**0.018**	0.071		Goetze
GGG with 3.7-4.2 wt.-% C (KV1)	1.207	0.250	**0.346**	0.878	310	Goetze

Scale: 500 µm **APS Mo (PL 72) coating** **Scale: 20 µm**

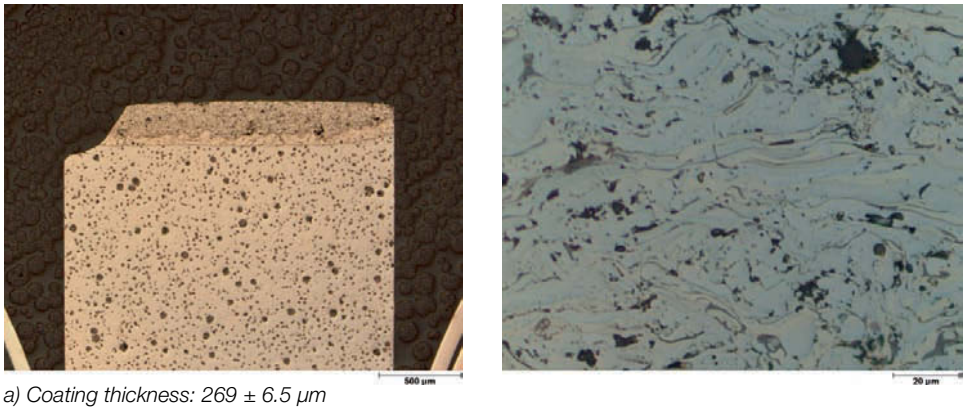

a) Coating thickness: 269 ± 6.5 µm

APS Ti_nO_{2n-1} coating

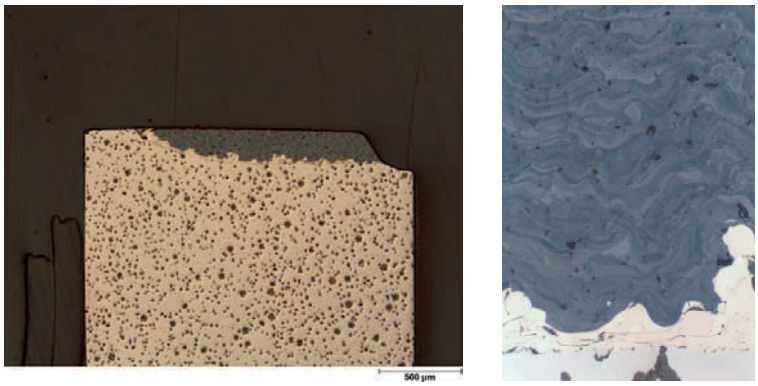

b) Coating thickness: 204 ± 9.6 µm

Figure 5
Optical micrographs of cross sections of APS coatings (TARABUSI) on grey cast iron piston rings: a) Mo and b) Ti_nO_{2n-1}

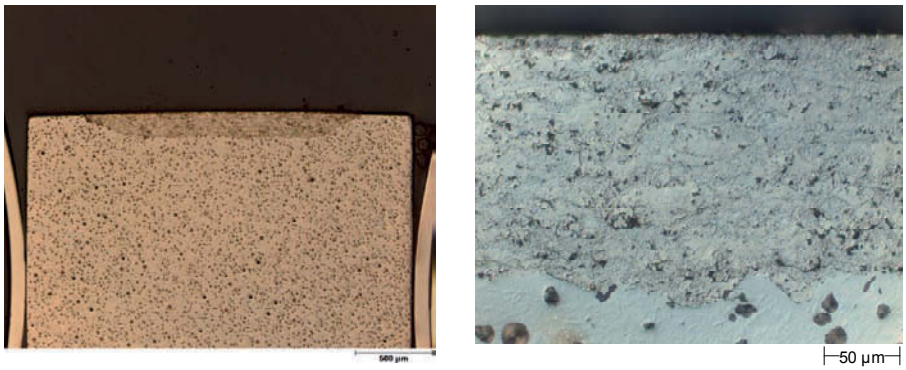

Figure 6
Cross sections of HVOF-MKJet502® coated piston ring

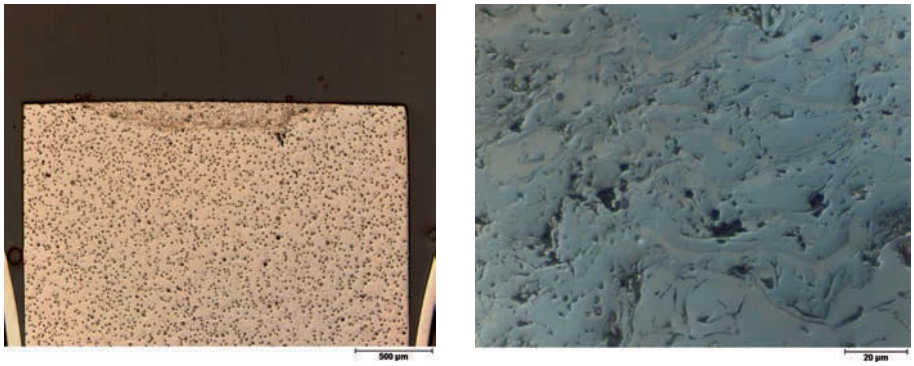

Figure 7
Optical micrograph of cross section of commercial Mo (MKP81A®) coated piston ring

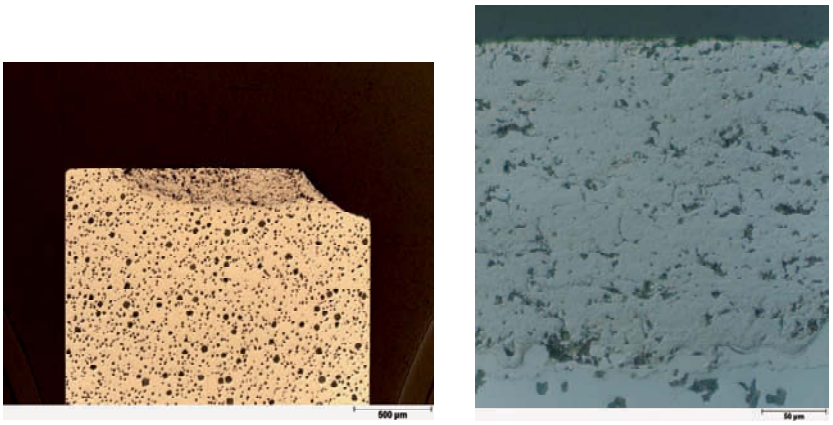

Figure 8
APS-(Ti,Mo(C,N)-23NiMo piston ring coating deposited by TARABUSI (TM23-2)

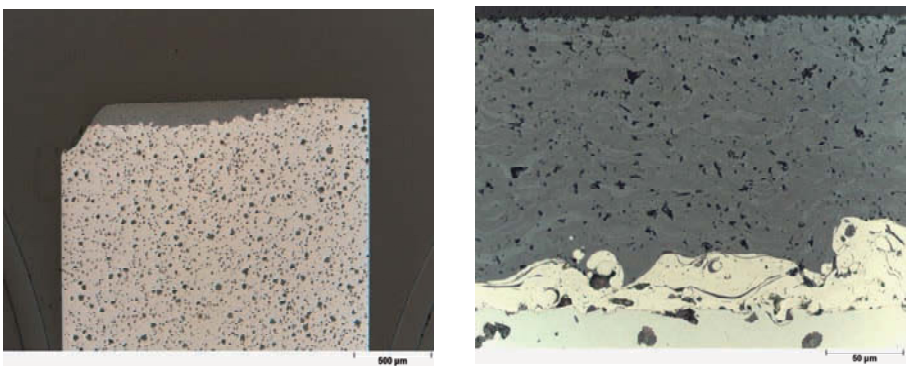

Figure 9
APS $Ti_{n-2}Cr_2O_{2n-1}$ piston ring coating deposited by TARABUSI

Besides a good bonding APS Ti_nO_{2n-1} is characterized by a dense, typical lamellar morphology.

Dark and bright grey areas visible in cross sections of APS Ti_nO_{2n-1} coating can be attributed to different oxygen contents. The hardness of the triboactive piston ring coating is slightly lower than for the triboactive cylinder liner coatings.

The HVOF-sprayed WC/Cr_3C_2-based hard metal ring coating (MKJet502®) with NiMo-binder has a dense structure. The tribological surfaces were superpolished. Due to the at least two hard phases, the hardness values of MKJet502® vary between 879 and 1 330 $HV_{0.3}$.

GDC-50®, a plated chromium with up to 2.0 % by volume of fine diamond particles and CKS-36®, also plated chromium with up to 6 % by volume of fine alumina particles, were tribological characterised, too.

KV1 is a cast iron with globular graphite (3.5-4.0 wt.-% C).

The metallurgical characterizations of the piston rings supplied by Federal Mogul Goetze can be found in reference [25].

Despite the functional references of molybdenum-based piston rings, some concerns grow more and more. Common sense precautions are necessary in repeated exposures of human beings especially in dusts and fumes of molybdenum and trioxide products as they occur during thermal spraying. Another aspect are the stock exchange prices for Ferromolybdenum and Molyoxide as they increased from ca. 3 US-$/lb in first quarter 1999 to ca. 7 US-$/lb in third quarter 2003. By 30th September 2005, the average price for Molyoxide reached 34 US-$/lb and by 17. March 2006 25 US-$/lb or 62 US-$/kg for Ferromolybdenum by 26th May 2006. There exist in consequence drivers for substituting molybdenum.

Coated $Ti_{n-2}Cr_2O_{2n-1}$-rings were machined to R_{PK} ca.0.14 µm remaining a functional thickness of ca. 187 µm.

3.7.4 Unlubricated sliding wear

Dry running or “oil-off” is a frequent operation mode for the piston ring/cylinder liner system requiring sliding couples free of adhesive wear.

The tribological behavior under unlubricated sliding conditions of APS-$Ti_{n-2}Cr_2O_{2n-1}$ machined to R_{pK} ca. 0.61 µm was characterized up to 800 °C and 7.5 m/s using stationary specimen in 99.7 % alumina. The results were elaborated in a high-temperature tribometer described elsewhere in reference [26].

In the work presented in references [27, 28], it is clearly visible, that the APS-$Ti_{n-2}Cr_2O_{2n-1}$, even with a quite elevated roughness of R_{pK} ca. 0.61 µm, runs best with low wear rates above 400 °C and 1 m/s associated with wear rates of the alumina below 10^{-7} mm³/Nm.

At 800 °C and 7.5 m/s under unlubricated sliding conditions, the lowest wear rate was kv = 1.62 10^{-6} mm³/Nm and of the alumina toroid kv = 9.9 10^{-8} mm³/Nm associated with P · V-values of 60.8 MPam/s and a coefficient of friction of 0.27.

Under dry friction, the self-mated couples of monolithic (sinterHIPpped) (Ti,Mo)(C,N)-15NiMo [TM10] displayed in a temperature range up to 800 °C and sliding speeds up to 5 m/s total wear rates lower than 10^{-6} mm³/Nm, which lie on a level comparable to those known for mixed/boundary lubrication. Compared to ceramic-ceramic composites, the tribosystem composed of self-mated (Ti,Mo)(C,N)+15NiMo couples achieved a further wear reduction at 22 °C and up to 800 °C. At 800 °C, the wear rate of the stationary (pin, shell) specimen decreased from 3.82 · 10^{-7} mm³/Nm at 0.12 m/s down to 9.5 · 10^{-8} mm³/Nm at 3.68 m/s, whereas the wear rate of the rotating (disc, shaft) specimen was only detectable at 3.68 m/s with a wear rate of 3.5 · 10^{-7} mm³/Nm. The lowest wear rate for TM10 was achieved at 6.17 m/s and 800 °C with 2.9 · 10^{-7} mm³/Nm for the stationary specimen and 5.7 · 10^{-7} mm³/Nm for the rotating specimen or as total wear rate of 8.6 10^{-7} mm³/Nm with an associated PV-value of 42 MPam/s.

Magnéli-phases of titania, Ti_nO_{2n-1}, are also part of the family of triboactive/-reactive materials with a prone dry running ability [17, 29].

4 Results of the measurements of viscometric and thermophysical properties

For a set of 28 different lubricants, the following properties have been measured in the temperature range from 20 °C to 150 °C:

- viscosity at ambient pressure
- density at ambient pressure
- dynamic viscosity at pressures up to 100 MPa = 1 kbar

For reasons discussed in chapter 4.6, functions $\alpha(T)$ and $\eta(T)$ have been derived.

In addition, three other properties have been measured for some of the oils:

- specific heat capacity (20 oils) in the temperature range from 20 °C to 150 °C
- thermal conductivity (10 oils) in the same temperature range
- dynamic viscosity at 150 °C and at a shear rate of up to 3 ·10^6 s^{-1} (6 oils)

The upper temperature limit of 150 °C is considered to be the maximum temperature in the oil sump.

4.1 Density

The results of the density measurements are presented in *Figure 10*, *Figure 11* and *Figure 12*. These data are needed for several calculations, namely:

- volumetric heat capacity $c_p \cdot \rho$

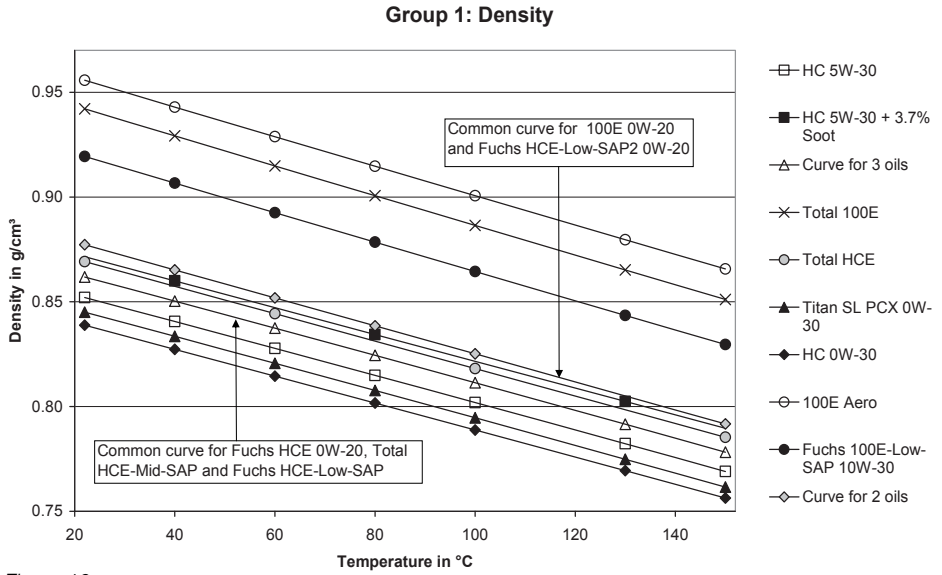

Figure 10
Density of the oils in group 1

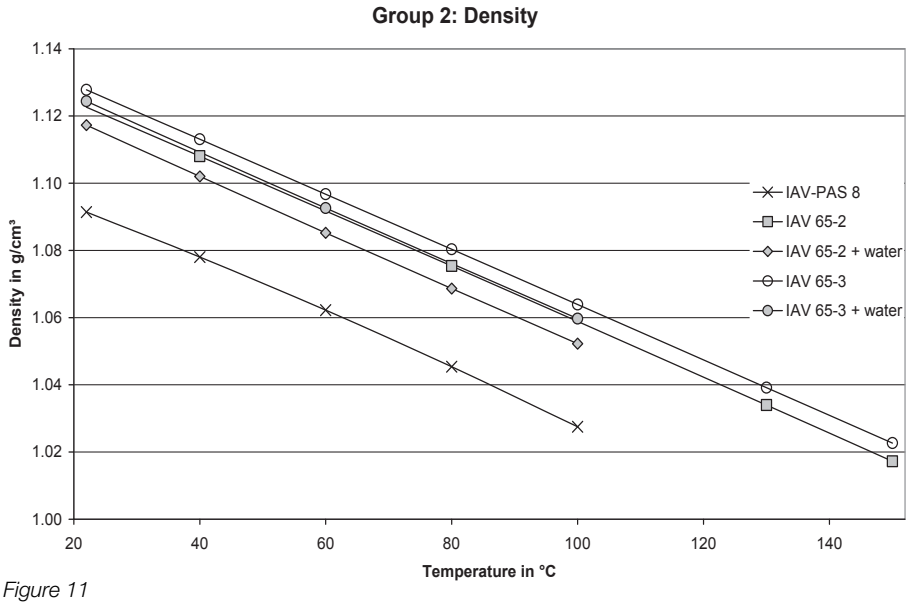

Figure 11
Density of the oils in group 2

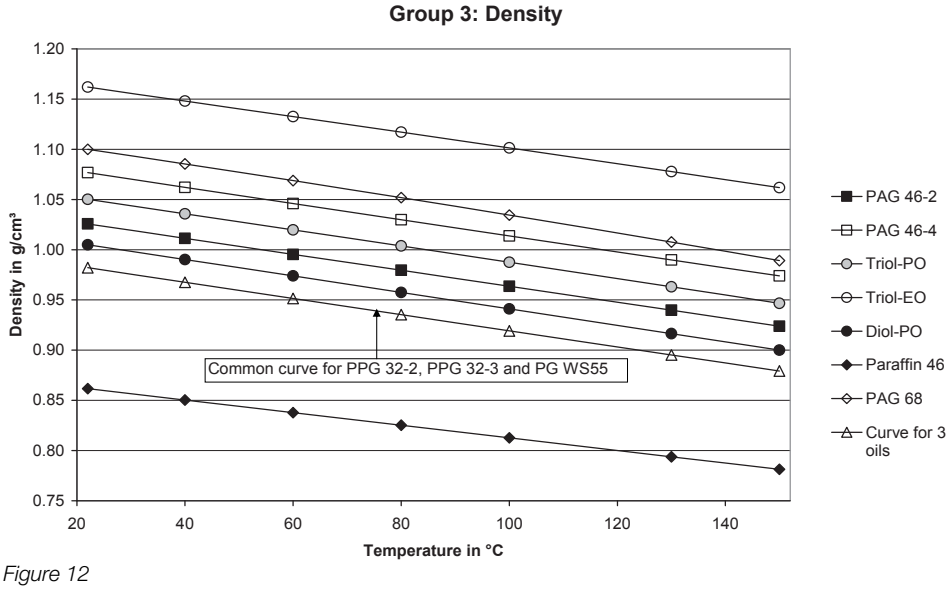

Figure 12
Density of the oils in group 3

– conversion between dynamic and kinematic viscosity, and

– buoyancy of the ball in the rolling-ball viscometer

Comparison of the diagrams shows that the oils in group 1 have a lower density than those in group 2 and 3, with the exception of Paraffin 46 from group 3.

4.2 Heat capacity

In most diesel engines, the piston crown is cooled by an oil jet to the piston bowl. Assuming a constant volume flow of the oil pump, the volumetric heat capacity (the product of the specific heat capacity c_p and the density ρ) has to be determined therefore to obtain the ability of oils to carry out heat. Engine designers are concerned about possible losses in the cooling efficiency of the piston by alternative fluids. Another aspect related to the heat capacity is the heating-up of the lubricating film during shearing, which results in an individual loss of viscosity and film-forming ability. Also, the film itself is defined by the volume of the bearing gap.

Figure 13 and *Figure 14* show the specific heat capacity of 9 oils from group 1, 3 oils from group 2, and 7 oils from group 3 as a function of the temperature. The oils of group 1 have a very similar heat capacity, with the exception of Total 100E. The lubricants IAV-PAS 8, IAV 65-2 + water and PAG 68 contain 20 wt.-% water, which results in a high heat capacity.

The product of specific heat capacity c_p and density ρ is plotted in *Figure 15* and *Figure 16*. The ranking of the oils is different, compared to the situation of in *Figure 13* and *Figure 14*.

The diagrams show that the volumetric heat capacities of the hydrocarbon-based oils HC 5W-30 and Titan SL PCX 5W-30 are the lowest that occurred in the experiments.

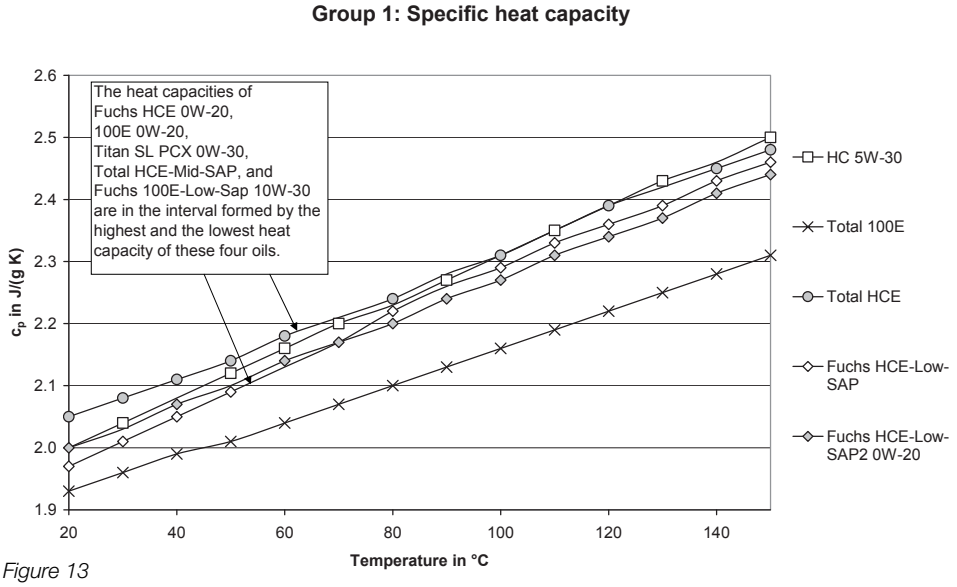

Figure 13
Results of the heat capacity measurements having been carried out with a power-compensated differential scanning calorimeter (10 oils of group 1).

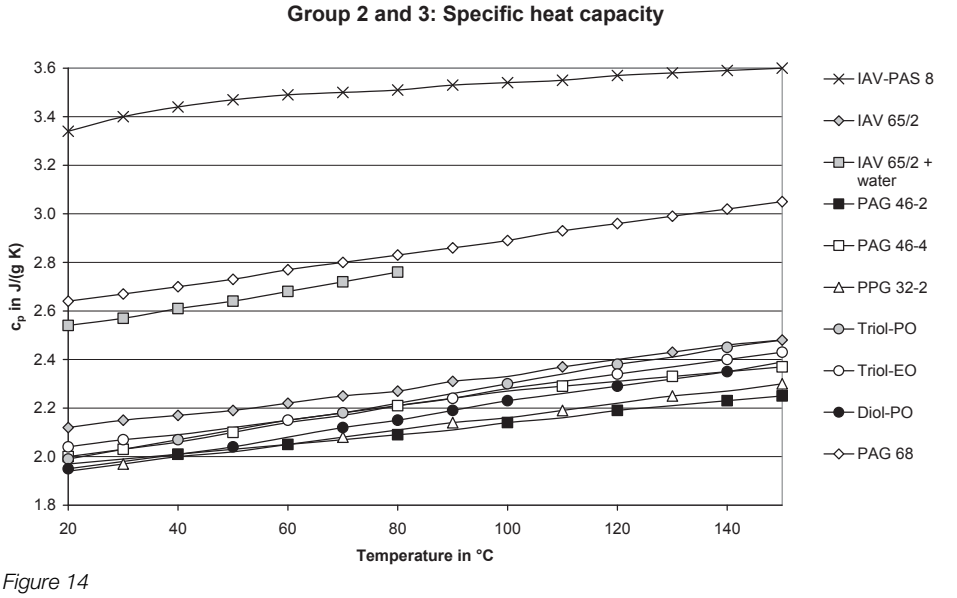

Figure 14
Results of heat capacity measurements for 10 oils of group 2 and group 3

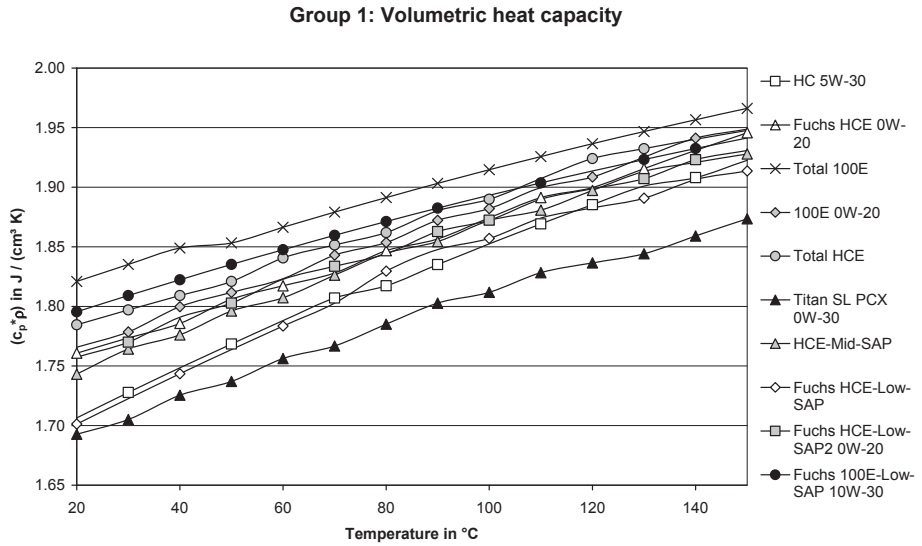

Figure 15
Volumetric heat capacity for 10 oils of group 1

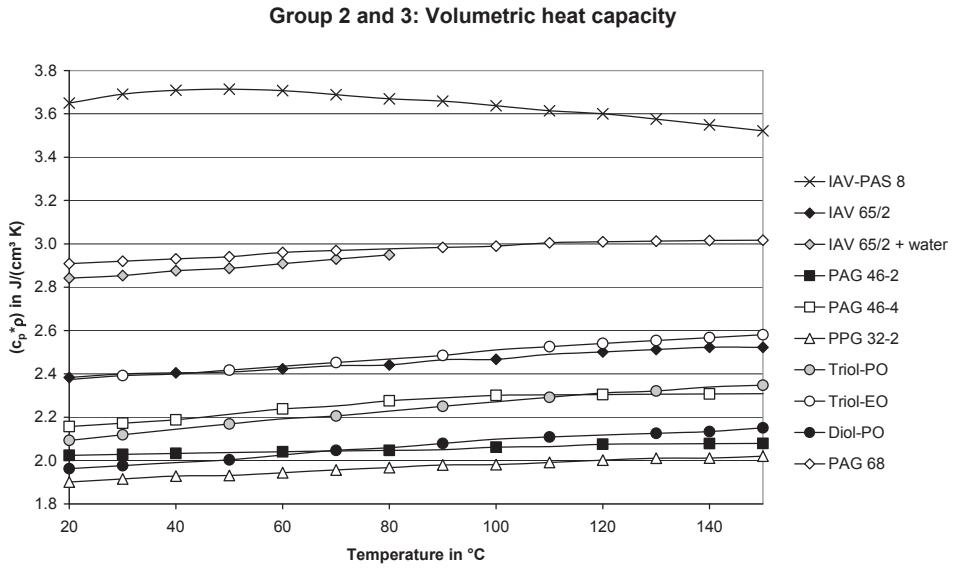

Figure 16
Volumetric heat capacity for 10 oils of the groups 2 and 3

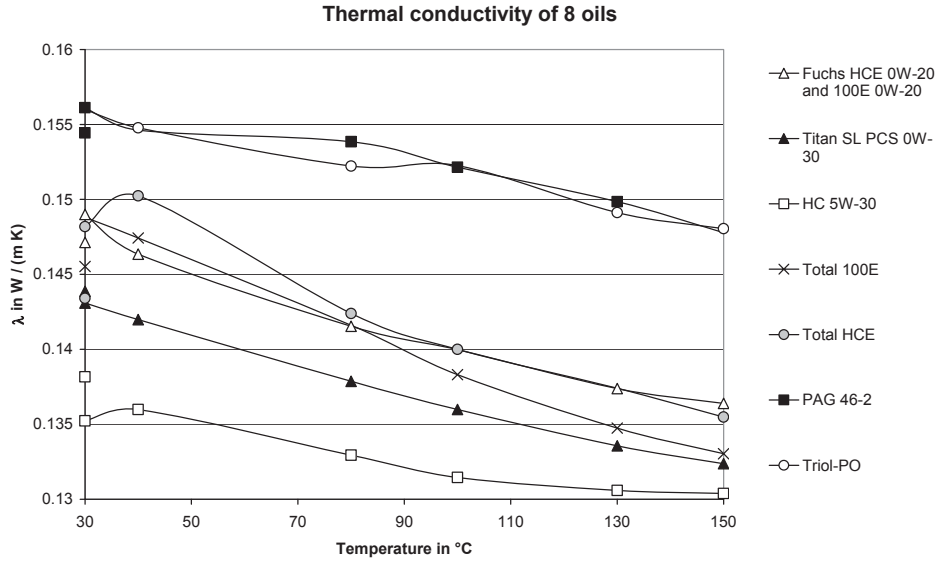

Figure 17
Thermal conductivity of 8 lubricants

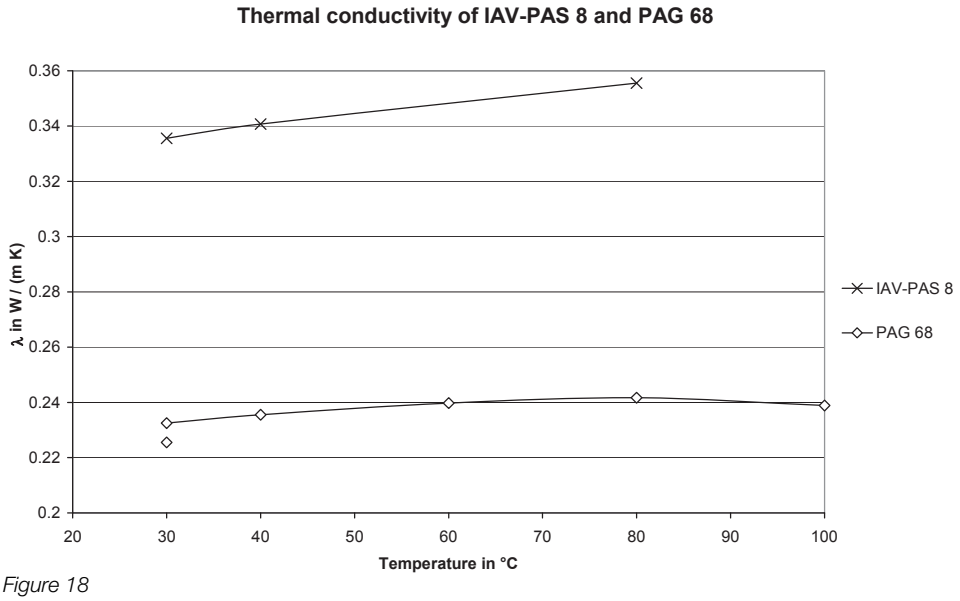

Figure 18
Thermal conductivity of IAV-PAS 8 (group 2) and PAG 68 (group 3)

The oils Total 100E, PAG 46-2 and PPG 32-2 compensate their low specific heat capacity with a comparatively high density, resulting in volumetric heat capacities that surpass that of the factory-fill oils significantly. The GT1, GTE and HCE oils, too, present a volumetric heat capacity that is slightly higher than that of the hydrocarbon-based factory-fill oils. Consequently, at the thermal management of the pistons, there should be no problems related to the tested esters and polyglycols. As oil films are sheared adiabatically, the loss in viscosity by heating is minimized by an increased oil heat capacity. Consequently, the thermal management of the pistons should be improved by the tested esters and hydrocarbons.

4.3 Thermal conductivity

The thermal conductivity affects the heat transfer at the liquid-solid interface of the oil film. The results of the measurements are given in *Figure 17* for eight oils and in *Figure 18* for two additional lubricants. These samples could be examined only at temperatures up to 80 °C or 100 °C because they approached their boiling point. The thermal conductivity of these two lubricants is by far higher than that of the other samples.

As shown in *Figure 17*, the thermal conductivities of these seven oils did not show any significant differences. It is therefore considered not to determine the final oil selection between hydrocarbons, esters and polyglycols. The relatively high conductivity of PAG 46-2 will enhance the transfer of heat generated during film shearing to the rubbing surfaces. Thus, the loss in viscosity due to the higher temperature will be minimal in comparison.

4.4 Viscosity at ambient pressure

The viscosity itself represents a key property for safe and durable operation, especially for the crankshaft bearings.

On the one hand, the OEMs require comparatively high values of the high-temperature high-shear (HTHS) viscosity at 150 °C. Depending on the operation cycle, at least 2.6 mPas are needed. In most cases, 2.9 to 3.0 mPas are required, in some others even more than 3.5 mPas.

On the other hand, low viscosities at low temperatures are advantageous for minimizing the fuel consumption in city driving and for short drives.

To respect these requirements, a low change in viscosity with temperature is required, which is equivalent to a high viscosity index (VI). A polymer-free formulation with a viscosity index of VI > 170 would represent a challenge to hydrocarbons in ISO VG 32-46.

4.4.1 Viscosity of the oils in group 1

Figure 19 presents the kinematic viscosities of the hydrocarbon- or ester-based oils of group 1 as a function of the temperature. The measurements have been carried out at ambient pressure using capillary viscometers of the Ubbelohde type or the rolling-ball viscometer. Hence, the diagram shows the viscosity at very low shear rates.

The oils show a very similar kinematic viscosity in the temperature range of interest, with two exceptions:

– HC5W-30+3.7 % soot shows a significantly higher viscosity in the whole temperature range. Only the rolling-ball viscometer could be used for this measurement because the soot would not pass through a capillary.

– 100E Aero has a viscosity which is significantly higher at 40 °C, but similar to the other oils at 150 °C. The viscosity is more temperature-dependent than that of the other oils.

Compared to fresh HC5W-30, the 3.7 wt.-% soot increased the viscosity and also the pressure-viscosity coefficient. From the hydrodynamic point of view, soot presented no disadvantages, but under mixed/boundary conditions the wear increased significantly (see chapter 6.12 and *Figure 46*), which affects the top dead region and/or the cams.

The average viscosity ν_{avg} of the remaining 11 oils of group 1 has been calculated for all of the seven measurement temperatures. In *Figure 20*, the relative deviation to this

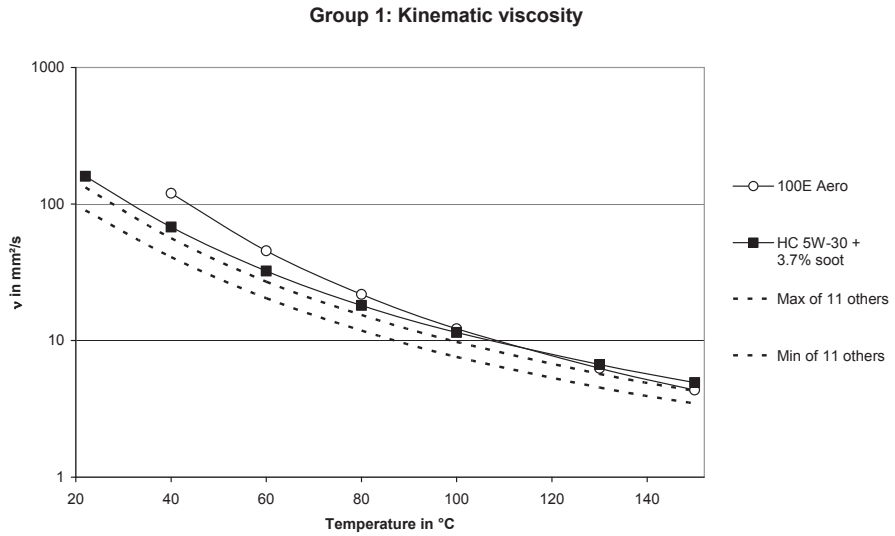

Figure 19
Kinematic viscosity of the oils in group 1 in a logarithmic scale

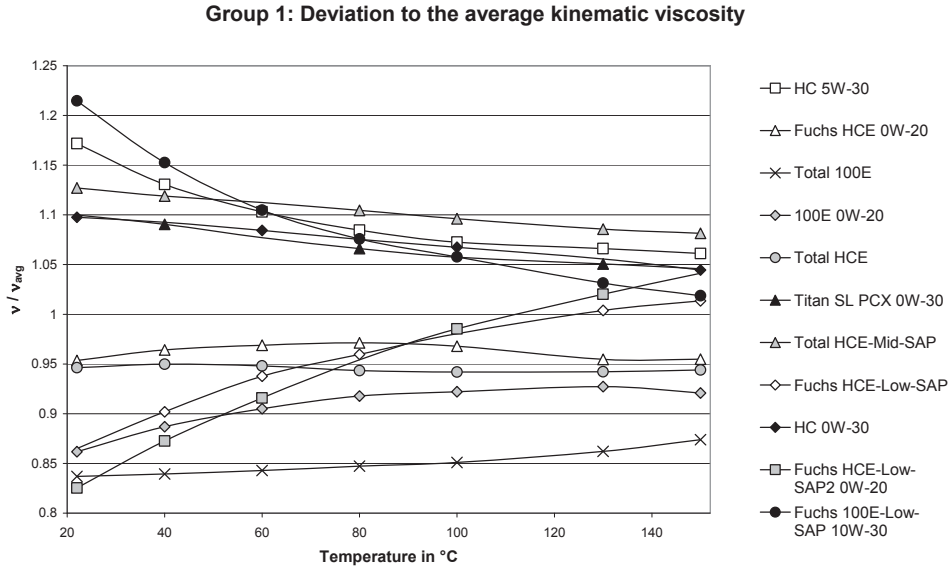

Figure 20
Deviation of the kinematic viscosity to the average value. For 100E Aero and HC 5W-30 + 3.7% soot, refer to Figure 23.

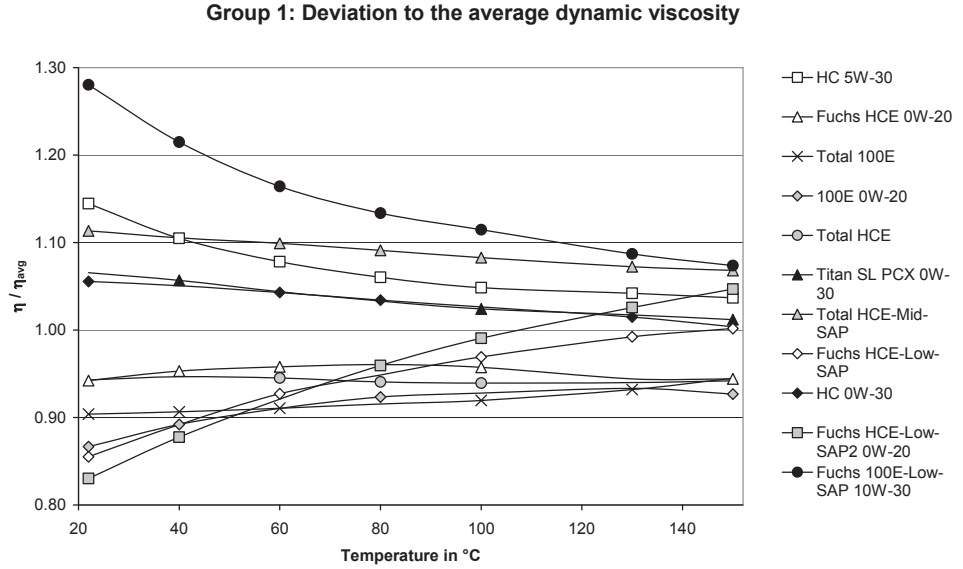

Figure 21
Deviation of the dynamic viscosity to the average value for 11 oils of group 1. For 100E Aero and HC 5W-30 + 3.7 % soot, refer to Figure 24.

average viscosity is plotted as a function of the temperature. Oils with $\delta(\nu/\nu_{avg})/\delta T > 0$ show a comparatively low change of viscosity with temperature, which is equivalent to a high viscosity index and advantageous for the use as a lubricant in an engine. A big positive deviation of ν/ν_{avg} is found for Fuchs HCE-Low-SAP2 0W-20 and Fuchs HCE-Low-SAP.

The relation of the dynamic viscosity η to the average dynamic viscosity of the 11 prementioned fluids η_{avg} is plotted in *Figure 21*. The lubricants with a comparatively high density show higher values η/η_{avg}, compared to ν/ν_{avg}. These fluids are mainly the ester-based lubricants Fuchs 100E-Low-SAP 10W-30 and Total 100E.

4.4.2 Viscosity of the oils in group 2

Figure 22 shows measurement data for the five lubricants which have to be tolerant to water. Three of the samples contain water and could not be examined at 130 °C and 150 °C. IAV 65-2 and IAV 65-3 both show a loss of viscosity if they are mixed with water. The relative loss of viscosity is roughly the same in the temperature range from 20 °C to 100 °C.

Figure 23 shows the relation ν/ν_{avg} for the five oils of group 2 as well as two oils of group 1. For ν_{avg}, the same values as in *Figure 20* have been used. The high viscosity index of the water-based lubricant IAV-PAS 8 (VI= 265!) is shown by the positive derivation of the corresponding curve, as well as the low viscosity index of 100E Aero by the negative derivation. The lubricants IAV 65-2, IAV 65-2 + water, IAV 65-3, IAV 65-3 + water and HC 5W-30 + 3.7% soot have a viscosity index similar to the average value of group 1.

The corresponding diagram for the dynamic viscosity *(Figure 24)* shows higher values η/η_{avg} for all lubricants with the exception of HC 5W-30 + 3.7% soot, which is due to the relatively high density of these fluids.

4.4.3 Viscosity of the oils in group 3

In group 3 (see *Figure 25*), the viscosity at 22 °C is between 17.1 mm²/s (PG WS 55) and 443 mm²/s (Triol-PO). Thus, the range is by far bigger than in the groups 1 and 2.

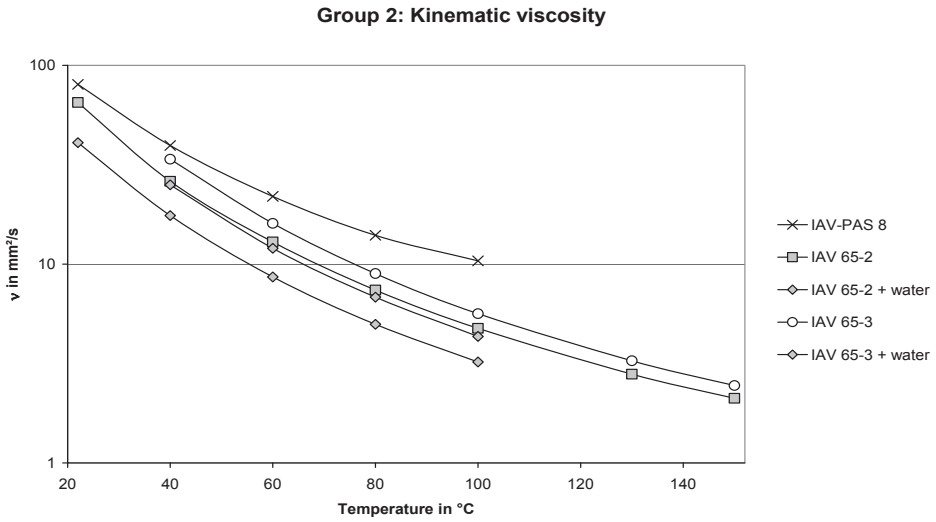

Figure 22
Kinematic viscosity of the lubricants for the Rankine power cycle

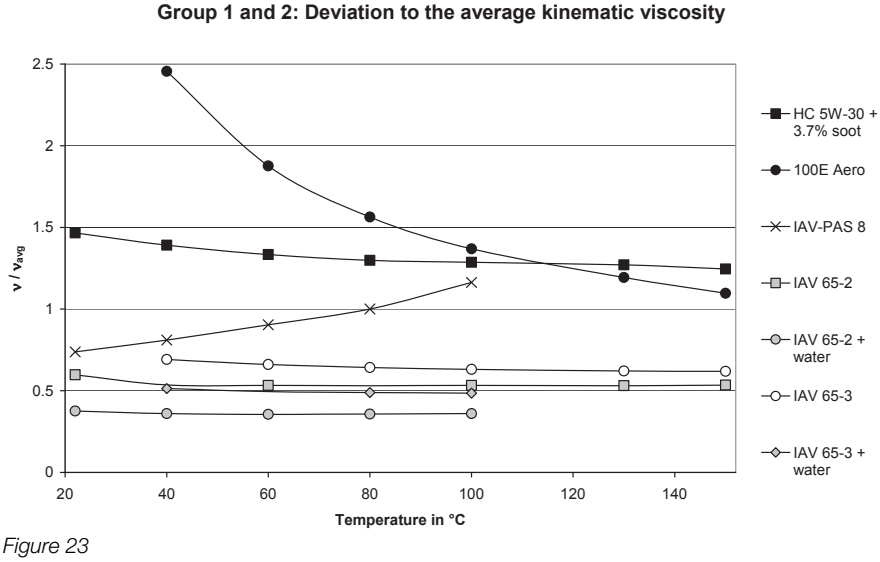

Figure 23
Deviation of the kinematic viscosity to the average value for the oils of group 2 as well as two oils of group 1.

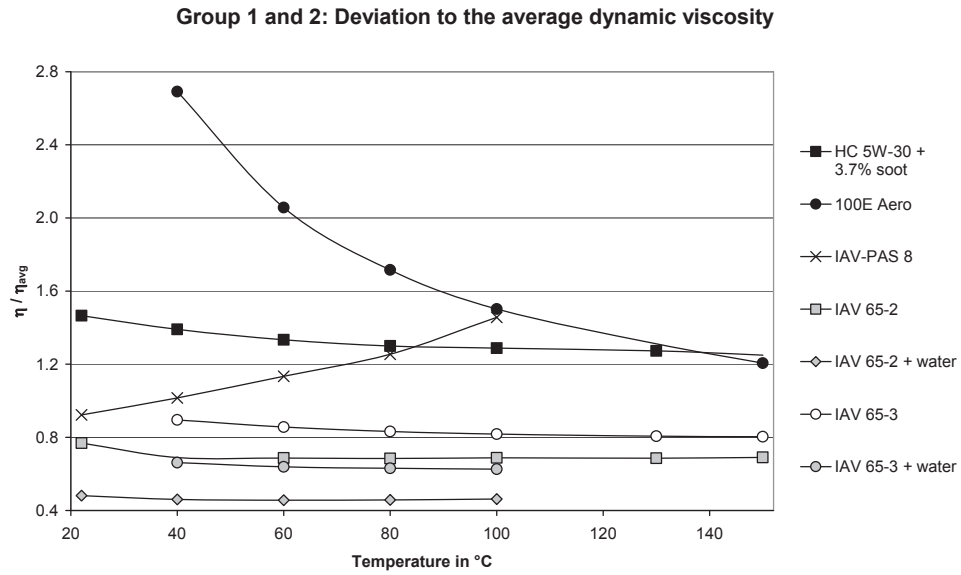

Figure 24
Deviation to the average dynamic viscosity for the oils of group 2, for 100E Aero, and HC 5W-30 + 3.7% soot (Group 1)

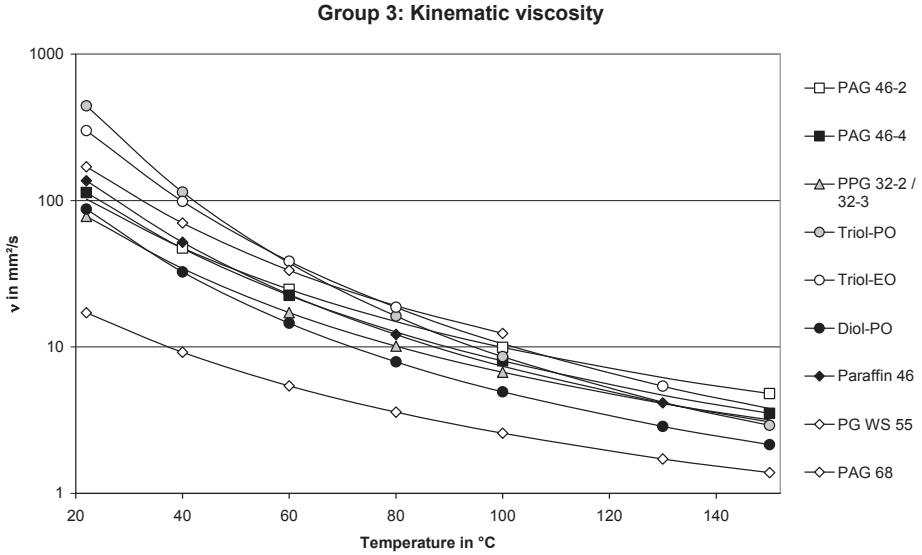

Figure 25
Kinematic viscosity of the lubricants in group 3

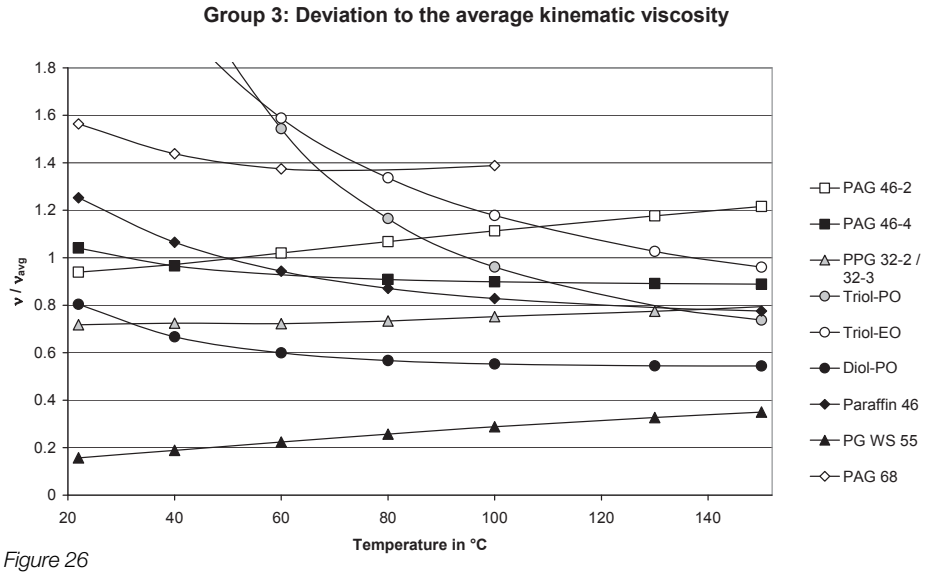

Figure 26
Deviation of the kinematic viscosity to the average value $\nu_{avg}(T)$

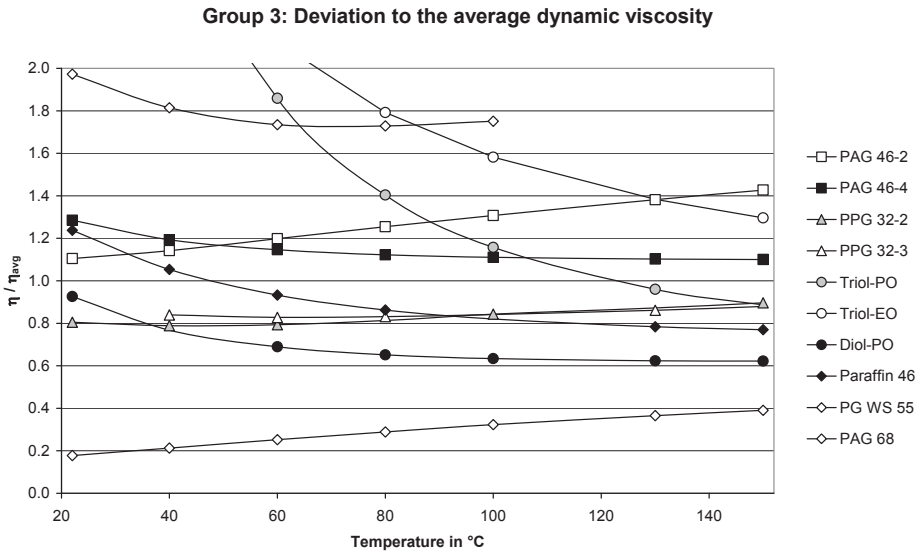

Figure 27
Deviation to the average dynamic viscosity to the average value $\eta_{avg}(T)$ for the oils of group 3.

Figure 26 shows that PAG 46-2, PAG 46-4, PPG 32-2, PPG 32-3 and Paraffin 46 have a kinematic viscosity $\nu(T)$ which is similar to the reference average of group1, while the other five oils show a deviation of more than 40 % to this average in at least a part of the temperature range.

As most oils in group 3 have a higher density than those of group 1, *Figure 27* shows for most oils higher values for η/η_{avg}, compared to the previously mentioned values for ν/ν_{avg}. An exception is Paraffin 46, which has a density similar to the oils determining the average.

4.4.4 The function $\eta(T)$

For the calculation of $\eta(T)$, which is needed to calculate the film thickness (see 4.6), the Vogel equation has been used:

$$\eta(T) = 1\,\mathrm{mPas} \cdot \exp\left(c \frac{T-a}{T-b} \right) \tag{3}$$

An equivalent form of this equation is given in Bauer [30]. The coefficients *a, b,* and *c* have been calculated based on the measurement results at seven different temperatures in the range from 22 °C to 150 °C.

4.5 High-Pressure-viscosity

The viscosity at high pressures up to 100 MPa and temperatures up to 150 °C has been measured using the rolling-ball viscometer that has already been described. The calculation of the pressure-viscosity-coefficient α is based on the measurement results.

4.5.1 Measurement program

The measurements are performed for most oils at three temperatures. These are 22 °C (or 40 °C), 80 °C (or 100 °C) and 150 °C. The viscosity has been measured for every temperature at ambient pressure, at 10 MPa, at 100 MPa and at least at two additional pressures between 10 MPa and 100 MPa (e.g. at 40 MPa and 70 MPa). Three lubricants (IAV-PAS 8, IAV 65-2 + water, IAV 65-3 + water) could not be examined at 150 °C, because their boiling point is below 150 °C.

4.5.2 Qualitative results

For all lubricants, the relative increase in viscosity with pressure is the highest at the minimum measurement temperature and the lowest at maximum temperature.

At 22 °C, the viscosity of many lubricants increases by a factor of typically 6 if the pressure increases by 100 MPa. At 150 °C, this factor is only about 3. These qualitative results are in accordance with measurements of other authors for other oils, for example those of Schmidt [31] and Blume [32]. Note that some of the measurement results presented in this publication are fairly different from this behavior, namely those for lubricants containing water.

4.5.3 Data analysis and presentation

The pressure-viscosity-coefficient α for a defined temperature T is a coefficient in the following equation:

$$\eta(p) = \eta_0 \cdot \exp(\alpha p) \tag{4}$$

where $\eta_0(T)$ is the dynamic viscosity at ambient pressure and at the temperature T and η is the dynamic viscosity at the same temperature and at the pressure p.

This equation can only be used as a rough estimation if a constant value for α is used. Therefore, the α-value for a defined temperature is given in dependence on the pressure. For high pressures, the calculation results in lower α-values. This means that the viscosity increases less than exponentially if the pressure is increased. The pressure-viscosity-coefficient α is calculated using the formula

$$\alpha(p,T) = \frac{1}{p} \ln\left(\frac{\eta(p,T)}{\eta_0(T)} \right) \tag{5}$$

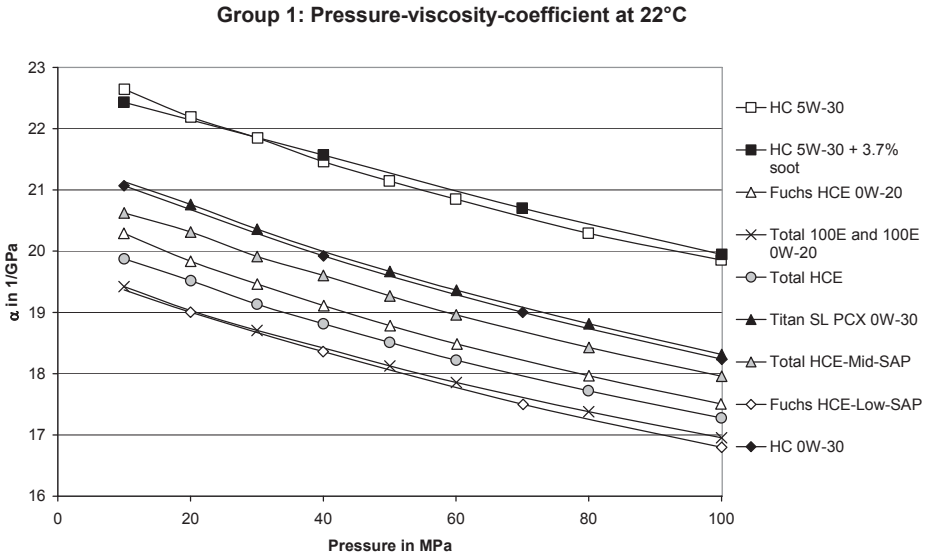

Figure 28
Pressure-viscosity-coefficient α(p) for ten oils of group 1 at 22 °C

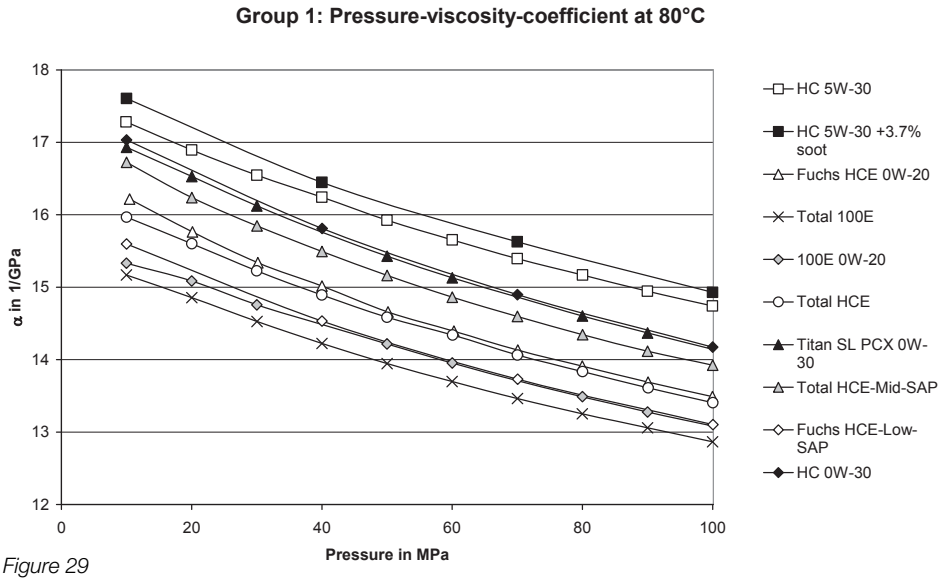

Figure 29
Pressure-viscosity-coefficient α(p) for ten oils of group 1 at 80 °C

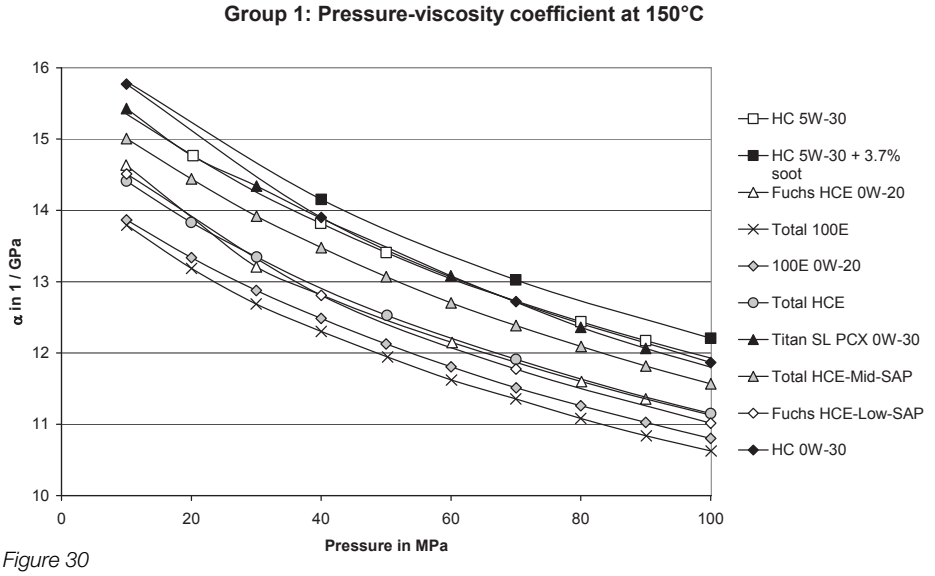

Figure 30
Pressure-viscosity-coefficient α(p) for ten oils of group 1 at 150 °C

4.5.4 Shape of the function α(p)

First, for three measurement temperatures (22 °C, 80 °C and 150 °C), the values for α(p) for ten oils of group 1 are presented (see *Figure 28*, *Figure 29*, and *Figure 30*). This is done to show the qualitative shape of the curves α(p), which is typical for all oils which have been examined in this measurement program. As discussed later, the function α(T) for $p = p_{max} = 100$ MPa is by far more important for tribological calculations. Therefore, the function α(p) is not presented for the remaining oils of group 1, which have been measured at other temperatures, and for the oils of group 2 and group 3.

The diagrams show that the hydrocarbon-based oils HC 5W-30, HC 5W-30 + 3.7 % soot, HC 0W-30 and Titan SL PCX 0W-30 have high pressure-viscosity coefficients. But among the 18 oils which are not represented in the diagram, five have values of the same range.

Additionally, it can be seen that the pressure-viscosity-coefficient of HC 5W-30 is slightly increased by soot in the oil, especially at high temperatures.

4.5.5 The function α(T)

The calculation of film thicknesses requires a function α(T) for $p = p_{max}$ = constant. The pressure-viscosity coefficient α has been measured at only three temperatures (22 °C, 80 °C, and 150 °C or 40 °C, 100 °C and 150 °C). For all lubricants, α decreases, if the temperature increases. Based on these measurement results, it is possible to calculate for every lubricant three coefficients A, B, and C to achieve

$$\alpha(T) = AT^2 + BT + C \qquad (6)$$

where T is the temperature in °C. An analysis of the resulting parabolas α(T) shows that for all fluids, the parameter A is positive. Thus, the parabola has a minimum which is found at temperatures between 140 °C (IAV 65-2) and 176 °C (100E 0W-20). A minimum of the parabola at T<150 °C results in $\delta\alpha/\delta T>0$ at T ≈150 °C, which is physically wrong.

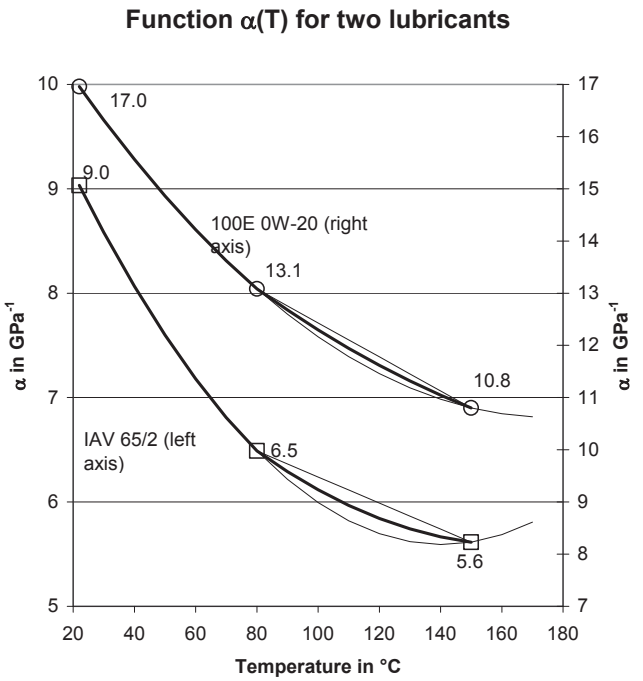

Figure 31
Measured α-values and possible functions α(T) for two of the tested lubricants. Between 80 °C and 150 °C, the average of the parabolic and the linear fit was used as a function α(T). At temperatures below 80 °C, the parabolic fit is used.

If the minimum is only slightly above 150 °C, the value of $\delta\alpha/\delta T$ has the correct sign, but it is unrealisticly small. These problems have been avoided by using the average of the parabolic fit and a linear fit in the temperature range of 80 °C<T<150 °C (see *Figure 31*). Between 22 °C and 80 °C, the parabolic fit didn't cause any problems.

The pressure-viscosity coefficient of IAV-PAS 8, IAV 65-2 + water, IAV 65-3 + water and PAG 68 has been measured only at temperatures up to 100 °C because the boiling point of these water-containing lubricants is below 130 °C. If measurements have been carried out only at two temperatures, a linear fit was used for calculating α(T).

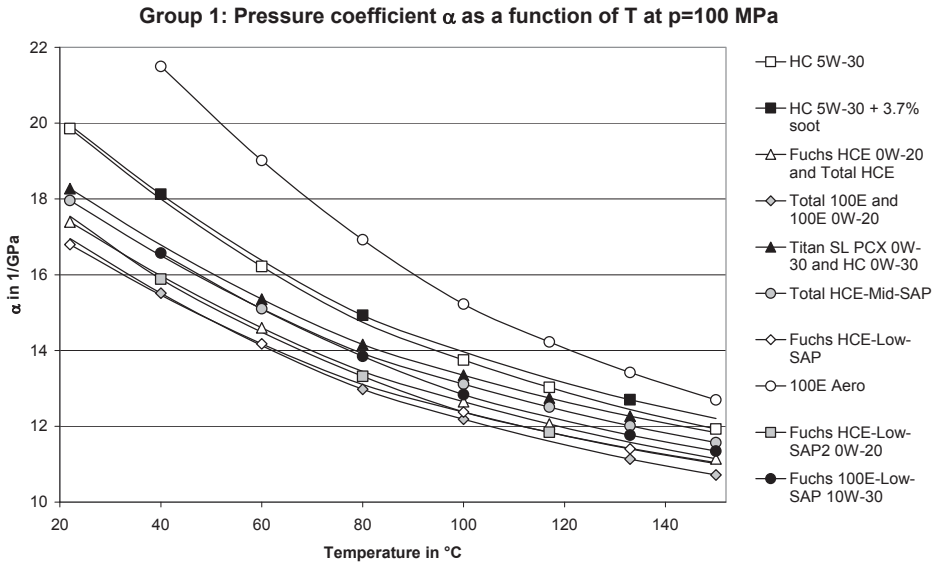

Figure 32
α(T) for p=100 MPa and group 1

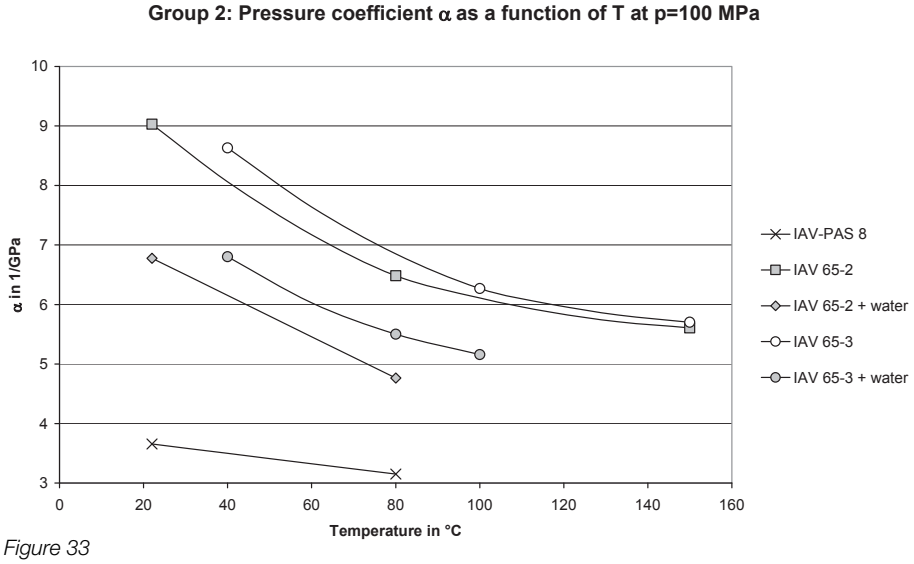

Figure 33
α(T) for p=100 MPa and group 2

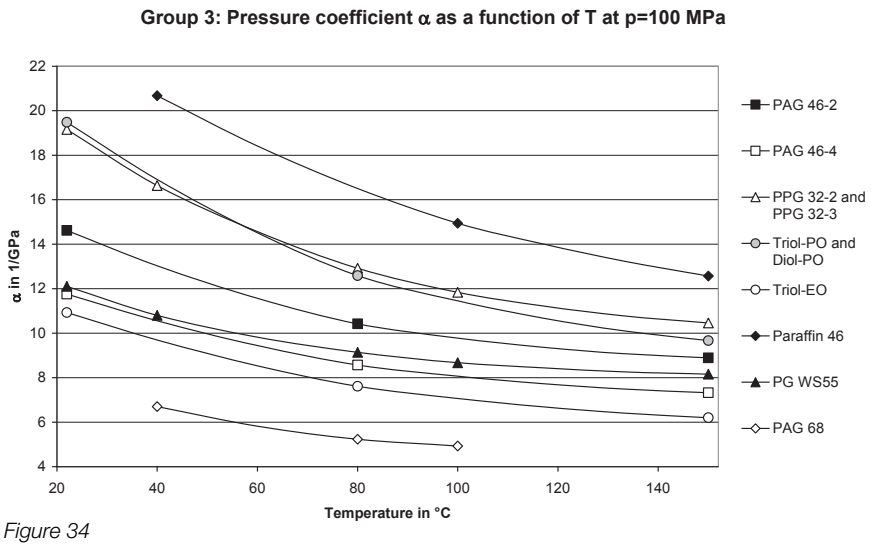

Figure 34
α(T) for p=100 MPa and group 3

4.5.6 Results for α(T)

The functions α(T) are presented in *Figure 32*, *Figure 33*, and *Figure 34*.

The oils of group 1, based on hydrocarbons and/or esters, have all very high and very similar pressure-viscosity coefficients. Therefore, additional points had to be drawn into *Figure 32* so that the curves can be distinguished.

The water-tolerant lubricants of group 2 have by far lower α-values, especially if they are really mixed with water. IAV-PAS 8 consists to nearly one half of water and has the lowest pressure-viscosity-coefficient that occurred in the test program.

In group 3, a wide variety of α-values can be seen. Paraffin 46 (which is a hydrocarbon (aliphatic), too) has, after 100E Aero, the second highest pressure-viscosity coefficient of all oils tested. The polypropylene glycols show a behavior similar to most oils of group 1, while the polyalkylene glycols have quite low pressure-viscosity coefficients. This is especially true for PAG 68, a water-containing oil for hydraulics, which has α-values only slightly higher than those of IAV-PAS 8.

4.6 Film-forming behavior

The engine oil specifications of standardization bodies and OEMs refer to the kinematic viscosities in mm²/s and the **h**igh-**t**emperature-**h**igh **s**hear viscosity (HTHS in mPas). The latter can be determined using the ASTM D4741 (rotating tapered-plug viscometer) and ASTM D4683 (tapered bearing simulator-viscometer).

The kinematic viscosity and the HTHS are considered by OEMs to be key properties for safe and durable operation, especially for the crankshaft bearings, as two main tasks for engine lubricants are energy saving (friction) and wear prevention. The hydrodynamic design of engine components is actually based only onto the kinematic viscosity and HTHS. This might be no problem, if only hydrocarbon-based formulations are considered, because there exists a practical background for correlation.

In order to differentiate hydrodynamic film forming behavior of alternative oils (hydrocarbons, esters and polyglycols), the dynamic viscosity taking into account the differences in density and the pressure-viscosity-coefficients "α" have to be used, because the equations for film forming behavior of fluids contain these two parameters.

The pressure-viscosity coefficient is up to now not mentioned in engine oil specifications, but it has a strong influence on the film thickness and in consequence also on the frictional losses associated to the film shearing. It was recently shown that the fuel efficiency [33, 34, 35] of an engine is correlated with the pressure-viscosity coefficient. Further correlations exist with the high-temperature-high-shear (HTHS) viscosity (a second viscometric property of the lubricant) and with the coefficient of friction under mixed/boundary lubrication.

4.6.1 Equations describing minimum film thickness

Tribological problems are considered to be elastohydrodynamic if the deformation of the solid bodies in the contact region is not negligible compared to the film thickness. Two of the three critical tribosystems have full EHD lubrication: the cam/follower system and the crank shaft. The piston ring/cylinder system has a mixed lubrication which is not the object of this paper, but at surface asperities, the contact can be elastohydrodynamic, too.

A detailed discussion of EHD contacts yields different equations for the film thickness, depending on the geometrical situation: The contact region might be

- a line, if a cylinder contacts a planar surface or if two parallel cylinders contact each other
- a rectangle if the height of at least one of the cylinders is small
- an ellipse if an elliptic body contacts a plane, a sphere or another elliptic body
- a point, if a sphere contacts a planar surface or another sphere.

The point contact is a special case of the elliptic contact. The individual increase of contact area as function of load or oil film pressure conducts to different exponents in the equations (13) to (15).

4.6.2 Parameters

Jacobson [36] and Jones [37] outlined a numerical method that allows the calculation of the fluid dynamics in a Hertzian contact, taking into account the shape and elasticity of the solids as well as their speed and the load on them. Further, three properties of the lubricant are used in the calculation: the viscosity, the compressibility and the increase of its viscosity due to the pressure.

To shorten the notation, two abbreviations are introduced:

The equivalent radius of curvature r for a line contact of two parallel cylinders A and B or a point contact of two spheres A and B which have the radii of curvature r_A and r_B is defined by the following equation:

$$\frac{1}{r} = \frac{1}{r_A} + \frac{1}{r_B} \tag{7}$$

Replacing cylinder or sphere B by a plane ($r_B \to \infty$) yields $r = r_A$.

In a similar way, the equivalent elasticity modulus E‘ is calculated using

$$\frac{1}{E'} = \frac{1}{2}\left[\frac{\left(1-\mu_A^2\right)}{E_A} + \frac{\left(1-\mu_B^2\right)}{E_B}\right] \tag{8}$$

where E is the elasticity modulus and μ is the Poisson ratio.

The equations for the film thickness depend on three non-dimensional groups of parameters:

1.) The materials parameter G:

$$G = \alpha E' \tag{9}$$

where α is the pressure-viscosity coefficient of the lubricant.

2.) The speed parameter U_e:

$$U_e = \frac{\eta_0 u}{rE'} \tag{10}$$

where η_0 is the dynamic viscosity at ambient pressure and operating temperature, while u is the entraining velocity:

$$u = \frac{1}{2}\left(u_A + u_B\right) \tag{11}$$

3.) The load parameter W_e‘ (for a line contact) or W_e (for a point or elliptical contact)

$$W_e' = \frac{F'}{E'r} \qquad \text{and} \quad W_e = \frac{F}{E'r^2} \tag{12}$$

where F‘ is the force per unit length, while F is the total force on the contact.

Equations

A repeated simulation of the minimum film thickness with varied dimensionless parameters G, U_e and W_e‘ results in data for the minimum film thickness which can be correlated by the following equations:

Line contact [37, 38]:

$$\frac{h_{\min}}{r} = 2{,}65\,\frac{U_e^{0.70} G^{0.54}}{W_e'^{0.13}} \tag{13}$$

Rectangular contact [36]:

$$\frac{h_{\min}}{r} = 3{,}07\,\frac{U_e^{0.71} G^{0.57}}{W_e'^{0.11}} \tag{14}$$

Elliptical contact [37]:

$$\frac{h_{\min}}{r} = P^* \frac{U_e^{0.68} G^{0.49}}{W_e^{0.073}} \quad (15)$$

P* is the following parameter:

$$P^* = 3.68 \cdot \left[1 - \exp\left(-0.67 \left(\frac{r_s}{r} \right)^{2/3} \right) \right] \quad (16)$$

where r is the radius parallel to the fluid entrainment, while r_s is the radius normal to this direction. For a point contact, r_s = r yields P*= 1.797, while r_s= 20·r yields P*= 3.65.

4.6.3 Influence of lubricant properties

The pressure-viscosity coefficient is up to now not mentioned in engine oil specifications, but it has a strong influence on the film thickness and in consequence also on the frictional losses associated to the film shearing.

Two of the previously mentioned parameters are influenced by fluid properties:

G is proportional to the pressure-viscosity-coefficient α of the lubricant

U is proportional to the viscosity at ambient pressure η_0.

The other elements in the definitions of G, U_e and W_e (or W_e') depend on the geometry, the solid material properties, the speed of the moving surfaces and the load on them. For a comparison of different lubricants which shall be used in the same engine, they can be treated as constants. This yields to three equations of the form

$$h_{\min} = C_{Tr} \eta^j \alpha^k \quad (17)$$

where C_{Tr} is a constant of the tribosystem. As shown in equations (13) to (15), different exponents j and k are used for different contact situations:

Table 5
Exponents j and k for different contact situations

Contact situation	Exponent *j*	Exponent *k*
Line	0.70	0.54
Rectangle	0.71	0.57
Ellipse or point	0.68	0.49

The exponents are quite similar in the equations that have been derived for different contact situations. The discussion shows that a comparison of several oils requires data for the dynamic viscosity and for the pressure-viscosity-coefficient at high temperatures (e.g. 150 °C). Both η and α are temperature-dependent and have a negative temperature coefficient. Thus, the film thickness h_{min} decreases if the temperature increases. Functions η(T) and α(T) which are based on measurement results have been discussed in 4.4.4 and 4.5.5, respectively.

4.7 Relative film thicknesses

The comparison is based on the fact that HC 5W-30 which is widely used as factory fill oil in passenger cars of a European car manufacturer obviously limits the wear of the engine elements in a satisfactory way at temperatures of up to 150 °C. Therefore, HC 5W-30 at 150 °C is used as reference oil. The reference film height h_{ref} in an engine tribosystem with a constant C_{Tr} is

$$h_{ref} = C_{Tr} \eta_{ref}^{\ j} \alpha_{ref}^{\ k} \quad (18)$$

where α_{ref} and η_{ref} are α and η of HC 5W-30 at 150 °C.

The relative film thickness h* for any lubricant at any temperature T is defined by

$$h^*(T) = \frac{h_{\min}(T)}{h_{ref}} = \frac{C_{Tr} \eta(T)^j \alpha(T)^k}{C_{Tr} \eta_{ref}^{\ j} \alpha_{ref}^{\ k}} = \left(\frac{\eta(T)}{\eta_{ref}} \right)^j \left(\frac{\alpha(T)}{\alpha_{ref}} \right)^k \quad (19)$$

and can be calculated without knowledge of the constant C_{Tr}, which depends on the properties of the tribosystem. The contact situation must be known to calculate h*, because there are different exponents j and k for different situations.

For a line contact, j = 0.70 and k = 0.54:

$$h_{\min} \propto \eta^{0.70} \alpha^{0.54} \quad (20)$$

For all tested fluids, the relative film thicknesses have been calculated in dependence of the temperature. In *Figures 35* to *37*, the results are plotted for low temperatures of maximal 100 °C.

At 22 °C, most fluids have relative film thicknesses between 10 and 16. The higher values for 100E Aero, HC 5W-30 + 3.7% soot, EO-Triol, and PO-Triol are due to a high viscosity at low temperatures, while the low values of film thickness for all oils of group 2 as well as for PAG 68 are mainly caused by their low pressure-viscosity coefficient α.

At any oil temperature, only a relative film thickness of h* ≈1 is needed. This supports the strategy to use engine oils with a high intrinsic viscosity index in order to reduce the fuel consumption especially during cold engine operation.

The relative film thicknesses at high temperatures are plotted in *Figure 38*, *Figure 39*, and *Figure 40*. Three lubricants show relative film thicknesses h*(150 °C)>1:

– 100E Aero, mainly because of its high pressure-viscosity coefficient,

– HC 5W-30 + 3.7 wt.-% soot, an oil with a similar α-value but a higher viscosity, compared to HC 5W-30

and

– PAG 46-2, an oil with a low pressure-viscosity coefficient and a high dynamic viscosity at 150 °C (4.45 mPas, HTHS = 4.3 mPas).

For the other oils, h*(150 °C) < 1. For these oils, a critical temperature T* is defined by h*(T*) = 1. The use of these lubricants with the same tribologic safety that is provided by HC 5W-30

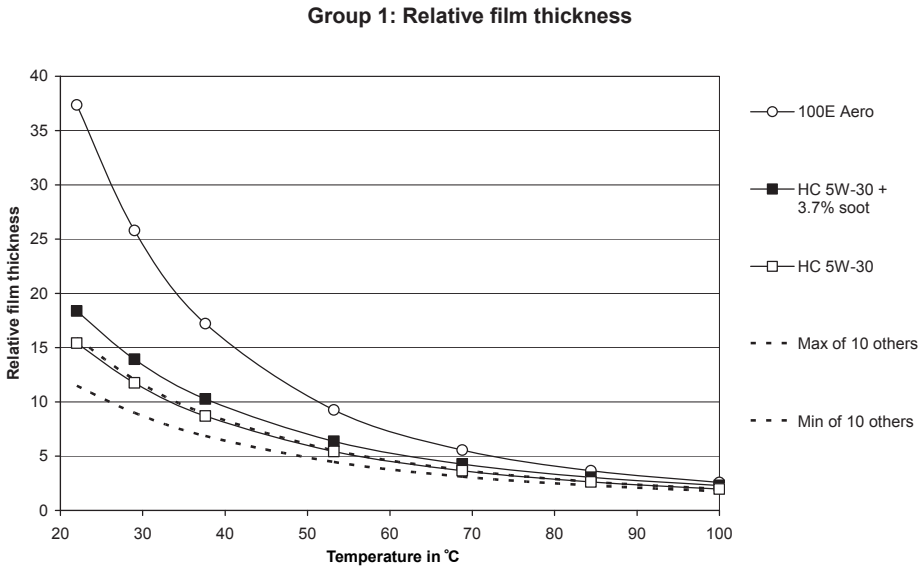

Figure 35
Relative film thickness of the oils in group 1 at low temperatures

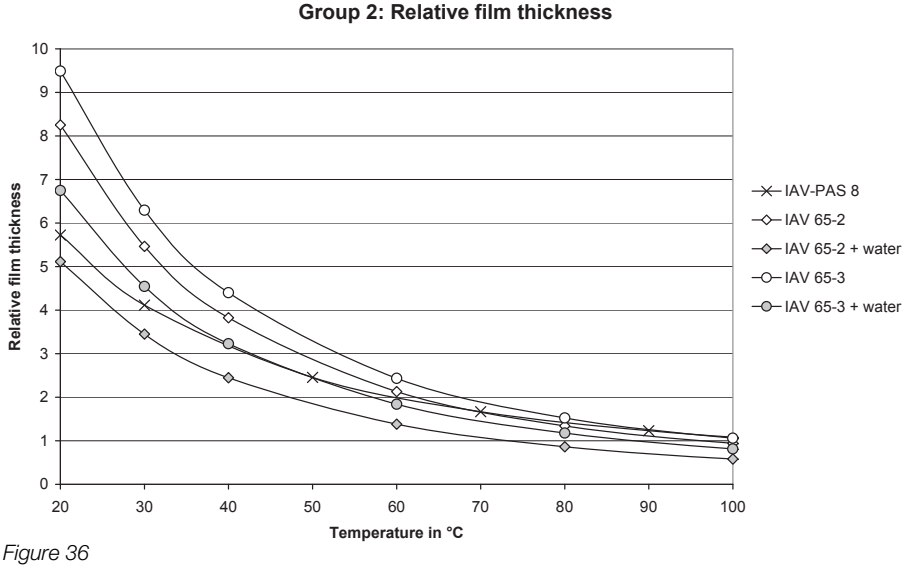

Figure 36
Relative film thickness of the oils in group 2 at low temperatures

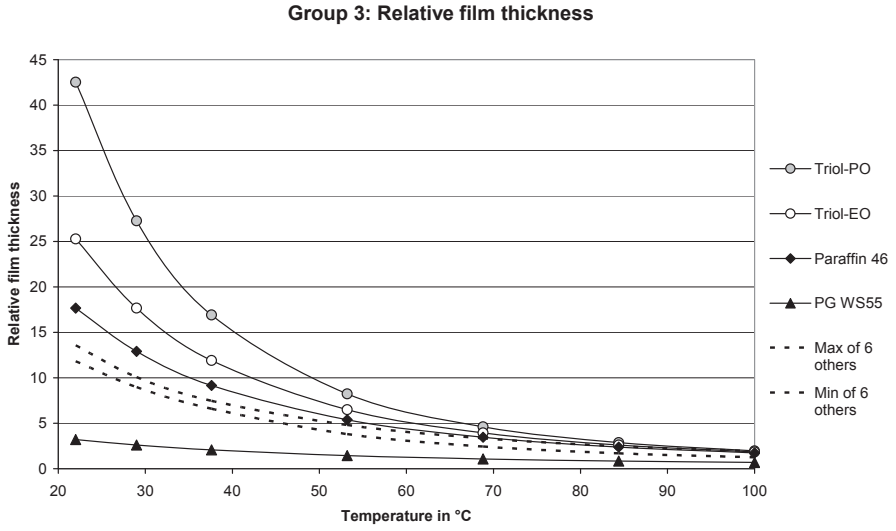

Figure 37
Relative film thickness of the oils in group 3 at low temperatures

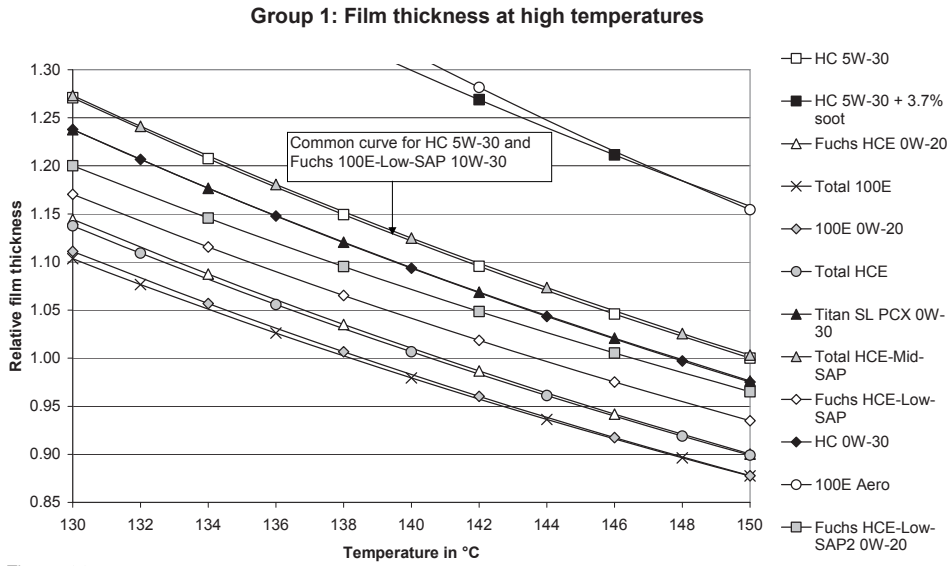

Figure 38
Relative film thickness of the oils in group 1 at high temperatures

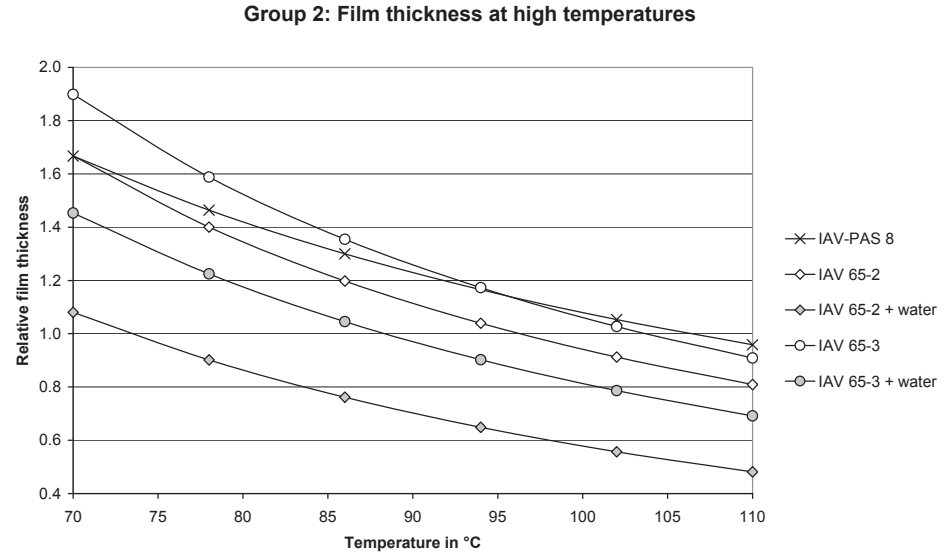

Figure 39
Relative film thickness of the oils in group 2 at high temperatures

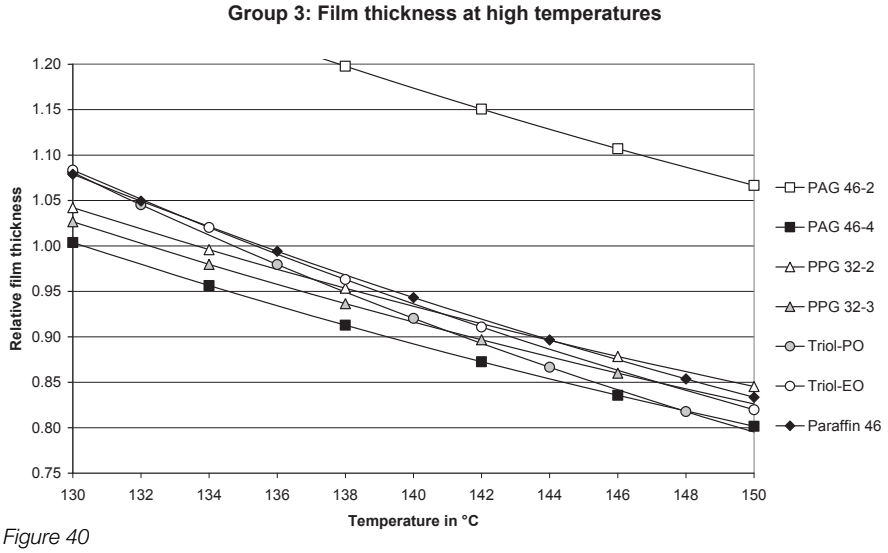

Figure 40
Relative film thickness of the oils in group 3 at high temperatures

requires a limitation of oil sump temperature to T^*, which can be achieved by an enlargement of the cooling system, high oil fill volume or by a reduction of the maximal power in case of a high engine temperature. But to avoid misunderstandings, three things should be pointed out:

– The oil Titan SL PCX 0W-30 with T^*=148 °C is actually used without problems in a lot of car engines, just like the reference oil HC 5W-30. This proves that a relative film height h* slightly below 1 is not dangerous for the engines which are actually in use.

– Low film thicknesses are equivalent to a lower power loss by friction, which is mainly important if the engine is used at a low temperature. Thus, lubricants with $h^*<1$ can contribute to decrease the fuel consumption of the engine if they show relatively low film thicknesses in the whole temperature range and if the lowest h^*-values which occur in operation are not dangerous for the engine.

– For engines which will be manufactured in future, it is possible to reduce the required minimum film height of the lubricant by lowering the surface roughness as well as the clearance of the bearings. In this way, the potential to reduce the fuel consumption can be used.

5 Viscosity measurement at high shear rates up to 3,4 · 10^6 s^{-1}

The determination of the HTHS viscosity using a capillary viscometer is standardized in ASTM D4624 for capillaries made of glass or stainless steel. The experience shows that the rotational method (D4741, D4683) has a better repeatability and reproducibility, compared to the capillary method. However, it is by far easier to extend the measuring range to high shear rates using the capillary method.

The heating of the oil passing through the PTB capillary viscometer under very high shear rates is limited to 2-3 K. This is one of the main causes for the comparatively small uncertainty.

The instruments described in ASTM D4624, ASTM D4741 and ASTM D4683 allow viscosity measurements at shear rates up to 1 · 10^6 s^{-1} provided the instruments are calibrated using special reference oils. The viscosity of these reference oils is certified at high shear rates of up to about 1 · 10^6 s^{-1}. It is important that there is no need to calibrate the PTB capillary viscometer using a reference oil certified at high shear rates.

5.1 Description of the apparatus

The high-shear viscometer HVA 6, manufactured by *Anton Paar* (www.anton-paar.com), Austria, was used at PTB to determine the Newtonian range of numerous viscosity reference liquids [39]. The working principle is as follows: The liquid under test is pressurized by nitrogen from a cylinder by means of a pressure regulator and a specially formed membrane made of viton for the separation of nitrogen and liquid. When the ball valve is opened, the liquid is driven through the capillary and a parabolic distribution of velocity develops. Behind the capillary, the volume flow of the liquid is measured using a precision glass tube of wide diameter in conjunction with two optical sensors and an interface for the separation of the liquid under test and the liquid used in the precision glass tube. According to the standard [40], the shear stress at the wall of the capillary is

$$\tau = \frac{R \cdot \Delta p}{2 \cdot L} \quad , \tag{21}$$

with R being the inner radius of the capillary, Δp the differential pressure along the capillary, and L the length of the capillary. In the case of a Newtonian liquid, the shear rate at the wall is

$$D = \frac{4 \cdot Q}{\pi \cdot R^3} \quad . \tag{22}$$

Q is the volume flow rate. The dynamic viscosity is

$$\eta = \frac{\tau}{D} \quad . \tag{23}$$

The instrument is designed for a maximum shear rate of 1·10^6 s^{-1}, which can be achieved with a capillary of 100 mm in length, 0.15 mm in diameter and a differential pressure of 12 MPa for a typical engine oil.

This instrument had to be modified in order to meet the following requirements:

measuring temperature: up to 150 °C

measuring shear rate: up to 3·10^6 s^{-1}

From equation 22 it can be seen that at a constant flow rate smaller diameters result in higher values of D. An increase of pressure to keep Q constant is not possible due to safety reasons. Therefore, a shorter capillary with 25 mm in length and 0.1 mm in diameter is used. The small bore is advantageous to reduce the flow rate (during one measurement series, a total volume of only about 300 cm^3 of test fluid is available) as well as the Reynolds number [41]

$$\mathrm{Re} = \frac{2 \cdot Q \cdot \rho}{\pi \cdot \eta \cdot R} \quad . \tag{24}$$

ρ is the density of the liquid. The radius of the capillary is determined from measurements with a viscometric reference liquid at low shear rates:

$$R = \sqrt[4]{\frac{8 \cdot \eta \cdot Q \cdot L}{\pi \cdot \Delta p}} \tag{25}$$

The maximum value Re =1256 occurred in the measurement series on 100 E 0W-20. This is in accordance with [41] or D 4624, where Re < 2000 is stated. The resulting volume flow rate at pressures of the order of 0.1 MPa is too small to detect the flow rate using the optical system. It is not designed for a slowly moving meniscus. For that reason, and

due to problems with decoupling the flow rate measuring device from that part of the apparatus, that has to be kept at a temperature of 150 °C, the mass flow is measured instead of the volume flow. A stainless steel tube was installed at the outlet of the capillary with 425 mm in length and an inner diameter of 1.5 mm, allowing the fluid to flow into a glass cup situated on a 200g-balance. The mass flow measurement is carried out as follows: Until stable temperatures are reached, the flow is directed into an additional cup. The reading of the balance is taken. With the start of the measurement, the flow is directed into the cup on the balance. At the end, the flow is switched to the additional cup and the second reading of the balance is taken. The time is taken by means of an electronic stopwatch. The buoyancy correction is used. Using the density, the volume flow is obtained from the mass flow. It is advantageous to have a considerably larger measuring range and no problems with thermostatisation. The small pressure loss in the stainless steel tubing is indeed very small, but it is taken into account in the analysis.

Three calibrated 100 Ω platinum resistance thermometers are installed to measure the temperature of the vessel containing the liquid and in the volumes at the inlet and the outlet of the capillary. At 150 °C, the ambient temperature seriously influenced the thermometer readings. The thermal insulation of just the thermometer bearings was not sufficient. For that reason, an air thermostat with a fan, an electric heater and a pid-controller was installed on the top plate of the HVA-instrument. The vessel containing the liquid is thermostated using a circulating thermostat, and the capillary is – in contrast to the original design – directly thermostated using the air thermostat.

Smart piezo-resistive pressure transducers with the ranges 1.6 MPa and 16 MPa and a relative measurement uncertainty of 0.05 % of the maximum value are installed outside the air thermostat. A needle valve is installed in the tubing to the pressure transducer in order to allow a changing of the transducers during one measurement series. This tubing is connected to the vessel containing the liquid at the top. Although the oil under test was heated up to 150 °C before the measurement in order to degas it, gas bubbles sometimes occur and can be allowed to escape through the needle valve (with the pressure transducers removed) before starting the experiment. The hydrostatic head $\rho \cdot g \cdot h$, with g being the acceleration of free fall and h the difference in the height between the pressure transducer and the capillary, is taken into account and is important at small pressures.

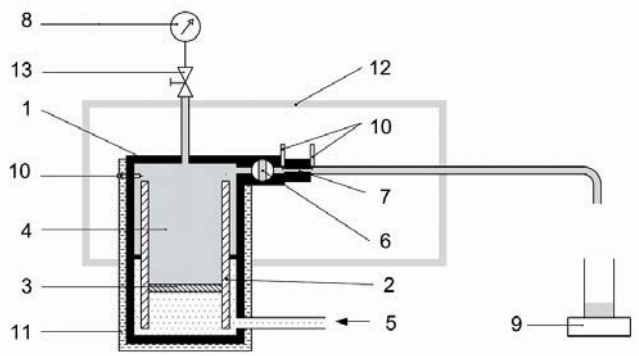

Figure 41
Schematic diagram of the modified HVA 6 viscometer: 1: pressure vessel, 2: cylinder for gas-liquid separation, 3: piston with O-ring seal, 4: liquid under test, 5: driving nitrogen, 6: ball valve, 7: capillary, 8: pressure transducer, 9: balance with cup, 10: 100 Ω platinum resistance thermometers, 11: thermostated oil, 12: heat-insulated box of the air-thermostat.

At a temperature of 150 °C and elevated pressures, considerable diffusion of nitrogen occurred through the Viton membrane which was intended for the gas-liquid separation. A two-phase mixture came out of the capillary which did not allow any reproducible measurements. Changing the material of the membrane did not turn out to be successful. The problem was solved by replacing the membrane by a piston-cylinder assembly made of stainless steel. The gap between the piston and the cylinder is only about 0.1 mm and an O-ring seal (Viton) was used. During the experiment (which took several hours), no more gas bubbles were observed leaving the capillary. *Figure 41* is a schematic diagram of the modified HVA 6 viscometer.

The most important correction at high shear rates is the Bagley-correction. It is determined according to the standard [41] with the aid of a reference liquid on hydrocarbon basis. Three capillaries, 10 mm, 25 mm and 40 mm in length, all with the same inner diameter of 0.1 mm, were used to measure the volume flow rate as a function of the driving differential pressure along the capillary. The result is approximated by the fit $\rho = a \cdot Q + b \cdot Q^2$ for each capillary with coefficients a, b and the corresponding standard deviations s_a, s_b. Thus it is possible to calculate the pressure p and its standard deviation s_p at additional values of Q within the measuring range. The result is shown in *Figure 42* with the differential pressure p as a function of the length L of the capillaries at constant volume flow rate (parameter). The slope of the curve is calculated from the difference of the pressures between 10 mm and 40 mm.

This is identical with the arithmetic mean value of all three slopes at equidistant points:

$$\frac{1}{3}\left[\frac{p_3 - p_2}{15\,\mathrm{mm}} + \frac{p_2 - p_1}{15\,\mathrm{mm}} + \frac{p_3 - p_1}{30\,\mathrm{mm}}\right] = \frac{p_3 - p_1}{30\,\mathrm{mm}} \tag{26}$$

From each of the three pressures p_1, p_2, and p_3 at 10, 25, and 40 mm one intersection with the ordinate is calculated. The arithmetic mean value of these three results is the Bagley-correction. The corresponding standard deviation to the degree of freedom 1 is s_{p1}. The Bagley-correction as a function of the flow rate, as shown in *Figure 43*, is

$$p_B = 4.8616 \cdot 10^{10} Q + 1.1057 \cdot 10^{19} Q^2 \ , \tag{27}$$

with Q in m^3/s and p_B in Pa. This equation is obtained from measurements with the reference liquid. The maximum difference in viscosity at high shear rates between the fluids and the reference liquid is only 33 %. Therefore it is assumed that equation 27 is also valid for the fluids under investigation. To achieve smallest uncertainties it is necessary to determine the Bagley-correction for each individual liquid.

From the measurements with the fluids under investigation equation 21 is used with $\Delta p = p - p_B$ and the apparent shear rate is calculated [40]:

$$D_{ap} = \frac{4 \cdot Q}{\pi \cdot R^3} = A \cdot \tau + B \cdot \tau^2 \tag{28}$$

Figure 42
Pressure as a function of the length of the capillary for different flow rates:
◊ : 2.0·10⁻⁸ m³/s, □ : 6.0·10⁻⁸ m³/s, Δ: 1,0·10⁻⁷ m³/s, x : 1,4·10⁻⁷ m³/s,
∗ : 1,8·10⁻⁷ m³/s, 0 : 2,2·10⁻⁷ m³/s, + : 2,6·10⁻⁷ m³/s

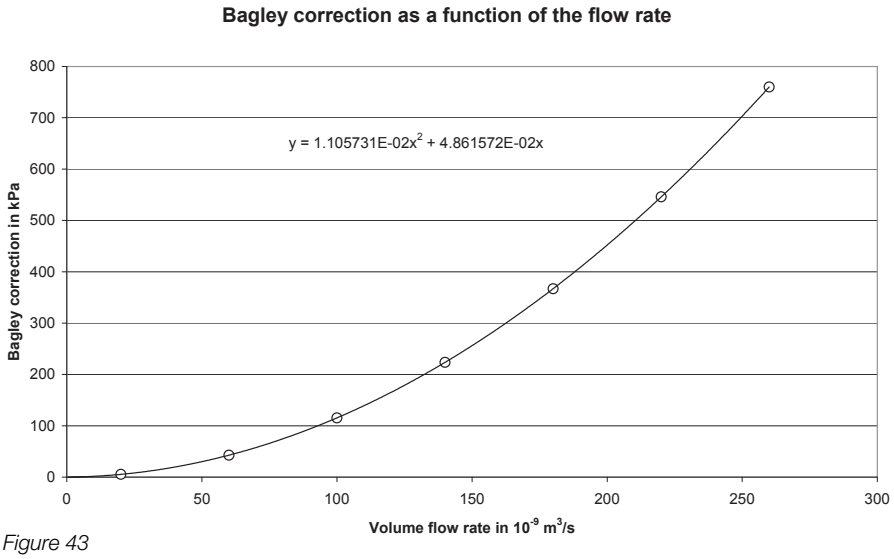

Figure 43
Parabola of Bagley

and fitted with the coefficients A and B. From the apparent shear rate, the true shear rate is calculated [40]:

$$D_{true} = \frac{D_{ap}}{4} \cdot \left(3 + \frac{\tau}{D_{ap}} \cdot \frac{\mathrm{d}D_{ap}}{\mathrm{d}\tau} \right) = \frac{3}{4} \cdot D_{ap}$$

$$+ \frac{1}{4} \cdot A \cdot \tau + \frac{1}{2} \cdot B \cdot \tau^2 \qquad (29)$$

In the case of the liquids under test, the difference between the apparent and the true shear rate is moderate. The maximum difference occurs in the liquid Titan SL PCX 0W-30. The relative difference between the flow curves is only 3 %. Equation 23 with D = D_{true} yields the dynamic viscosity.

The dynamic viscosity $HTHS_{150\ °C}$ is related to the ambient pressure p_{amb}. For that reason, the viscosity measured at the pressure p_m (arithmetic mean pressure in the capillary) has to be corrected according to [41]:

$$\eta(T, p_{amb}) = \eta(T, p_m) \cdot [1 - p_m \cdot (\alpha - \kappa)] \,, \qquad (30)$$

with α being the pressure coefficient of viscosity and K the compressibility of the liquid under test. Values for α are available from measurements with the high pressure rolling-ball viscometer. From the compression of the liquid at 100 MPa at room temperature T_{room} from the volume V to V-ΔV, only a rough estimate of the compressibility is possible according to the empirical formula

$$\kappa(150°\mathrm{C}) = 2.5 \cdot \frac{\Delta V}{100\ \mathrm{MPa} \cdot V} \,, \qquad (31)$$

which is based on investigations with oils used for heat exchange.

During the measurement it is not possible to keep the temperature exactly at 150 °C. At high shear rates, the temperature increases at the capillary outlet due to friction. After starting the flow through the capillary, it takes about 20s until a stable temperature is reached and the flow measurement can be started. In the analysis, the arithmetic mean of the temperatures, measured by the platinum resistance thermometers, is used. The temperature differences to 150 °C are corrected using the temperature-viscosity coefficient β obtained from a Vogel equation, which is set up for each liquid under investigation by measurements at ambient pressure:

$$\eta(150°\mathrm{C}, p_{amb}) = \eta(T, p_{amb}) \cdot [1 + \beta \cdot (T - 150°\mathrm{C})] \quad (32)$$

5.2 Results

The result of the corrected HVA 6 measurements is shown in *Figure 44*. The polyalkylene glycol PAG 46-4 shows an almost perfect Newtonion behavior with no indications for a shear thinning. The polymer-free Fuchs HCE 0W-20 and 100E 0W-20 are quite similar. The shear thinning of the polymer-containing FUCHS HCE-Low-SAP and Titan SL PCX 0W-30 is visible. All four liquids show a very weak pseudoplastical behavior. In rheology, *Figure 44* is normally shown with a double logarithmic axis. As a result, 5 nearly horizontal curves are obtained. If only the D-axis is logarithmic, *Figure 44* changes to *Figure 45*.

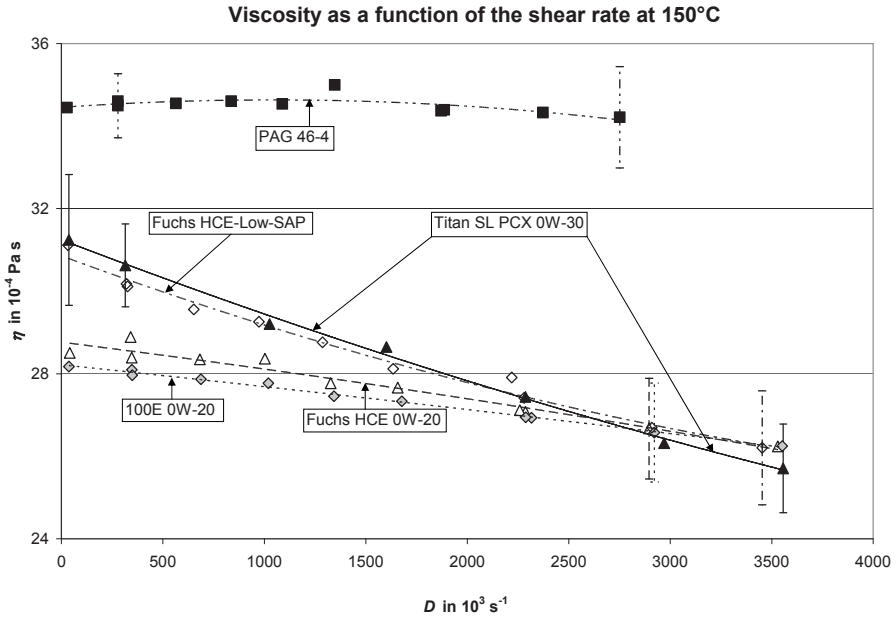

Figure 44
Viscosity curves depending on the shear rate for five different liquids

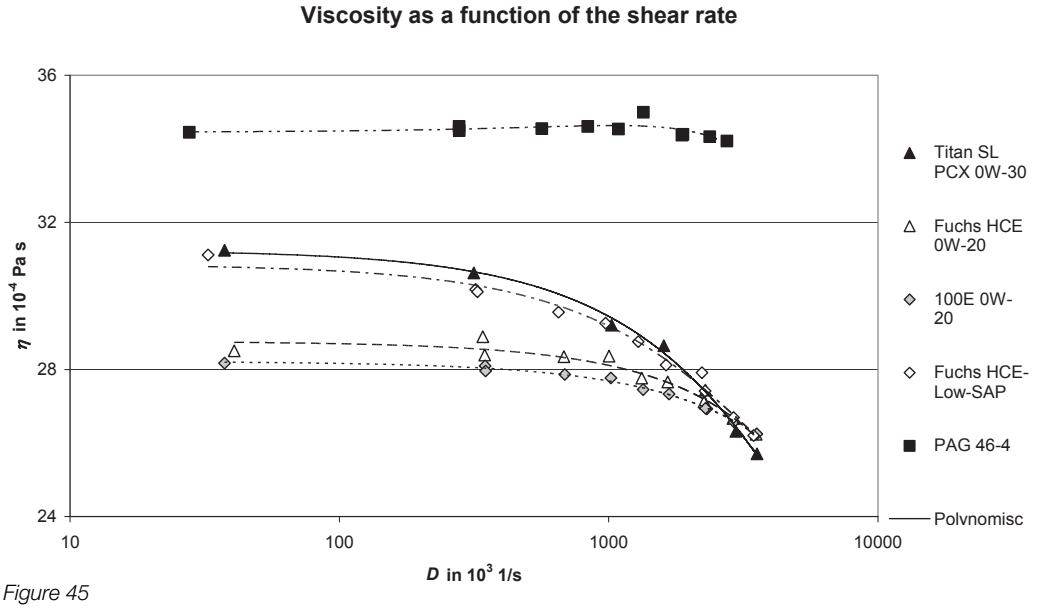

Figure 45
Viscosity curves depending on the shear rate for five different liquids

5.3 Estimation of the measurement uncertainty

The uncertainty calculations according to [9] are performed with the aid of the GUM Workbench. The working equations 25, 21, 28, 29 and 23 are entered, and after that the input quantities including an appropriate measure of uncertainty. One contribution to the Bagley-correction is the already defined s_{p1}, which is correlated with the uniformity of the inner diameter of the three capillaries of different length. In addition, the standard deviation s_{p2} belonging to $s_a \cdot Q + s_b \cdot Q^2$ is calculated. This contribution is a measure for the quality of the fit $p = a \cdot Q + b \cdot Q^2$. For each capillary, at least 11 measurements are carried out to determine the coefficients a and b. Hence, the degree of freedom 9 is used for s_{p2}. At high shear rates the Bagley-correction yields the leading term in the uncertainty budget.

Another important contribution is due to coefficient B in equation 28. The corresponding standard deviation s_B is calculated from the measurements of the liquid under investigation.

For example, in the case of the liquid Titan SL PCX 0W-30 at a volume flow rate of 340 mm³/s (corresponding shear rate: $3.4 \cdot 10^6$ s^{-1}) in the uncertainty budget, the index of s_{p1} is 37.5 %, that of s_{p2} 24.9 %, and that of s_B 16.1 %. The contribution for the determination of the capillary radius yields 4.2 % (small volume flow rate of 5.56 mm³/s) and the measurement of low pressure 4.3 %. The remaining three influence quantities with indices higher than 0.7 % are: the volumetric flow rate at the high shear rate (4.5 %), temperature measurement including control (4.3 %), and the coefficient A (2.7 %). As a result, the expanded relative measurement uncertainty for the viscosity 4.9 % is obtained.

The uncertainty of viscosity as a function of the shear rate $\eta = \eta(D)$ and not as a function of the flow rate $\eta = \eta(Q)$ is of interest. For that reason the relative standard uncertainty (denoted by ‘) along the viscosity curve is

$$s'^2\left(\eta(D)\right) = s'^2\left(\eta(Q)\right) + \left[\frac{D}{\eta} \cdot \frac{\mathrm{d}\eta}{\mathrm{d}D}\right] \cdot s'^2(D)$$

$$+ s'^2(\mathrm{fit}), \qquad (33)$$

provided the input quantities are not correlated. The relative standard deviation s‘(fit) is calculated from the differences between the viscosity curve and the measuring points. The GUM Workbench yields the result 2.7 % for the expanded relative measurement uncertainty of the shear rate (same example as before). Thus, the expanded relative measurement uncertainty at $D = 3.45 \cdot 10^6$ s^{-1} is 5.1 %. At $D = 2.90 \cdot 10^6$ s^{-1} this value is reduced to 4.2 % and at $D = 0.31 \cdot 10^6$ s^{-1} to 3.3 %. These results and uncertainties for the other tested liquids are shown in *Figure 44* as error bars.

6 Tribological behavior under continuous sliding (BAM-method)

The following figures in this chapter contain not only the wear rates under mixed/boundary lubrication for each triboelement, but also to each couple the coefficient of friction. They were achieved by using the BAM-test procedure [14]. The wear rate (or wear coefficient) is defined by the wear volume divided by sliding distance and load.

6.1 TOTAL HC 5W-30 fresh oil and as engine aged with soot

Depending from the combustion process in an internal combustion engine, the generation of soot in the oil concerns wear, as the primary particles of 20-50 nm agglomerate to some micrometers and became larger than the oil film thicknesses. The *Figure 46* bench mark nine metallurgically different piston rings under mixed/boundary lubrication. In any cases, the 3.7 wt.-% soot increased the ring wear by one to two orders of magnitude. The only exception was the “GDC50®”, a hard chrome coating with diamond particles. The GGL20HCN liner wear was accelerated by up to one order of magnitude.

Based on the viscometric results, it can be concluded, that soot has an adverse effect on component life only under the regime of mixed/boundary lubrication.

The abrasive action of soot can be limited, but not eliminated, by using hard metal or cermet (see also *Figure 58*) as well as GDC50® ring coatings.

6.2 FUCHS Titan GT1

The ester-based TITAN GT1 (HCE) displayed no indications for accelerated wear under mixed/boundary lubrication of the piston ring coatings and cylinder liner materials. The wear rates and coefficients of friction of cast iron (GGL20HCN) in GT1 are in the same range as those in HC 5W-30. MKJet 502® presented the lowest ring wear, but associated also the highest liner wear of triboactive liner coatings (See *Figure 47*). MKJet 502® and TM23-1 are in GT1 responsible for high/excessive liner wear.

The “zero” liner wear of quite rough finished ($R_{PK} \approx 0.36$ µm) TM23-liner was associated with intensive Ti_nO_{2n-1}- and MKP81A®-ring wear.

6.3 TOTAL HCE midSAP

The wear rates of the reference couple MKP81A®/GG20HCN in HCE midSAP were similar to those measured in HC 5W-30. A friction reducing action of HCE lowSAP was not observed. “Zero” liner wear in HCE mid SAP was observed when using smoothly machined APS-$Ti_{n-2}Cr_2O_{2n-1}$ and HVOF-(Ti,Mo)(C,N)-23NiMo liner coatings (See *Figure 48*). The wear rates of APS-$Ti_{n-2}Cr_2O_{2n-1}$ coated rings are in HCE midSAP in the same order of magnitude than those of MKP81A®, even the wear rates of GG20HCN- and Ti_nO_{2n-1}-liner tend to be slightly increased by the APS-$Ti_{n-2}Cr_2O_{2n-1}$ ring coating.

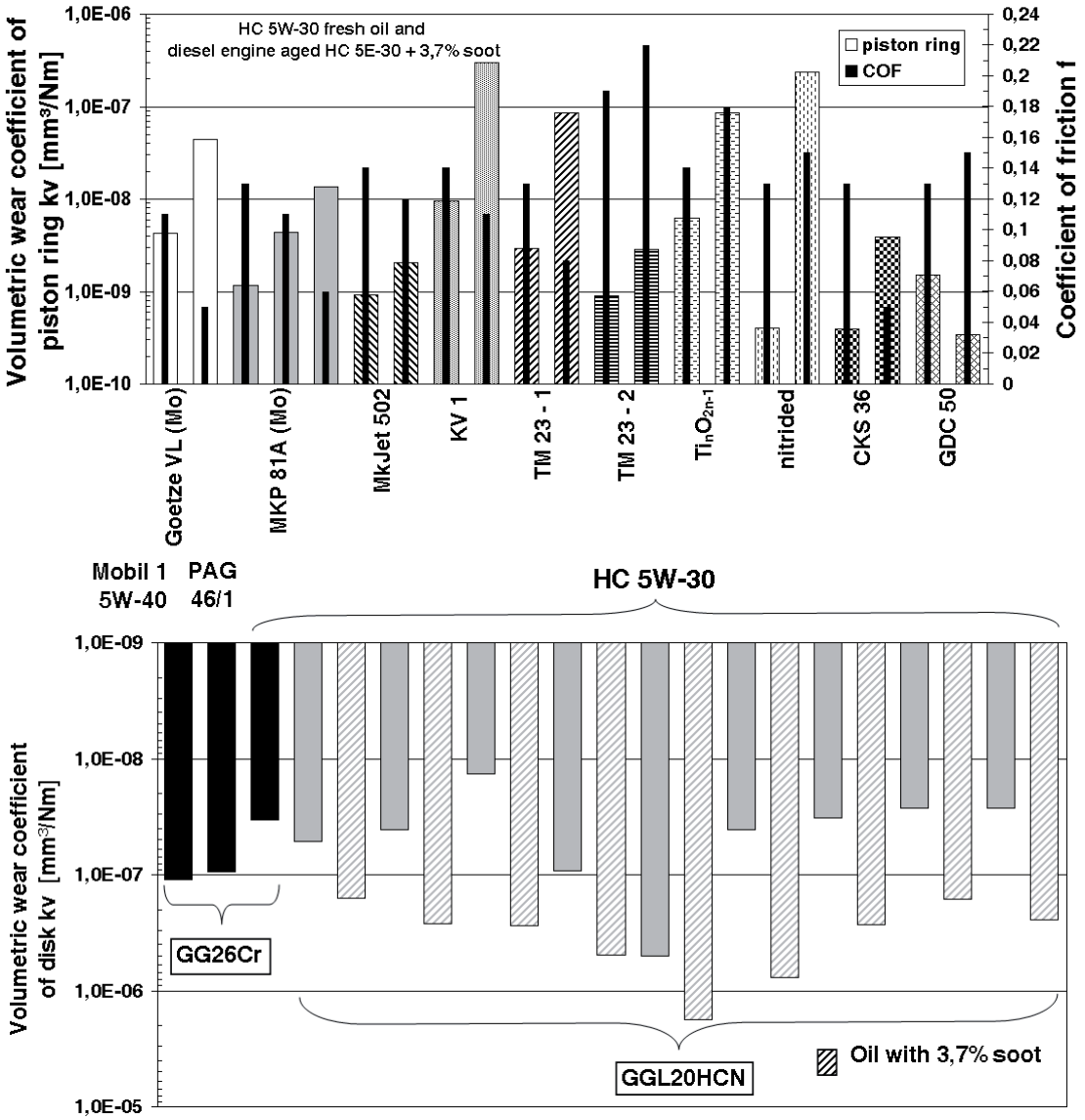

Figure 46
Volumetric wear coefficients of coated piston rings and uncoated grey cast iron using HC 5W-30 fresh oil and diesel engine aged HC 5W-30 (1.9 liter TD, 89 kW) under mixed lubrication conditions

6.4 FUCHS HCE lowSAP

The “hard/hard” couples MKJet 502®/TM23 were not significantly more wear resistant than MKP81A®/GG20HCN using the HCE LowSAP formulation. The lowest liner and system wear was observed in HCE LowSAP with the smooth finished (Ti,Mo(C,N)-23NiMo liner coating (See *Figure 49*).

The HCE lowSAP formulation displayed a trend to increase under mixed/boundary lubrication the coefficients of friction.

6.5 PPG 32-2

As with the PAG46-4 (see chapter 6.6), the coefficients of friction were significantly lowered also in PPG32-2. The GGL20HCN liner wear seemed to be slightly increased by PPG32-2. “Zero” wear and low friction can be achieved by using triboactive coatings and PPG32-2.

6.6 PAG 46-4

As the PAG46-4+2.65 Phopani contained no friction modifiers, the PAG-base oil molecules tend to halven down to ca. 0.04 the coefficients of friction compared to most other formulations of this test programme (See *Figure 51*).

Smoothly finished (Ti,Mo)(C,N)-23NiMo offer in PAG46-4 “zero” liner wear associated with reduced coefficients of friction. The lubrication of GGL20HCN with PAG46-4 did not affect the wear rates, but reduced the coefficients of friction for different ring metallurgies. In PAG46-4, the APS- Ti_nO_{2n-1}-liner was as wear resistant as the GGL20HCN.

It was surprising to observe, that in PAG46-4 the “nitrided” ring presented one of the highest wear resistances of the rings, which has an economic impact.

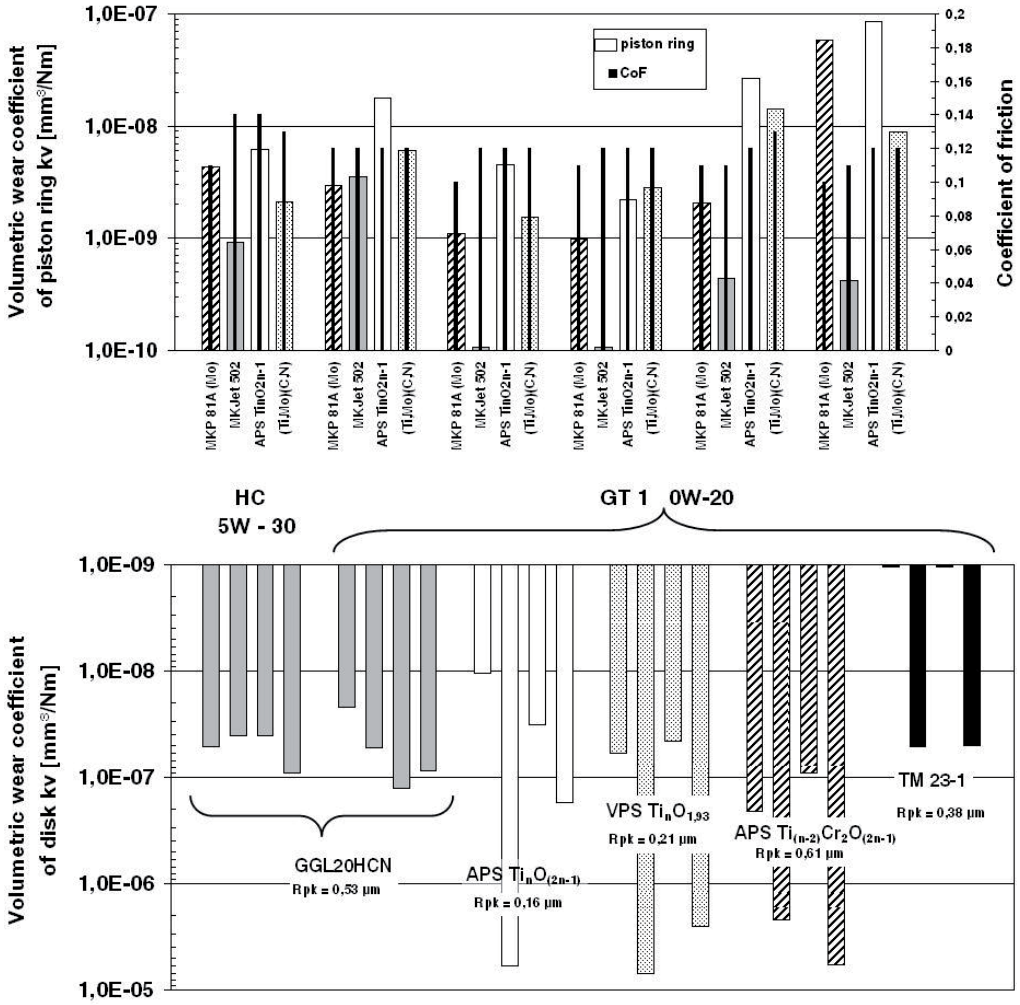

Figure 47
Volumetric wear coefficients of coated piston rings and of thermal sprayed triboactive cylinder liner coatings and uncoated grey cast iron using TITAN GT1 and factory fill oils under mixed lubrication conditions

6.7 GGL20HCN

Figure 52 summarizes the wear rates of the different piston rings (Mo (MKP81A® and VL®), Ti_nO_{2n-1}, TM23-1 and MKJet502®) sliding against an uncoated grey cast iron cylinder material with high carbon content (HCN) in different lubricants. For these combinations the wear rates of the piston rings with two Mo-based coatings are quite similar indicating a high reproducibility of the test method and coating process. As trend the wear rates of the GGL20HCN cylinder liner are "independent" of the used ring material and lubricant or "robust" against the selected ring materials or lubricant with exception in Titan GT1 sliding against MKP81A. The MKJet 502® seems to be sensitive to the lubricant used and does not always presents significant tribological benefits. On the other hand, the lowest friction was observed for the couples MKJet502®/GG20HCN and MKP81A®/GG20HCN in PAGs 46-3/-4. The PCX and the two PAGs displayed the lowest coefficients of friction.

The wear rates of APS coated piston rings are similar to that of the reference Mo-based coating with a trend of higher wear rates for APS-Ti_nO_{2n-1} (See chapter 6.10). The coefficient of friction can be halvened with Supersyn SL PCX and by a factor 2 – 3 with PAGs 46-3/-4. The PAGs 46-3/-4 reduces the coefficient of friction even though no friction modifiers were added, as well as in the PAG 46-1. Additionally, the wear resistance of piston rings in low additivated PAGs46 are comparable or even higher than in the hydrocarbon and ester based lubricants.

The figure of 4.51 10^{-8} mm³/Nm in *Figure 55* represents the average of 230 tests performed with GGL20HCN against different ring metallurgies and in several oils. This may act as a base line for validation of other liner metallurgies in the BAM test.

6.8 (Ti,Mo)(C,N)-23NiMo liner coating

The TM23-1 ring was finished to $R_{PK} \approx 0.8$ µm and the second TM23-2 grade to $R_{PK} \approx 0.18$ µm. Overall, the tribological data in *Figure 53* show clearly, that rings coated with (Ti,Mo)(C,N)-23NiMo present significantly reduced ring and liner wear rates, when they are smoothly machined.

The wear resistance of triboactive (Ti,Mo)(C,N)+23NiMo (TM23) piston ring coatings is similar or even higher than for widespread used Mo-based coatings against grey cast iron in different lubricants. In Zinc-free PCX and PAG46-4 slightly reduced coefficients of friction were observed.

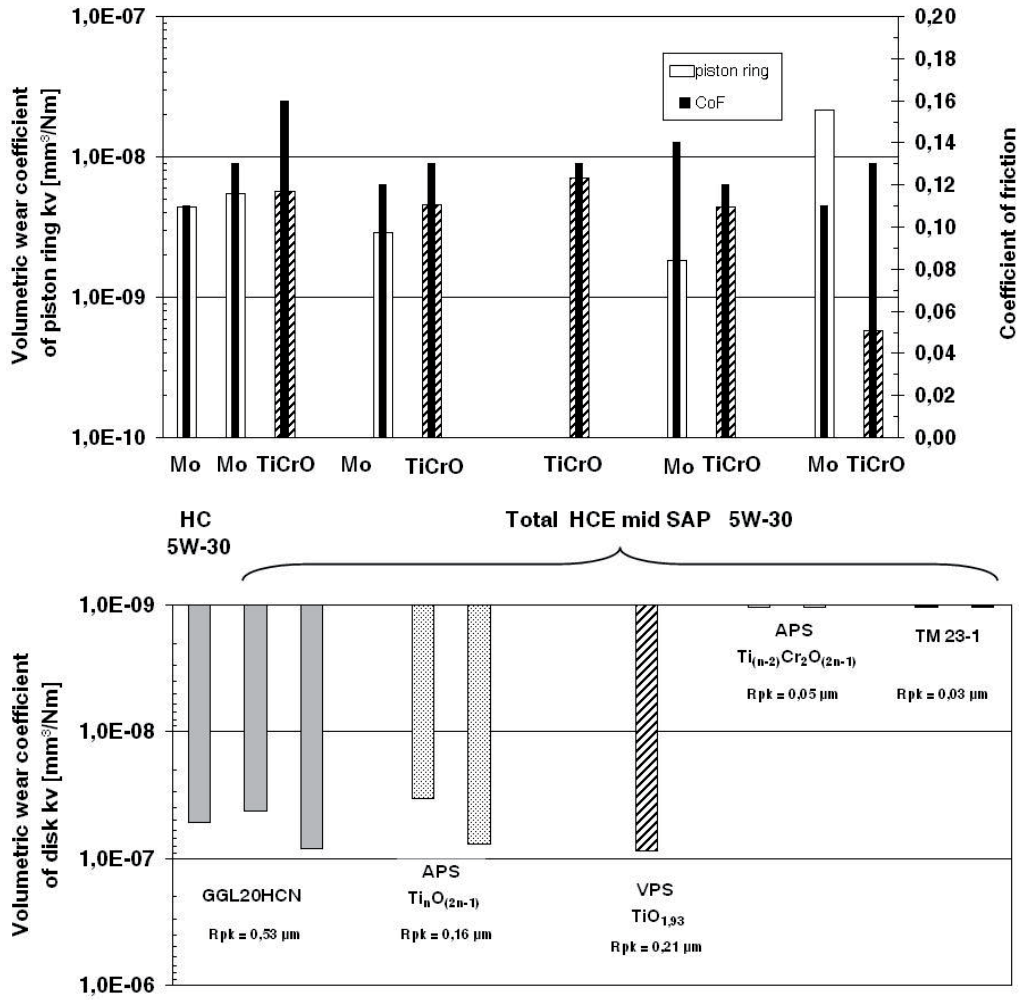

Figure 48
Volumetric wear coefficients of coated MKP81A® and APS-$Ti_{n-2}Cr_2O_{2n-1}$ piston rings and of thermal sprayed triboactive cylinder liner coatings and uncoated grey cast iron using Total midSAP under mixed lubrication conditions

Mating TM23 ring coatings with liners coated with $TiO_{1,93}$, Ti_nO_{2n-1} or $Ti_{2-n}Cr_2O_{2n-1}$ resulted in all formulations in excessive liner wear of the laters.

6.9 $Ti_{2-n}Cr_2O_{2n-1}$ liner coating

The APS-$Ti_{n-2}Cr_2O_{2n-1}$ liner wear rates ($R_{pK} \approx 0.61$ µm) in *Figure 54* displayed either no significant advantages in respect to GGL20HCN regarding wear resistance within the precision of the BAM test procedure between the fully-formulated hydrocarbon- and ester-based oils nor positive effects regarding a fluid-surface interaction.

Liners coated with APS-$Ti_{n-2}Cr_2O_{2n-1}$ presented in *Figure 54* and in *Figure 55 a* significant wear reduction by nearly two orders of magnitude in "HC" 5W-30 using all of the three types of Mo-based rings, when the liner surfaces were smoothly finished to $R_{PK} \approx 0.05$-0.1 µm. The same wear reduction was found in PCX and HC 5W-30 only mating with the PCF 251 and PCF 278 rings. Mating with the MKP81A® piston rings, the APS-$Ti_{n-2}Cr_2O_{2n-1}$ liner coating with $R_{pK} \approx 0.61$ µm is as wear resistant as the GG20HCN. Such a wear resistance was also determined for Ti_nO_{2n-1} liner coatings. This qualifies APS-Tin-2Cr2O2n-1 liner as a candidate liner coating for aluminium substrates.

The low APS-$Ti_{n-2}Cr_2O_{2n-1}$ liner wear in "HC" 5W-30 was confirmed by means of repeated tests.

The low coefficients of friction for "PCX" are in general not untypical for this Mo-free formulation. On the other hand, the friction modifier used in "PCX" not always interacts with all "ceramics" and "hard metals" resulting in low friction.

The most significant reduction in "system" wear was demonstrated by mating the APS-$Ti_{n-2}Cr_2O_{2n-1}$ coated piston rings with smooth machined HVOF-(Ti,Mo)(C,N) liner coating (See *Figure 58*), which was confirmed in BAM- and SRV-type tests. The APS-$Ti_{n-2}Cr_2O_{2n-1}$ coated piston rings offer a potential for substituing molybdenum and hard metal based rings.

In the case of PCX-oil, the friction modifier of PCX not acted beneficial in couples sliding against $Ti_{2-n}Cr_2O_{2n-1}$-liners.

6.10 Ti_nO_{2n-1} ring coatings

Figure 56 presents effects of liner materials for APS-Ti_nO_{2n-1} coated piston ring wear in factory fill HC 5W-30 as well as in the ester containing Titan GT1. Against GGH20HCN, the wear of the Ti_nO_{2n-1} coated piston ring is increased as well as slightly the wear rate of the cast iron using GT1, but tribocouples with Ti_nO_{2n-1} coated piston rings sliding against

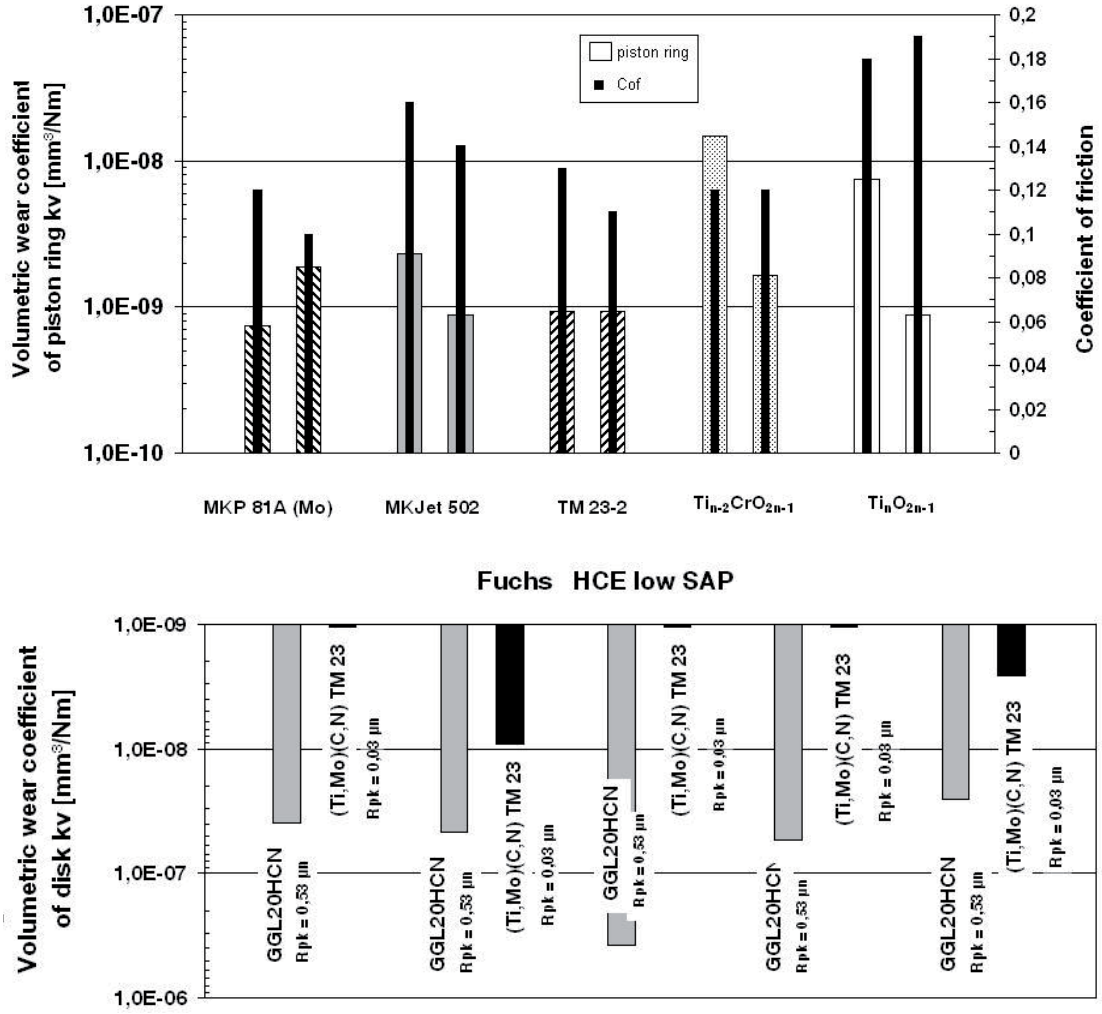

Figure 49
Volumetric wear coefficients of coated piston rings and of thermal sprayed triboactive cylinder liner (Ti,Mo)(C,N) coatings and uncoated grey cast iron using FUCHS lowSAP under mixed lubrication conditions

TiO_x liner coatings exhibit the same high wear resistance as commercial Mo/GGL20HCN couples. The wear coefficient of Ti_nO_{2n-1} coated piston rings is similar to that of Mo-based ring coating MKP81A® in HC 5W-30 and the wear of grey cast iron is not affected. TM23 liner coatings illuminated the highest wear resistance close to "zero" wear independent of liner roughness. The smoothing of TM23 liner roughness from $R_{pk} \approx 0.53$ µm to $R_{pk} \approx 0.03$ µm reduced the wear rates of Ti_nO_{2n-1}-rings by more than one order of magnitude.

Under unidirectional sliding a slightly higher system wear and under oscillating sliding conditions (SRV®) a reduced system wear was measured for APS-Ti_nO_{2n-1}/GG20HCN compared to Mo/GGL20HCN.

Overall, both ring coatings wear in the same order of magnitude. It is reasonable that thermally sprayed TiO_x-based coatings can substitute common materials and serve as a promising alternative to commercial piston rings coated of strategic molybdenum.

6.11 Ester oil

The wear rates of MKP81A® coated rings and those of the smoothly machined (Ti,Mo)(C,N)-23NiMo liner coatings were in GTE (100E) also close to the "zero" wear limit. In order to meet a "zero" wear target, MKJet502® is not consequently necessary to use this ester formulation. Also in GTE (100E), the MKJet502® increased the wear rates of coated Ti_nO_{2n-1} and $TiO_{1,93}$ liners. It has to be noted, that the APS-$Ti_{n-2}Cr_2O_{2n-1}$ liners presented on "abrasive" action against the hard metal-based MKJet 502®.

A specific friction reducing action under mixed/boundary lubrication against many couples was not observed with this ester-oil formulation.

6.12 Zero wear target

Compared to the MKP81A®, the APS-$Ti_{n-2}Cr_2O_{2n-1}$ ring coating (see *Figure 54*) sliding on GG20HCN displayed no advantages in wear resistance, except when lubed by the PCX-oil.

A synergistic, significant reduction of the „system wear" (summ of ring and liner) can be achieved by mating the APS-$Ti_{n-2}Cr_2O_{2n-1}$ coated piston rings with smooth finished HVOF-(Ti,Mo)(C,N)-23NiMo liner samples as the APS-$Ti_{n-2}Cr_2O_{2n-1}$ ring wear is reduced by one order of magnitude and those of HVOF-(Ti,Mo)(C,N)-23NiMo liner samples up to two orders of magnitude down to the resolution limit of the BAM-test using 24 km (see *Figure 58*).

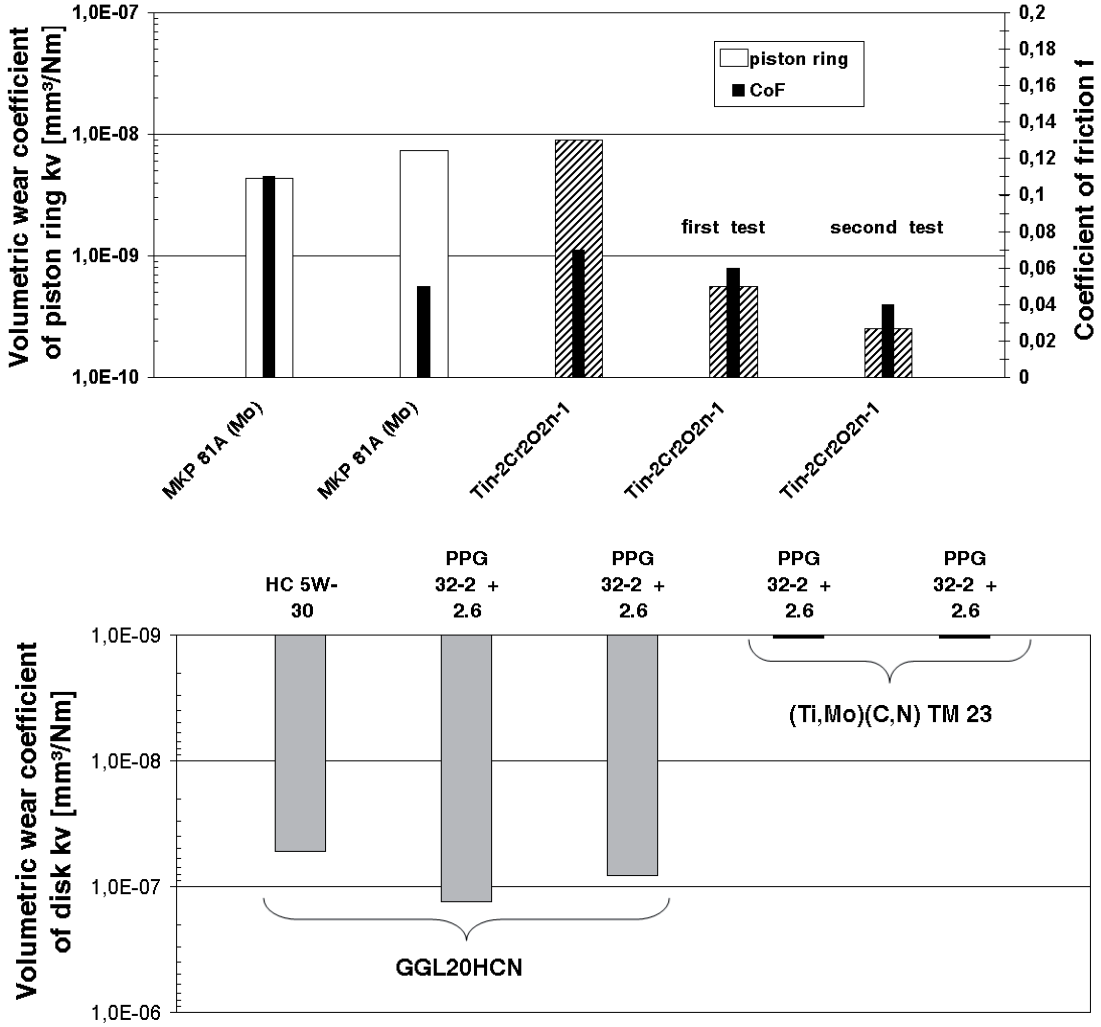

Figure 50
Volumetric wear coefficients of coated piston rings and of thermal sprayed triboactive cylinder liner coatings and uncoated grey cast iron using PPG32-2+2.65 Phopani and factory fill oils under mixed lubrication conditions

If the HC 5W-30 contains 3.7 wt.-% of soot (Diesel engine aged HC 5W-30), the wear rates of (Ti,Mo)(C,N) coated liner and APS-$Ti_{n-2}Cr_2O_{2n-1}$ coated piston ring increase under mixed/boundary lubrication by one order of magnitude close to the wear rates of MKP81A®/GGL20HCN in fresh HC 5W-30 without soot. The friction reducing effect of soot is probably related to the lapping movement (slip-rolling) of the soot particle in the tribocontact.

By using APS-$Ti_{n-2}Cr_2O_{2n-1}$/(Ti,Mo(C,N)-23NiMo, the zero wear target can be achieved in fully additivated hydrocabon-based or with alternative formulations with reduced contents of additives.

6.13 Summarizing friction and wear behavior in BAM test

Figure 59 and *Figure 60* summarize in two plots the coefficients of friction under mixed/boundary lubrication versus wear rate of different triboactive and state-of-the-art ring and liner coatings in five oils using the BAM test procedure.

The two polyglycols without and the FUCHS PCX containing an organic friction modifier displayed as a trend the lowest coefficients of friction under the regime of mixed/boundary lubrication. Depending from the portion of mixed/boundary lubrication, they will contribute to improve Fuel Economy.

The PPG32-2, PAG46-4 and the PCX offer, lubing the appropriate materials, a potential for “zero liner wear”, even they are polymer-, Zn- and Mo-free and respect bionotox criteria (Except bionotox for PCX!) and follow different strategies to reduce Zinc, phosphorus, sulphur and low ash.

Such lubrication concepts avoiding a different number of additives (VI, EP, AW) enable a retention of tribological properties over drain.

For given test conditions all APS coatings on piston rings showed no friction reducing effect. The coefficient of friction is more determined by the lubricants than by the materials or by an individual interaction between lubricants and a specific material or tribopairing.

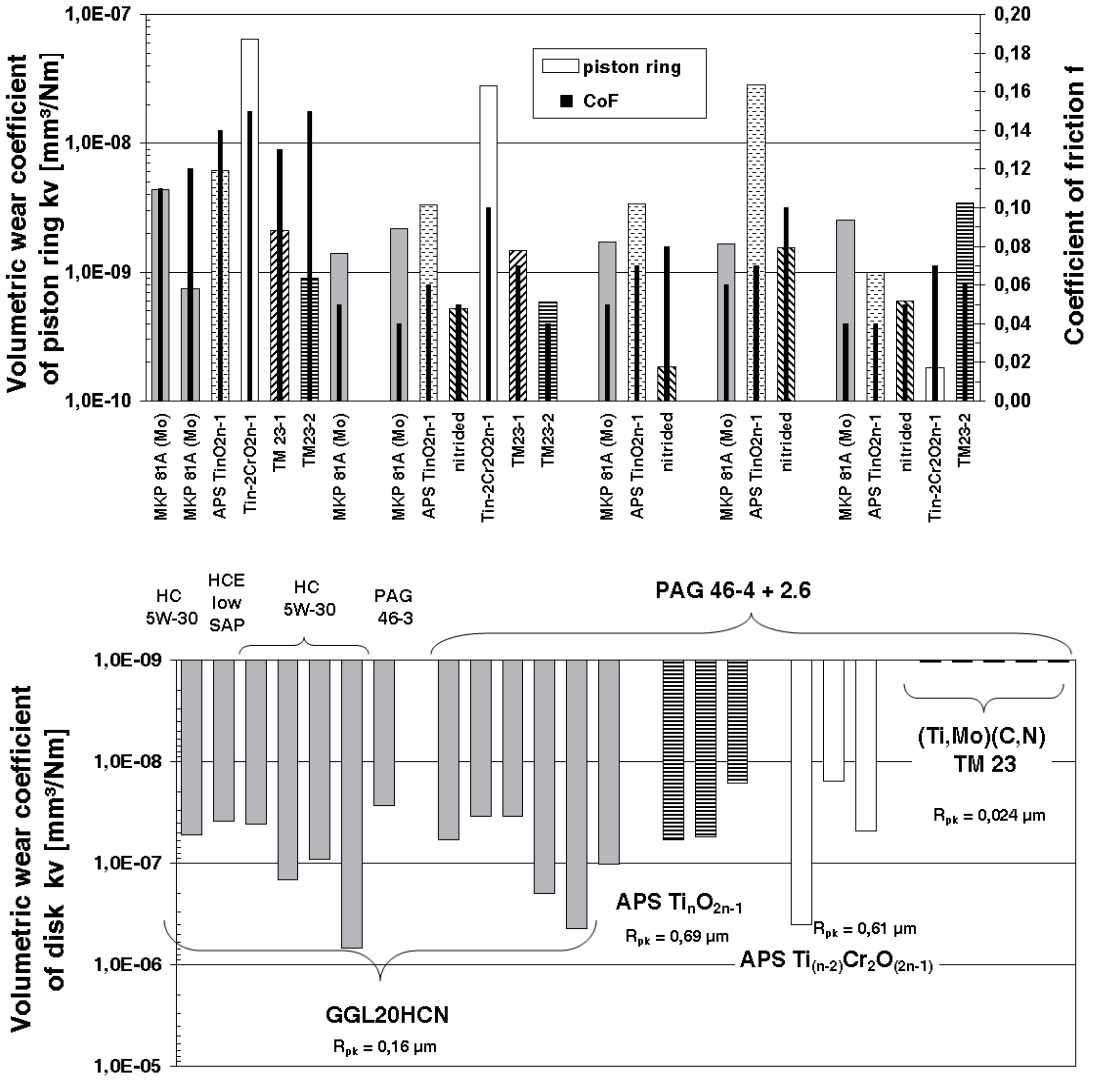

Figure 51
Volumetric wear coefficients of coated piston rings and of thermal sprayed triboactive cylinder liner coatings and uncoated grey cast iron using PAG46-4+2.65 Phopani and factory fill oils under mixed lubrication conditions

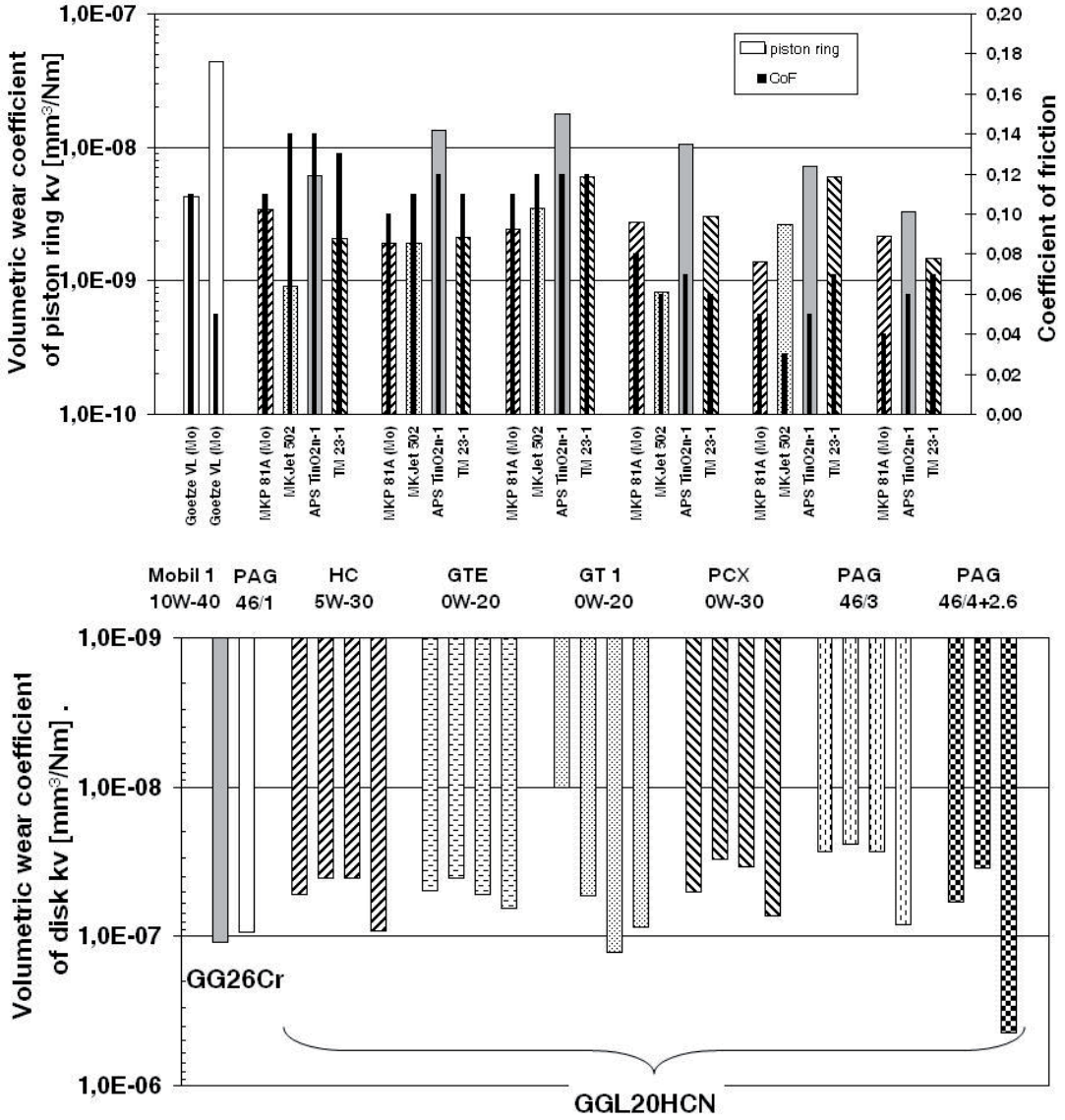

Figure 52
Volumetric wear coefficients of coated piston rings and uncoated grey cast iron GGL20HCN in different oils under mixed lubrication conditions

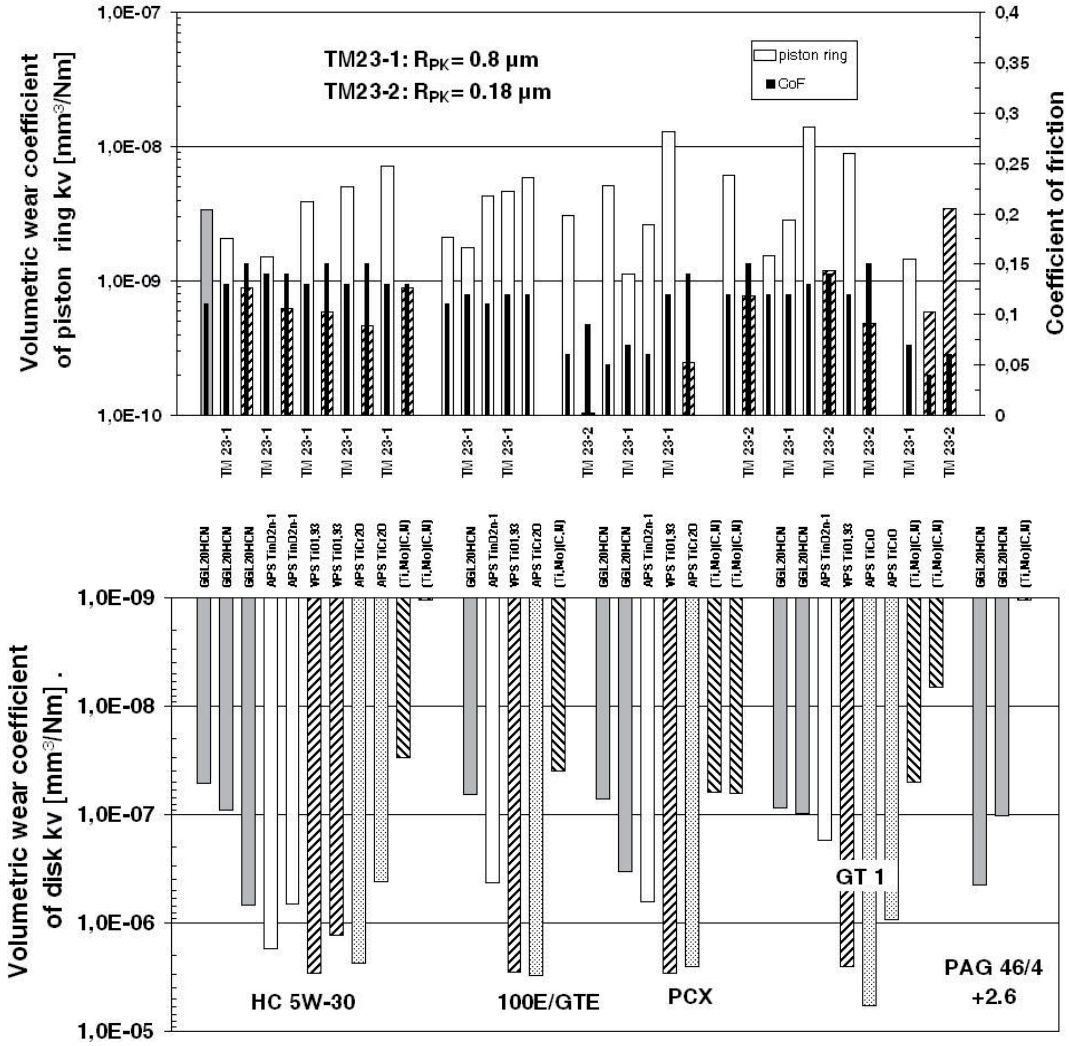

Figure 53
Volumetric wear coefficients of two finishing grades of APS-(Ti,Mo)(C,N) coated piston rings sliding under mixed lubrication conditions against cast irons and different coatings in different oils

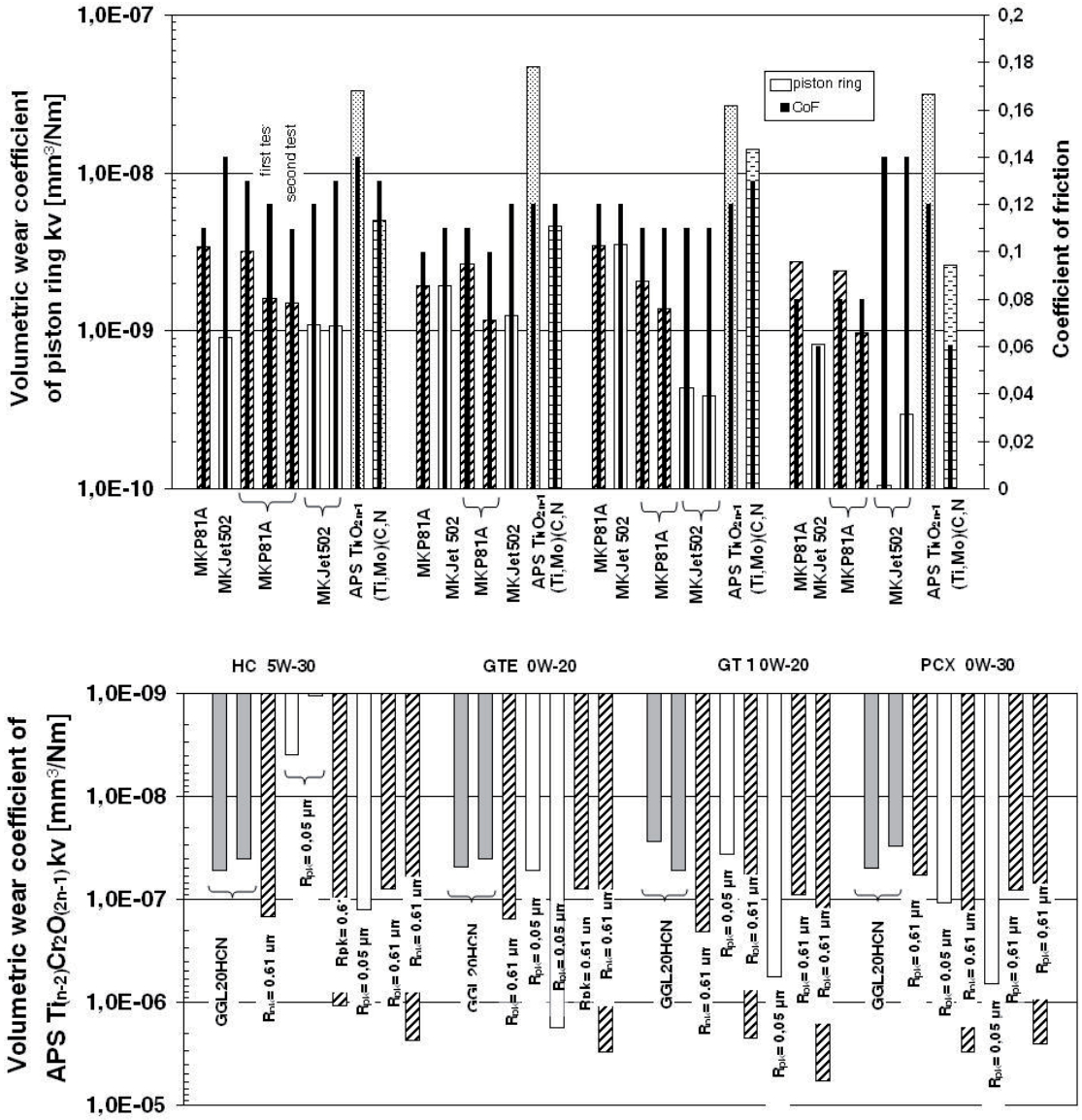

Figure 54
Volumetric wear coefficients of Ti_nO_{2n-1}, MKP81A® and MKJet502® coated piston rings sliding under mixed lubrication conditions against cast irons and APS-$Ti_{n-2}Cr_2O_{2n-1}$ in different oils

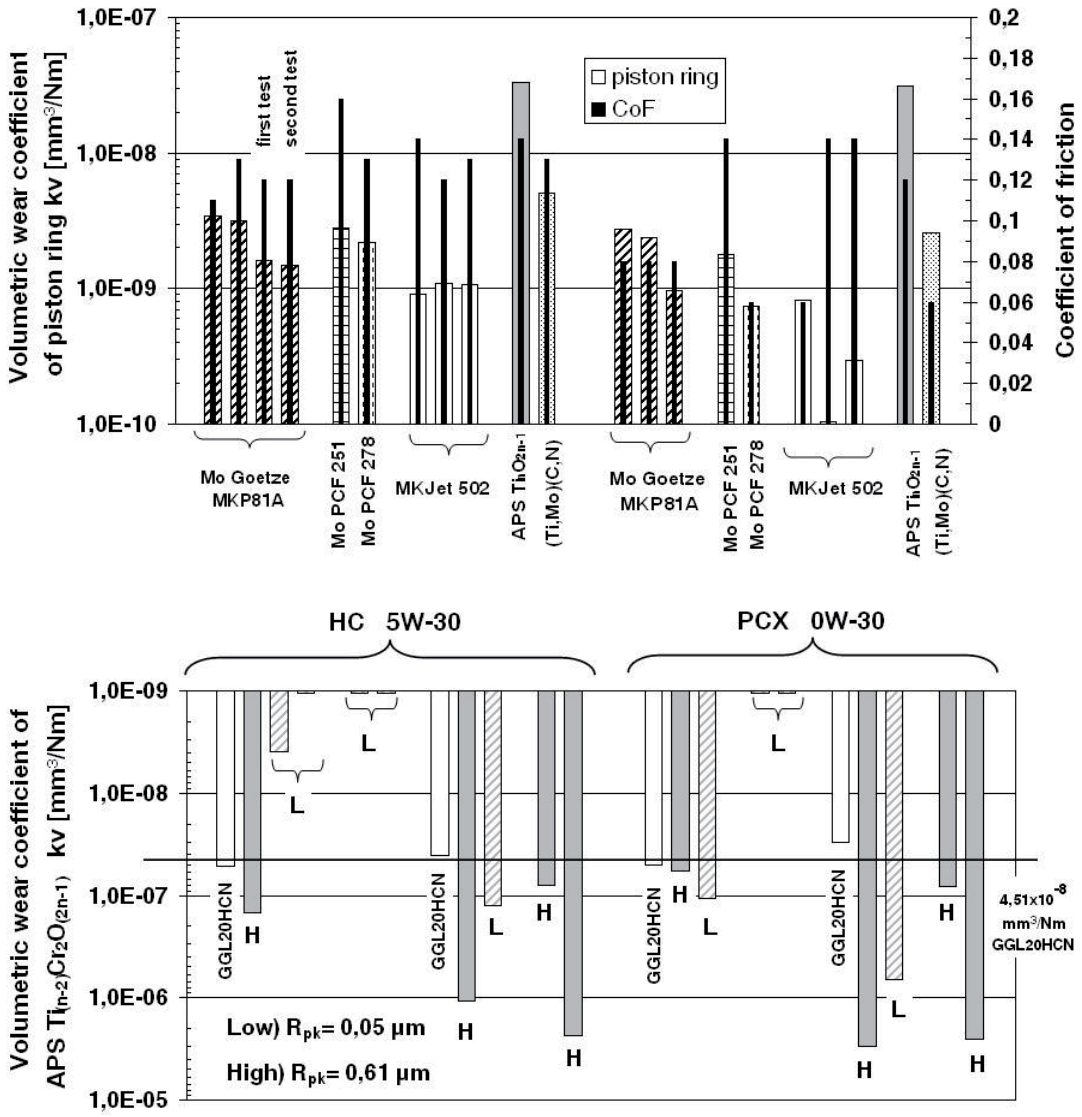

Figure 55
Volumetric wear coefficients of Mo-based and MKJet502® piston rings sliding under mixed lubrication conditions against cast iron and APS-$Ti_{n-2}Cr_2O_{2n-1}$ in two factory fill hydrocarbon-based lubricants.

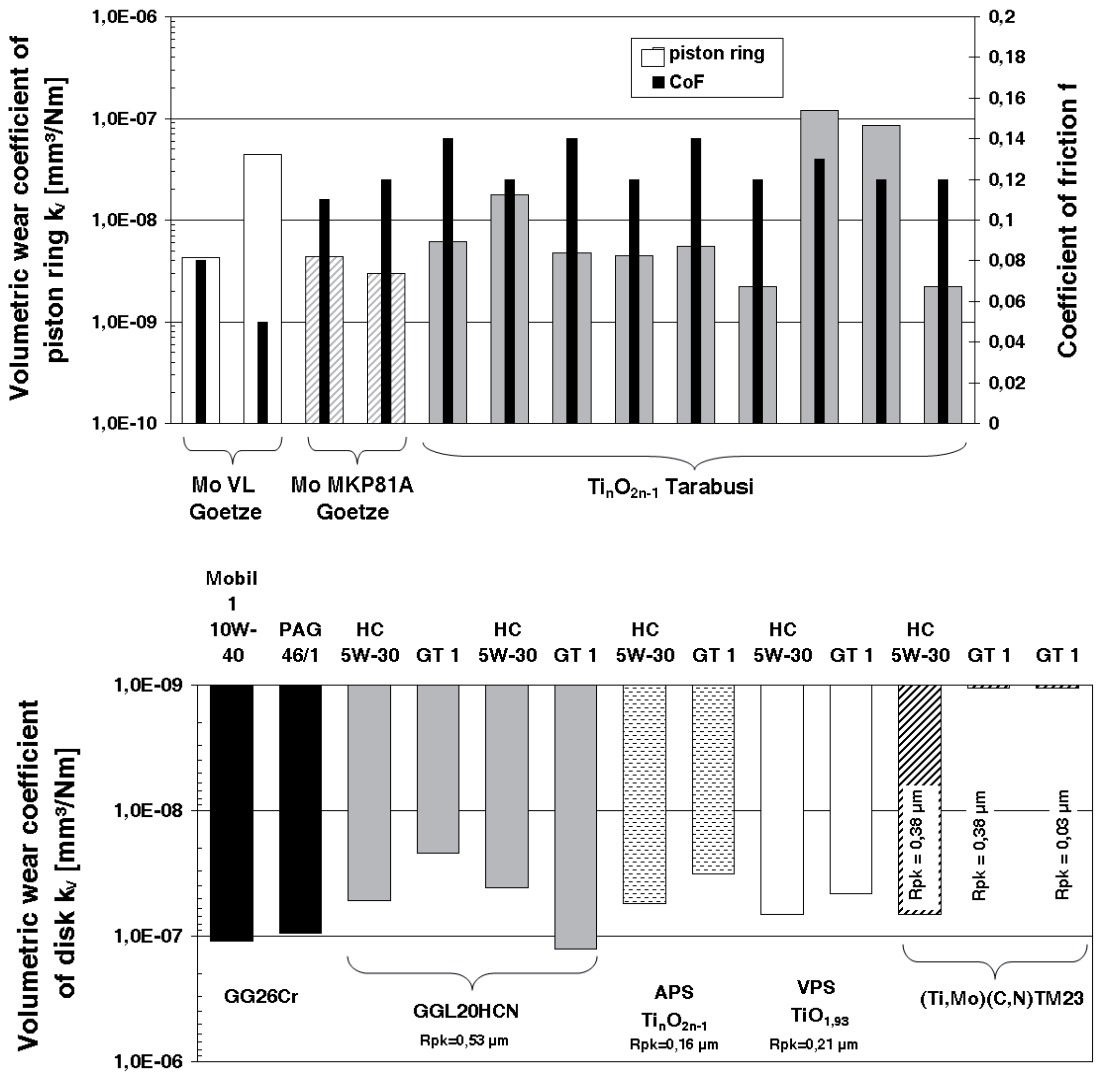

Figure 56
Volumetric wear coefficients of APS Ti_nO_{2n-1} coated piston rings and of different triboactive cylinder liner coatings in comparison to uncoated GGL20HCN using factory fill HC 5W-30 and an ester-containing Titan GT1 under conditions of mixed lubrication.

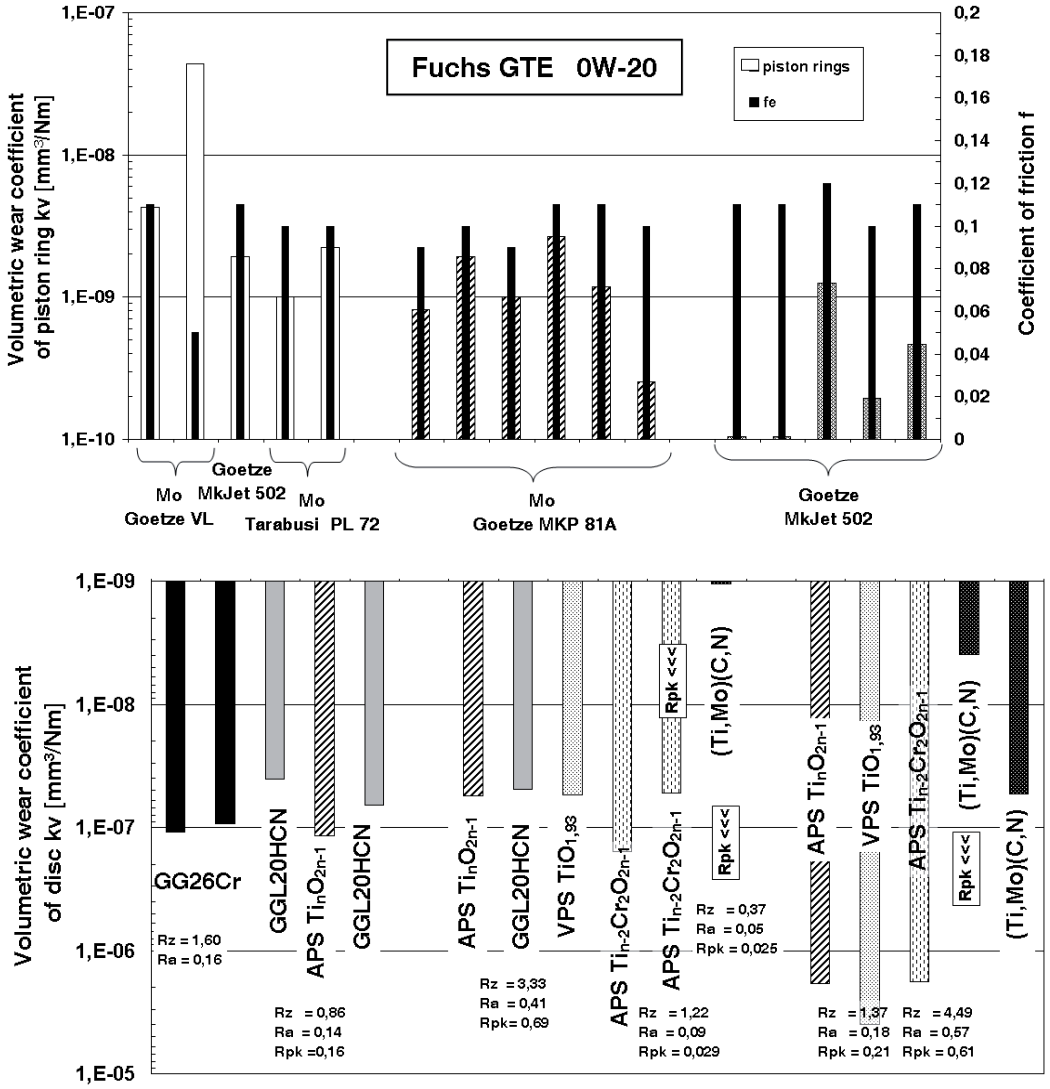

Figure 57
Volumetric wear coefficients of coated molybdenum-based and MKJet502® coated piston rings sliding against of thermal sprayed triboactive cylinder liner coatings and uncoated grey cast iron using TITAN GTE (100E) under mixed lubrication conditions

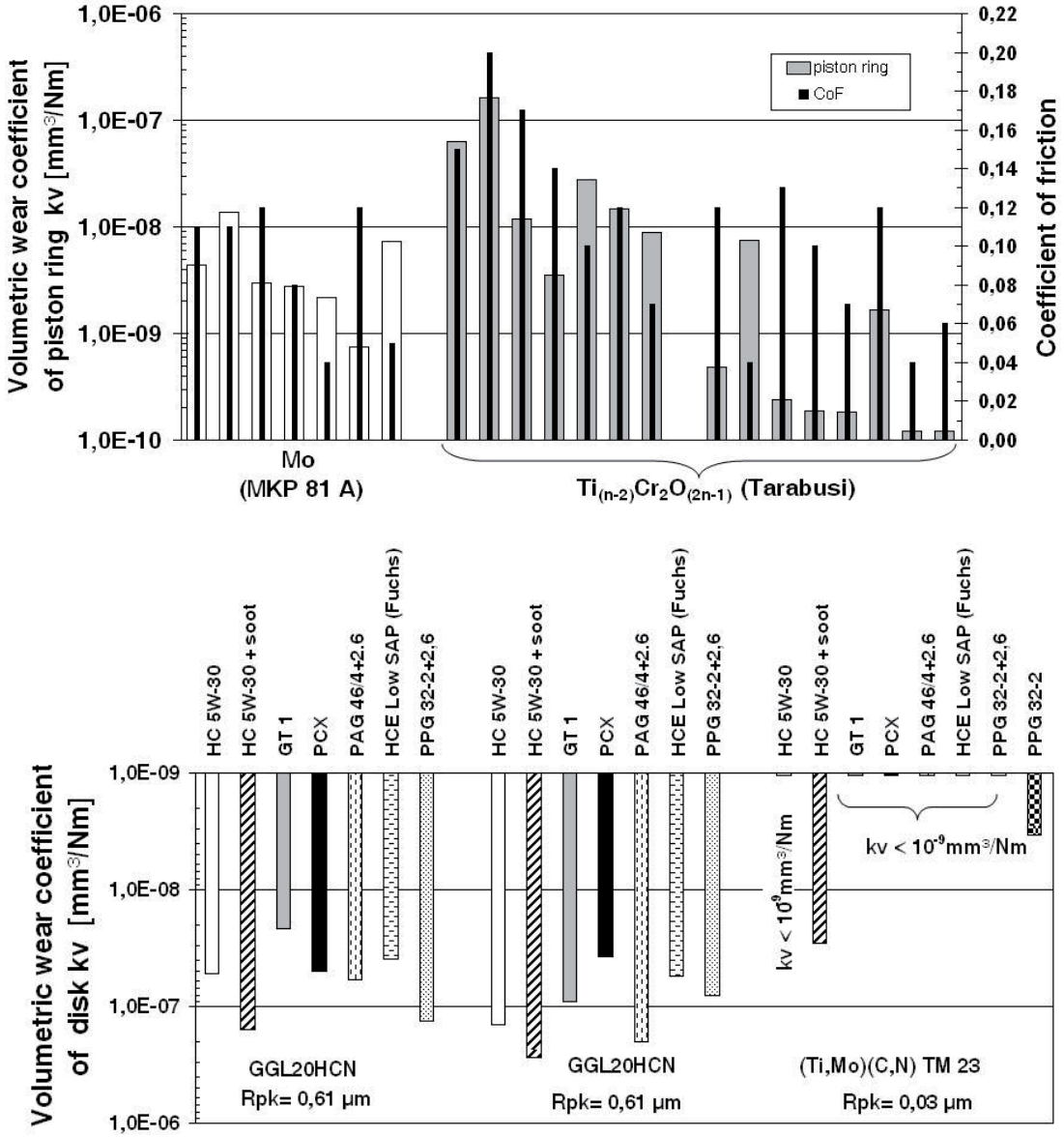

Figure 58
Volumetric wear coefficients of MKP81A® and APS-$Ti_{n-2}Cr_2O_{2n-1}$ coated piston rings sliding under mixed lubrication conditions against cast iron GGL20HCN and HVOF-(Ti,Mo)(C,N) in different oils

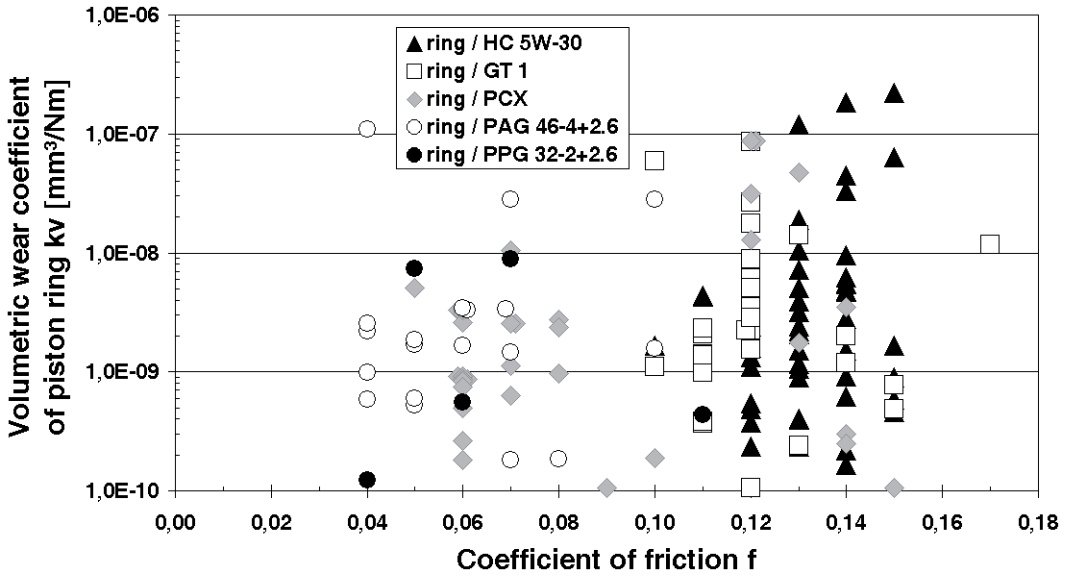

Figure 59
Summarizing plot of "coefficient of friction at test end" versus "Wear rate for ring" of sets of different tribo-couples in PAG 46-4+2.6 Phopani, PPG32-2+2.6 Phopani, SAE 5W-30 (HC), PCX 0W-30 and GT1 using the BAM test (F_N = 50 N ; v = 0.3 m/s ; T = 170 °C ; s = 24 km)

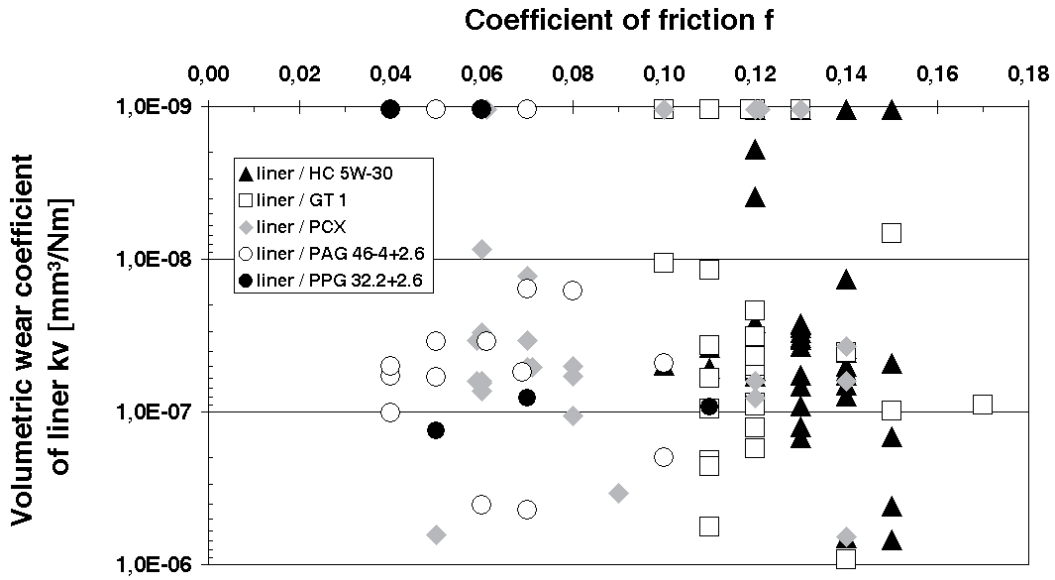

Figure 60
Summarizing plot of "coefficient of friction at test end" versus "Wear rate for liner" of a set of different tribo-couples in PAG 46-4+2.6 Phopani, PPG32-2+2.6 Phopani, SAE 5W-30 (HC), PCX 0W-30 and GT1 using the BAM test (F_N = 50 N ; v = 0.3 m/s ; T = 170 °C ; s = 24 km)

7 Tribological behavior under linear, oscillating sliding (SRV®-method)

7.1 Extreme pressure behavior in the SRV® test

The resistance against seizure of an iron based alloy (ball bearing 100Cr6H = AISI 52100) was determined for different lubricants with the SRV® test rig[2] according to ASTM D5706-05 under conditions of mixed lubrication and quoted as Hertzian contact pressure (for the last O.K. pressure before failure, see *Figure 61*). At 135 °C, the factory-fill oils ranged acceptable from 3000 MPa to 3500 MPa. The unadditivated polyglycols (base oil= b.o.) PAG46-4 b.o. and PPG32-2 b.o. itself achieved highest values of ~ 3700 MPa, which were lowered by antioxidants, and followed or on the same level by the ester-based formulations FUCHS 100E and TOTAL HCE. The formulations having low content of EP-additives or containing no “classic” EP-additives displayed no disadvantages exceeding the maximum design limit of today of 2000 MPa.

7.2 Friction and wear

The SRV® procedure applies a higher load of 300 N associated with a lower oil temperature of 135 °C than the BAM test procedure using 50 N and 0.3 m/s at 170 °C oil temperature. The different deposition techniques applied for the liner samples using HVOF in BAM test versus APS in SRV® test of the same spray powder play a key role and have to be taken into account as additional factors the lower oil temperature of 135 °C and higher roughness of the APS-(Ti,Mo)(C,N)-23NiMo liner samples.

The cast iron liner wear didn´t increase using the APS-$Ti_{n-2}Cr_2O_{2n-1}$ piston ring coating compared to MKP81A®. Also the APS-$Ti_{n-2}Cr_2O_{2n-1}$ piston ring coating wear remain on the same level as the MKP81A® coating ring wear. Thus, also the SRV® tests confirm the potential for substituting molybdenum-based rings by APS-$Ti_{n-2}Cr_2O_{2n-1}$ and also the significant reduction of liner wear when APS-$Ti_{n-2}Cr_2O_{2n-1}$ coated rings are mated with APS-(Ti,Mo)(C,N)-23NiMo. The wear rates of the liner samples coated with APS-(Ti,Mo)(C,N)-23NiMo lie in the range of k_V = 0.7 to 0.9 10^{-9} mm³/Nm (see *Figure 62*).

Figure 63 compiles friction and wear results determined with SRV® test rig under linear, oscillating sliding motion for mixed lubricated conditions for APS-Mo (MKP81A®) and APS-Ti_nO_{2n-1} coated piston rings running against GGL20HCN cylinder liner material (lamellar cast iron with high carbon content).

The coefficient of friction is overall not affected by the used Mo and Ti_nO_{2n-1} piston ring coatings with a small scatter of about 1 % between both coatings. Nevertheless both piston ring coatings exhibit the same dependency for the coefficient of friction in different lubricants. The lowest coefficient of friction was measured with polyalkylene glycoles, which corresponds to the results with unidirectional sliding motion (BAM test, see *Figure 56*). Compared with the factory fill hydrocarbon based HC 5W-30 the ester containing GT1 and GTE can reduce the coefficient of friction under oscillating and unidirectional sliding motion by about 0.01-0.03. PPG32-2 and modified PPG32-2 have in SRV tests a higher coefficient of friction than in the BAM test. The FUCHS Supersyn SL PCX presents

[2] SRV®, n – Schwingung, Reibung, Verschleiß (German); oscilation, friction, wear (English translation). Optimol Instruments GmbH, Westendstr. 125, D-80339 Munich, Germany. See ASTM D5706, D5707, D6425 and D7217.

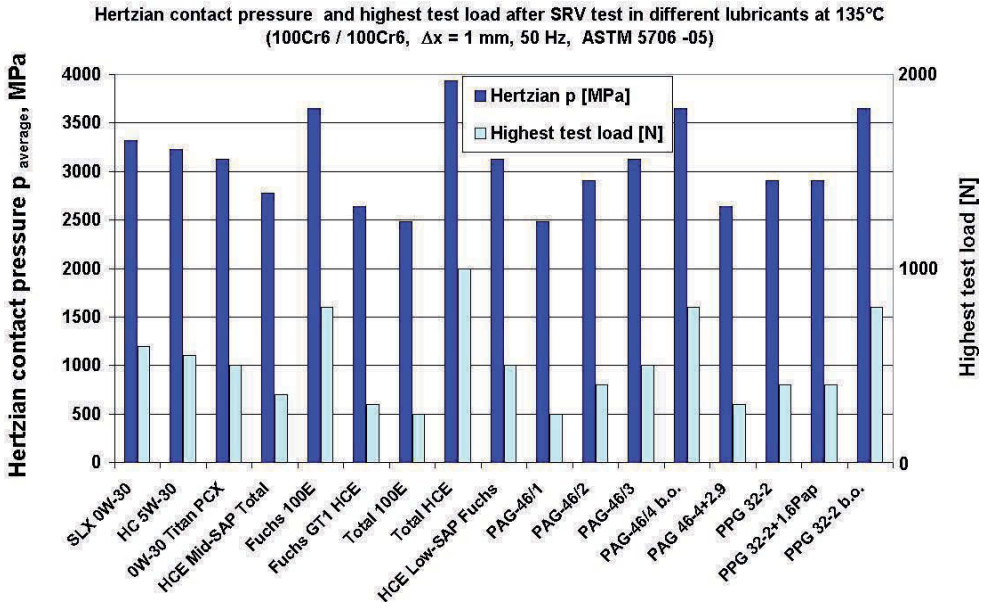

Figure 61
Resistance against seizure for different lubricants according to ASTM D5706-05 using 100/Cr6H/100Cr6H (AISI 52100) at 135 °C

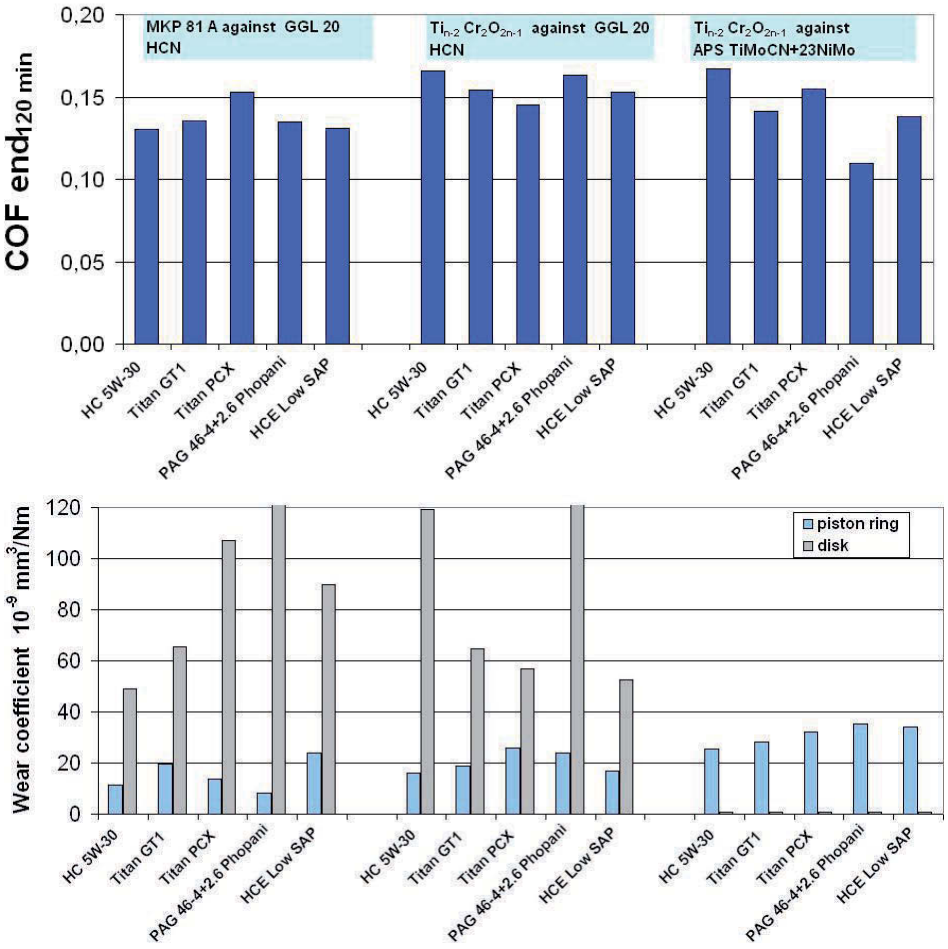

Figure 62
SRV® test results for MKP81A®- and APS-Ti$_{n-2}$Cr$_2$O$_{2n-1}$-coated piston rings sliding on GGL20HCN and APS-(Ti,Mo)(C,N)-23NiMo disks in different lubricants (Top: coefficients of friction; bottom: wear rates; F_N = 300 N, Δx = 2 mm, ν = 50 Hz, s = 1440 m)

under oscillation sliding a higher coefficient of friction as it was not found under unidirectional sliding according to the BAM test method.

The wear data under linear oscillation display, that the molybdenum coating can be substituted by the Ti$_n$O$_{2n-1}$ coating, since the wear rates of the Ti$_n$O$_{2n-1}$ piston ring coating are comparable or lower than those of the Mo-coating. The ranking was confirmed by BAM tests. Furthermore, the Ti$_n$O$_{2n-1}$ piston ring coating promotes a beneficial wear reducing action when lubed with alternative bio-no-tox oils as Titan GTE, PAGs 46 and PPG32-2 with 2.6 Phopani.

7.3 Precision of SRV® test

The *Figure 64* and *Figure 65* show the influence of two different test conditions (BAM and SRV® test) on friction and wear of molybdenum-based MKP81A® against cast iron GGL20HCN in the SRV® test with the associated standard deviation from five consecutive tests. Both, load and temperature were changed. For these comparisons in a meaningful two hours SRV® test, the stroke and frequency were identical.

The standard deviation bars indicate a high repeatability for these SRV® tests which is superior to those known from engine tests.

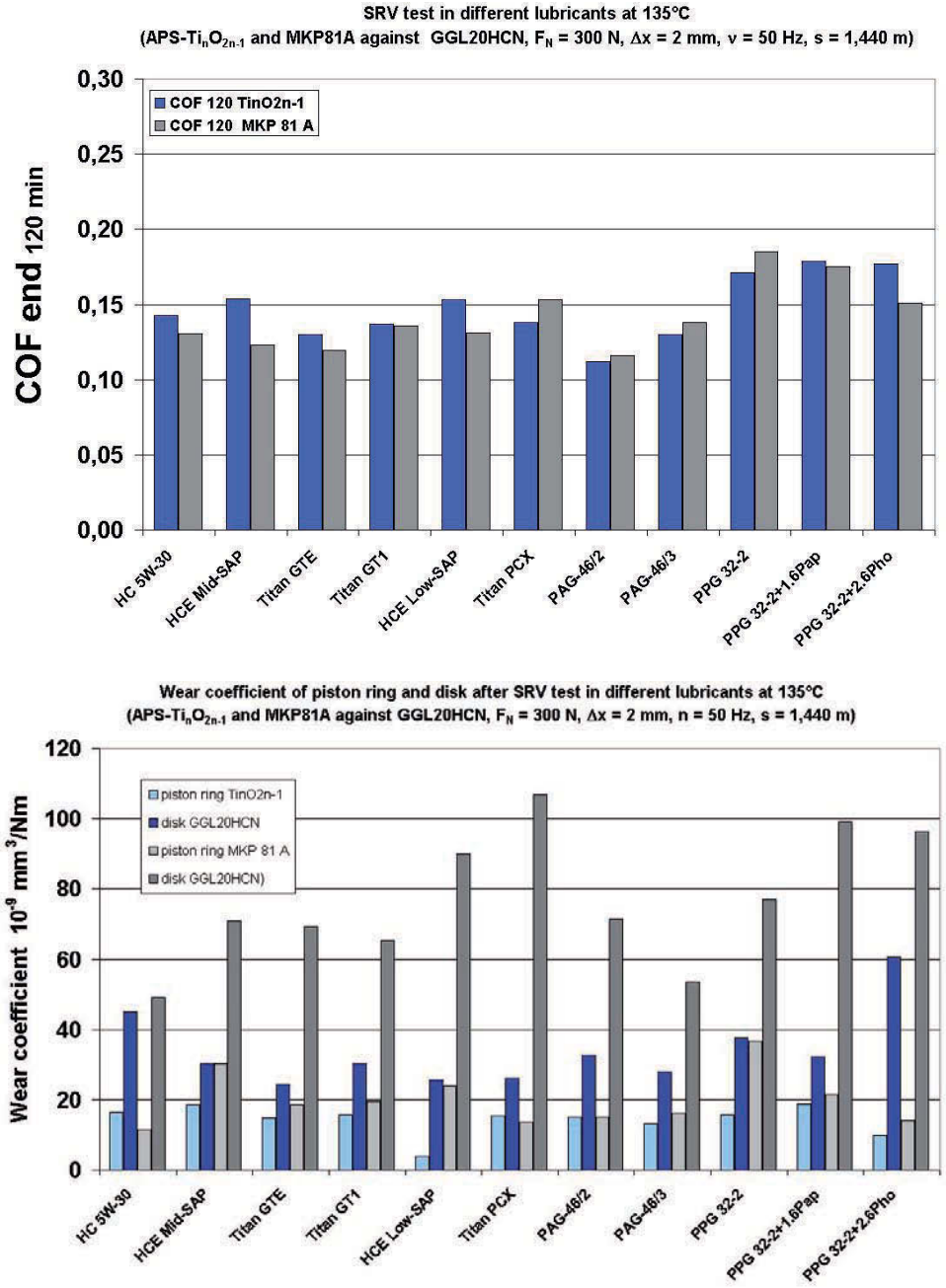

Figure 63
SRV® test results for MKP81A® coated and Ti$_n$O$_{2n-1}$ coated piston rings against GGL20HCN in different lubricants (Top: coefficient of friction, bottom: wear rates]

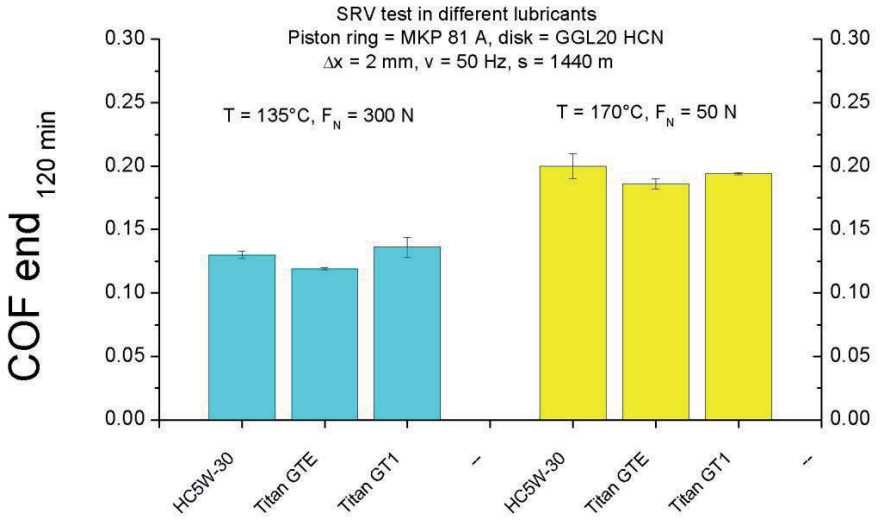

Figure 64
Repeatability and influence of test conditions on friction using SRV® for piston ring cylinder liner evaluation

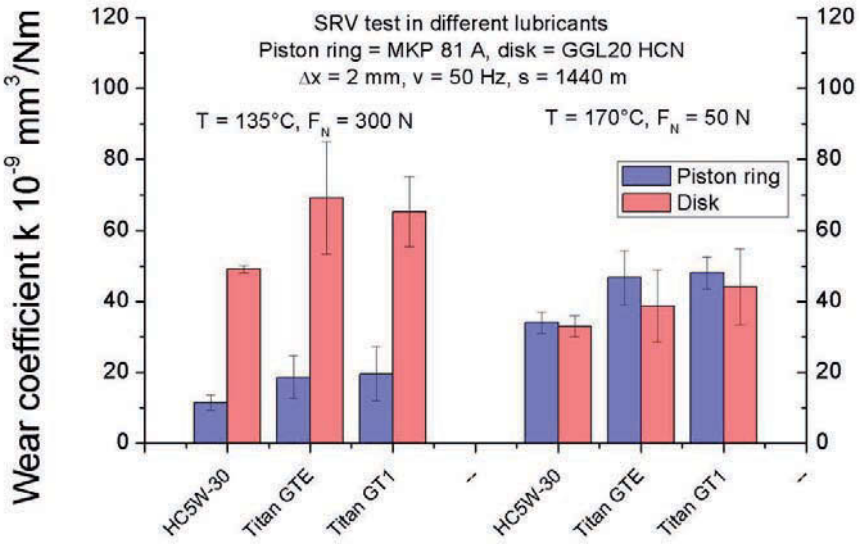

Figure 65
Repeatability and influence of test conditions on wear using SRV® for piston ring cylinder liner evaluation

8 Concluding summary

The present results from the test program revealed that in engine oil specifications the dynamic viscosity, especially measured under higher shear rates than 10^6 s^{-1}, the heat capacity and the pressure-viscosity-coefficients have to be introduced, especially when alternative oils of different chemistries have to be ranked. With these data, the oil film thickness of an individual formulation can be calculated. In order to differentiate viscometric properties of alternative oils, the dynamic viscosity taking into account the differences in density has also to be used. All viscometric lubricant properties should be determined at least at 150 °C.

Some polymer-free ester-type and polyglycol-based engine oils presented thermo-physical and viscometric properties conforming with hydrocarbon-based factory-fill oils or exceeding them.

The cooling ability (volumetric heat capacity $c_p \cdot \rho$) of polyglycols was the highest. The alternative ester- and polyglycol-based formulations offer additional benefits when criteria related to bio-no-tox, low NOACK evaporation, high VI, low/no ash content and reduced additive concentrations have to be respected.

Important properties such as price or polymer compatibility were not considered here, but they are the subject of other, parallel, validations. A favorable economical forecast can be seen in light of the sum of functional properties displayed by the alternative formulations.

Based on the piston ring/cylinder liner simulation tests performed outside of engines by means of the BAM and the SRV® tests, both performed under conditions of only mixed/boundary lubrication, it is reasonable to conclude, that

a. thermally sprayed TiO_x-based coatings ($Ti_{n-2}Cr_2O_{2n-1}$, $TiO_{1,93}$, Ti_nO_{2n-1}) can substitute common materials and serve as a promising alternative to commercial piston ring coatings using strategic molybdenum

b. "Zero wear" was displayed by mating the APS-$Ti_{n-2}Cr_2O_{2n-1}$ coated piston rings with smooth machined HVOF-(Ti,Mo)(C,N) liner coatings or molybdenum-based rings against smooth machined APS-$Ti_{n-2}Cr_2O_{2n-1}$ and (Ti,Mo(C,N) coated liners

c. The coefficient of friction is more determined by the lubricants than by the materials or by an individual interaction between lubricants and a specific material or tribopairing. For given tribological test conditions all APS coatings on piston rings showed no friction reducing effect.

The different bionotox and low ash prototype engine oils with reduced additive contents displayed isoperformance regarding the tribological behavior when lubing common and triboreactive materials. They presented no visible weakness in wear resistance, coefficient of friction and extreme pressure properties, but a distinct potential to reduce the coefficient of friction and to reduce the system wear.

The outcomes and data generated in the frame of this project, showing that ecological compatibility and technical performance can be reached simultaneously, supported the German Environmental Agency (www.umweltbundesamt.de) to draw the draft document with the criteria for the attribution of an ecolabel for engine oils.

Acknowledgements:

The authors are grateful to the German Ministry of Economics and Labour (www.BMWA.bund.de) funding the project BMWA14/02 "New lubrication concepts for environmentally friendly machines" related to thermophysical and viscometric properties of alternative lubricants interacting tribologically with triboreactive materials.

Some of the protoype oils were supplied within the framework of the parallel EC-funded project GROWTH Contract N° G3RD-CT-2002-00796-EREBIO, "-Emission reduction from engines and transmissions substituting harmful additives in biolubricants by triboreactive materials" focussing on triboreactive materials and bio-no-tox-properties.

The supply of oils is gratefully acknowledged by the authors. The alternative bio-no-tox-lubricants were supplied by the project partners Fuchs Petrolub AG (Mannheim, Germany) and via Renault SAS from Total SA (Paris, France). Factory-fill oils used at the project partner Renault SAS (Paris, France) were supplied by Total SA (HC 5W-30 fresh oil, aged in a turbodiesel engine having 3.7 wt.-% soot) and Fuchs Petrolub AG (Titan SL PCX 0W-30). Prototype oils were supplied by the same companies (Total: 100E, HCE and HCE-Low-SAP; Fuchs: Fuchs HCE 0W-20 and GTE (100E 0W-20), HCE low SAPs, 100E HDDO). All pre-blended polyglycols were modified by the Federal Institute for Materials Research and Testing (BAM), Berlin.

The authors are grateful for the active support received from industry and OEM members, namely to Dr. Michael Berg and Dr. Hubert Schultheiß of IAV GmbH as well as to Tom Linnemann, Gérard Desplanches, Bernard Criqui and Nathalie Davias of Renault SAS and to Rolf Luther of FUCHS Petrolub AG.

The experimental APS-Ti_nO_{2n-1}, APS-$Ti_{n-2}Cr_2O_{2n-1}$ and APS-(Ti,Mo)(C,N)+23NiMo coated piston rings were provided by Jesu Landa/Dr. Iñaki Illaramendi from Grupo CIE Automotive (Tarabusi), Barrio Urquizu 58, E-48140 Igorre, Spain.

Within BAM: Mr. Norbert Kelling and Manfred Hartelt are gratefully acknowledged for performing the tribological tests and profilometry. The assistance of our colleagues Ms. Sigrid Binkowski, Ms. Silvia Benemann and Ms. Birgit Strauß is gratefully acknowledged in carefully performing metallography, recording optical and SEM micrographs and Ms. Dagmar Nicolaides for XRD analysis and the measurement of particle size distribution.

Within PTB: The authors wish to thank Mr. Karl-Heinz Metzing for the construction and manufacturing of the rolling-ball viscometer as well as of important parts of the high-shear viscometer. He also did a lot of measurements with this two instruments. Thanks also go to Ms. Nicole Wloczek for carrying out the kinematic viscosity measurements using Ubbelohde viscometers. We are also grateful to Mr. Jörg Matthis, who performed the heat conductivity measurements according to Dr. Ulf Hammerschmidt. We have to thank Dr. Stefan Sarge for the specific heat measurements carried out by Mr. Peter Bartling, Dr. Dirk Boghun and Dr. Michael Müller–Wiegand as well. Dr. Harro Bauer is acknowledged for numerous discussions.

List of variables

Symbol	Dimension	Definition
a, b c	K -	Coefficients of the Vogel equation unless otherwise defined in the text
A	$m^2\ s^{-1}\ N^{-1}$	Linear coefficient of the apparent flow curve
A_c	m^2	Area of circular plates
B	$m^4\ s^{-2}\ N^{-2}$	Quadratic coefficient of the apparent flow curve
c_p	$kJ\ kg^{-1}\ K^{-1}$	Specific heat capacity at constant pressure
C_{Tr}		Constant, tribosystem
d	m	Gap
D	s^{-1}	Shear rate
D_{ap}	s^{-1}	Apparent shear rate
D_{true}	s^{-1}	True shear rate
E	MPa	Elasticity modulus
f	-	Coefficient of friction
F	N	Force on the contact
G	-	Material parameter
h^*	-	Relative film thickness
h_{min}	mm	Minimum film thickness
h_{ref}	mm	Film thickness of reference oil at 150°C
k_V	$mm^3/(Nm)$	Wear rate
L	mm	Capillary length
Mw	$g\ mol^{-1}$	Molar mass
p	MPa	Pressure
p_B	MPa	Bagley correction
p_m	MPa	Pressure, arithmetic mean
p_{amb}	MPa	Ambient pressure
r	mm	Equivalent radius of curvature
r_A	mm	Radius of curvature of cylinder/sphere A

Symbol	Dimension	Definition
r_B	mm	Radius of curvature of cylinder/sphere B
R	mm	Capillary radius
Re	-	Reynolds number
s	m	Sliding distance
s_z	Dimension of quantity z	Standard deviation
s'	-	Relative standard deviation
Q	$m^3\ s^{-1}$	Volume flow rate
$\dot{Q}$	W	Flow of thermal energy
T	°C	Temperature
U_e	-	Speed parameter
VI	-	Viscosity index
W_e	-	Load parameter
α	GPa^{-1}	Pressure coefficient of the dynamic viscosity
β	K^{-1}	Temperature coefficient of the dynamic viscosity
η	mPa s	Dynamic viscosity
η_{avg}	mPa s	Arithmetic mean of the dynamic viscosity within a group of oils
κ	GPa^{-1}	Compressibility
λ	$W\ m^{-1}\ K^{-1}$	Thermal conductivity
ν	mm^2s^{-1}	Kinematic viscosity
ν_{avg}	mm^2s^{-1}	Arithmetic mean of the kinematic viscosity within a group of oils
μ	—	Poisson ratio
ρ	$kg\ m^{-3}$	Density
τ	$N\ m^{-2}$	Shear tension

9 Literature/References

[1] RENAULT SAS
Dossier Zukunftssichere Entwicklung – "ELLYPSE", Radikal konstruiert-R&D –Wege der Innovation-, Das Magazin für Forschung und Entwicklung, Nr. 26, Oktober 2002, Publisher: Renault SAS, Direction de la Communication, rue du Vieux-Pont-de-Sèvres, F-92109 Boulogne-Billancourt (France), ISSN: 1289-009X or in press kit for the „Mondial de l´Automobile, 2002, Paris (www.planeterenault.com go to Protos go to Ellypse)

[2] Environmental Protection Agency (EPA)
"Oil pollution prevention and responses, non-transportation-related facilities, final rule", of 30. June 2000, 40 CFR part 112,

[3] R. Schmidt, G. Klingenberg, and M. Woydt
Thermophysical and viscometric properties of environmentally acceptable lubricants
Industrial Lubrication and Tribology, 4/2006, Vol. 58, p. 210-224

[4] R. Schmidt, M. Woydt
Viskosimetrische und thermophysikalische Eigenschaften umweltverträglicher Motorschmierstoffe
Tribologie und Schmierungstechnik Vol. 53 (2006), No 2, pp. 16-20

[5] G. Buschmann, H. Clemens, M. Hoetger, and B. Mayr
The Steam Engine – Status of Development and Market Potential
Motortechnische Zeitschrift Vol. 62 (2001) No. 5, pp. 2-10

[6] Spillingwerk GmbH
Werftstrasse 5, D-20457 Hamburg
Tel. +49/(0)40-789175-0, Fax +49/(0)40-7892836, Internet www.spilling.de

[7] M. Woydt, N. Kelling, M. Hartelt , A.Igartua, O. Areitioaurtena, C. Seyfert, and R. Luther
Tribological performance of bio-no-tox engine oils and new triboactive materials for piston ring/cylinder liner systems
Proc. 15th Int. Coll. Tribology, TAE Esslingen, 17.-19. January 2006, ISBN 3-924813-62-0

[8] M. Woydt and A. Igartua
Ashfree and bionotox engine oils
Virtual Tribology Institute (VTI) Internet site, 2005, www.vti-europe.org, ISBN 83-7204-449-X

[9] "Guide to the expression of uncertainty in measurement", International Organization for Standardization (Geneva, Switzerland) 1995

[10] E.S. Watson, J.J. O'Neill, and N. Brenner
A Differential Scanning Calorimeter for Quantitative Differential Thermal Analysis
Analytical Chemistry 36 (1963), pp. 1233-1238

[11] G. Höhne, W. Hemminger, and H.-J. Flammersheim
Differential Scanning Calorimetry
2nd edition, Springer-Verlag 2003

[12] U. Hammerschmidt
Thermal Conductivity of a Wide Range of Alternative Refrigerants. Measured with an Improved Guarded Hot-Plate Apparatus
Int. J. Thermophys.16 (1995), pp. 1203-1211

[13] ASTM D xxxx.yy draft „Tribological Characterization of Piston Ring and Cylinder Liner Materials and Lubricants using the translatory oscillation apparatus (SRV®)", supported by ASTM D02 "L" and "B" subcommittees

[14] M. Woydt and N. Kelling
Testing the tribological properties of lubricants and materials for the system "piston ring / cylinder liner" outside of engines
Industrial Lubrication and Tribology 55 (2003), No.5, pp. 213-222

[15] M. Woydt and J. Ebrecht
SRV-Testing of the Tribosystem Piston Ring and Cylinder Liner Outside of Engines
Proc. KSTLE – 41st Autumn Conference, 25. Nov. 2005, Seoul, pp. 158-168, publisher: Korea Military Academy.

[16] ASTM D5706-05 "Standard Test Method for Tribological Characterization of Piston Ring and Cylinder Liner Materials and Lubricants using SRV® Test Machine" (2005)

[17] M. Woydt
Review on Lubricious Oxides and Their Practical Importance
In: Handbook of Surface Modifications and Processing: Physical & Chemical Tribological Methodologies, edited by: G.E. Totten; Marcel Dekker, New York, ISBN 0-9247-4872-7 (2004)

[18] M.N. Gardos
The effect of anion vacancies on the tribological properties of rutile (TiO2-x)
Tribology Transactions 32 (1989), pp. 30-31

[19] M.N. Gardos
The Effect of Magnéli Phases on the Tribological Properties of Polycrystalline Rutile
Proc. 6th Int. Congress on Tribology (1993), Vol. 3, pp 201-206

[20] M. Woydt, J. Kadoori, H. Hausner, and K.-H. Habig
Development of engineering ceramics according to tribological considerations (bilingual)
Cfi/Ber. DKG, Vol. 67 (1990), No. 4, pp.123-130 (Journal of the German Ceramic Society)

[21] O. Storz, H. Gasthuber, and M. Woydt
Tribological properties of thermal sprayed Magnéli-type coatings with different stoichiometries (Ti_nO_{2n-1})
Surface and Coatings Technology 140 (2001), pp. 76-81

[22] M. Woydt, N. Kelling, and M. Buchmann
Thermisch gespritzte, keramische Zylinderlaufbahnen unter Misch-/Grenzreibung
DGM-Tagung „Reibung und Verschleiß“, 09.-11.03.2004, Fürth, in: Materialwissenschaft und Werkstofftechnik, ISSN: 0933-5137 (print), 1521-4052 (online), Vol. 35 (2004), No.10, pp. 824-829

[23] T. Naumann, L.-M. Berger, M. Ingwerth, and P. Vuoristo
Titanium suboxide coatings prepared by VPS spraying
Thermal Spray 2003: Advancing the Science & Applying the Technology, C. Moreau and B. Marple (eds.), ASM International, Materials Park, Ohio, USA (2003), pp. 1441-1445

[24] „Hochwertig legierter Grauguß“ (“High value alloyed grey cast iron”), Supply Specification DBL 4401 of Mercedes-Benz, December 2002, 4 pages

[25] Kolbenringhandbuch (Piston ring Handbook) , April 2003, Federal Mogul Burscheid GmbH, D-51399 Burscheid (Germany)

[26] M. Woydt and K.-H. Habig
High temperature tribology of ceramics
Tribology International, Vol. 22 (1989), No. 2, pp. 75-88

[27] M. Woydt, N. Köhler, and N. Kelling
Magnéli-type phases for dry high-speed sliding applications up to 800 °C
World Tribology Conference, WTC2005-63236, 12.-16. September 2005, Washington D.C., USA, In German in: Tribology&Schmierungstechnik, Jg. 52 (2005), Heft 4, pp. 5-12 as well as in English in: Proc. 15th Int. Coll. Tribology, TAE Esslingen, 17.-19. January 2006, ISBN 3-924813-62-0

[28] M. Woydt
Tribomaterials for axial and radial foil bearings,
DE 10 2004 046 320.4, filed 17.09.2004

[29] M. Woydt
Tribological characteristics of polycrystalline titanium-dioxides with planar defects
Tribology Letters, Vol. 8 (2000), No. 2-3, Special issue „Lubricious Oxides“, pp. 117-130

[30] H. Bauer (1986)
Flüssigkeiten mit NEWTONschem Fließverhalten
In: Fließverhalten von Stoffen und Stoffgemischen, Hüthig & Wepf Verlag, Basel, Heidelberg, New York, Kulicke, W.-M., ed., pp 100-146, ISBN 3-85739-115-4

[31] A. Schmidt
Untersuchung des Viskosität-Druck-Temperatur-Verhaltens der Bioöle B, K, N und S im Hochdruckbereich
Forschungsvereinigung Antriebstechnik, Vorhaben Nr. 265, (1998), Frankfurt a. M.

[32] J. Blume
Druck-und Temperatureinfluß auf Viskosität und Kompressibilität von flüssigen Schmierstoffen Ph.D. Thesis, RWTH Aachen University (1987)

[33] J. Sorab, S. Korcek, C.B. McCollum, and K. W. Schriewer
Sequence VIB engine test for evaluation of fuel efficiency of engine oils- Part II: Stage selection and time factor determination
SAE Technical paper 982624

[34] J. Igarashi
The mineral oil industry in Japan
Proc. 13th Int. Coll. Tribology, 15.-17. Jan. 2002, Esslingen, ISBN 3-924813-48-5, Vol. I, pp. 13-17

[35] R.I. Taylor, R.T. Dixon, F.D. Wayne, and S. Gunsel
Lubricants&Energy Efficiency: Life-Cycle Analysis
Leeds-Lyon Symposium on Tribology, September 2004

[36] B.O. Jacobson
Rheology and elastohydrodynamic lubrication
Elsevier Science Publishers, Amsterdam, The Netherlands, ISBN 0-444-88146-8 (1991), pp. 263-288

[37] D. A. Jones
Elastohydrodynamic Lubrication Theory
In Engine Tribology, Elsevier Science Publishers, Amsterdam, The Netherlands, Taylor, C.M., ed, ISBN 0-444-89755-0 (1993), pp. 15-50

[38] D. Dowson
Elastohydrodynamics, Proc. Inst. Mech. Eng., London, Vol. 182 (3A) (1968), pp 151-167

[39] N. Böse and H. Broeke
Reducing Measurement Uncertainty of a High Pressure Capillary Viscometer
Rheology 95 (1995), pp.190-195

[40] DIN 53014 Part 1: Viscometry, capillary viscometers with circular and rectangular cross section for determination of flow curves; principles, concepts, definitions (1994)

[41] DIN 53014 Part 2: Viscometry, capillary viscometers with circular and rectangular cross section for determination of flow curves; systematic deviations, sources and corrections (1994)